Russian Original Vol. 40, No. 4, April, 1976
October, 1976

SATEAZ 40(4) 349-444 (1976)

SOVIET ATOMIC ENERGY

АТОМНАЯ ЭНЕРГИЯ
(ATOMNAYA ÉNERGIYA)

TRANSLATED FROM RUSSIAN

CONSULTANTS BUREAU, NEW YORK

SOVIET ATOMIC ENERGY

Soviet Atomic Energy is a cover-to-cover translation of *Atomnaya Énergiya*, a publication of the Academy of Sciences of the USSR.

An agreement with the Copyright Agency of the USSR (VAAP) makes available both advance copies of the Russian journal and original glossy photographs and artwork. This serves to decrease the necessary time lag between publication of the original and publication of the translation and helps to improve the quality of the latter. The translation began with the first issue of the Russian journal.

Consultants Bureau journals appear about six months after the publication of the original Russian issue. For bibliographic accuracy, the English issue published by Consultants Bureau carries the same number and date as the original Russian from which it was translated. For example, a Russian issue published in December will appear in a Consultants Bureau English translation about the following June, but the translation issue will carry the December date. When ordering any volume or particular issue of a Consultants Bureau journal, please specify the date and, where applicable, the volume and issue numbers of the original Russian. The material you will receive will be a translation of that Russian volume or issue.

Subscription
$107.50 per volume (6 Issues)
2 volumes per year
Prices somewhat higher outside the United States.

Single Issue: $50
Single Article: $15

CONSULTANTS BUREAU, NEW YORK AND LONDON

c/b
227 West 17th Street
New York, New York 10011

Published monthly. Second-class postage paid at Jamaica, New York 11431.

Soviet Atomic Energy is abstracted or indexed in *Applied Mechanics Reviews, Chemical Abstracts, Engineering Index, INSPEC—Physics Abstracts and Electrical and Electronics Abstracts, Current Contents,* and *Nuclear Science Abstracts.*

SOVIET ATOMIC ENERGY

A translation of *Atomnaya Énergiya*

October, 1976

Volume 40, Number 4 April, 1976

CONTENTS

CONTENTS

(continued)

The Russian press date (podpisano k pechati) of this issue was 3/24/1976. Publication therefore did not occur prior to this date, but must be assumed to have taken place reasonably soon thereafter.

ARTICLES

PLUTONIUM CHARGING OF THE VVÉR-440 WATER-COOLED WATER-MODERATED REACTOR

H. Kaikkonen and P. Silvennoinen

UDC 621.039.512.45

The present delay in the adoption of commercial breeder reactors means that the repeated use of plutonium in the light-water reactors of the 1980's is a likely outcome. Whereas some plutonium-containing assemblies will probably be used in the BWR reactors [1], in the PWR reactors it will be most reasonable and economical to use plutonium in all the fuel assemblies [2]. Let us therefore consider the charging of a VVÉR-440 reactor with the secondary use of plutonium in all the fuel assemblies and a specific distribution of plutonium enrichment.

Limitations on the Use of Plutonium in the Active Zone of the VVÉR-440. The monitoring of reactivity and the distribution of energy evolution are the main problems involved in improving the use of nuclear fuel containing plutonium. It is essential to keep the characteristics of the active zone the same as in the case of uranium charging. The problem of determining the necessary "weight" of the control rods has never been examined, but a system of control rods with neutron traps will clearly not introduce any limitations into the shutting down of the reactor, since the neutrons will be thermalized and largely absorbed in the water filling the control assemblies, so that the system will be insensitive to changes in the neutron spectrum. The "pure" lattice and hexagonal geometry of the active zone of the VVER will lead to a geometrically simple disposition of the plutonium assemblies, despite the fact that the wider water gaps between the plutonium assemblies will increase the power evolution peaks. In our calculations we considered that plutonium fuel was incorporated in the initial fuel charge, for which the differences in the flux levels of the neutron spectra were the greatest. The results accordingly give a conservative estimate of the use of plutonium under practical recharging conditions.

From the point of view of recharging economics, all the fuel assemblies of the VVÉR-440 reactor being recharged should be provided with plutonium, since the incorporation of local plutonium-containing assemblies reduces the plutonium productivity of the reactor by a factor of 2. Typical problems which arose in organizing the recharging of the PWR reactor were solved in [3] by using at least three degrees of enrichment in the plutonium assemblies. We used this arrangement in our present calculations.

According to calculation, the degree of fuel enrichment in the steady state of recharging amounts to 2.4 and 3.6% for U and Pu, respectively. There is no need to use a plutonium enrichment exactly corresponding to the enrichment of the uranium fuel replaced. The foregoing degree of enrichment eases solution of the problem of repeatedly using the plutonium and satisfies the requirements imposed upon the fuel circulation, thus giving additional flexibility. In order to maximize the value of the plutonium, the highly enriched uranium fuel should be replaced by fuel consisting of oxide mixtures, and the envisaged rechargings should take account of this aspect.

Results of the Calculations. In order to obtain groups of parameters based on the ENDF/B data we used the computer programs FORM [4] and THERMOS [5]. The differential diffusion computing program TRIGON [6] designed for a triangular lattice configuration was used with two neutron-energy groups in the general reactor calculations, while four neutron-energy groups were used in the calculation for the fuel assembly. The boundary of the thermal neutrons was increased to 2.53 eV.

State Technical Scientific-Research Center. Laboratory of Nuclear-Power Technology, Helsinki, Finland. Translated from Atomnaya Énergiya, Vol. 40, No. 4, pp. 283-286, April, 1976. Original article submitted July 4, 1975.

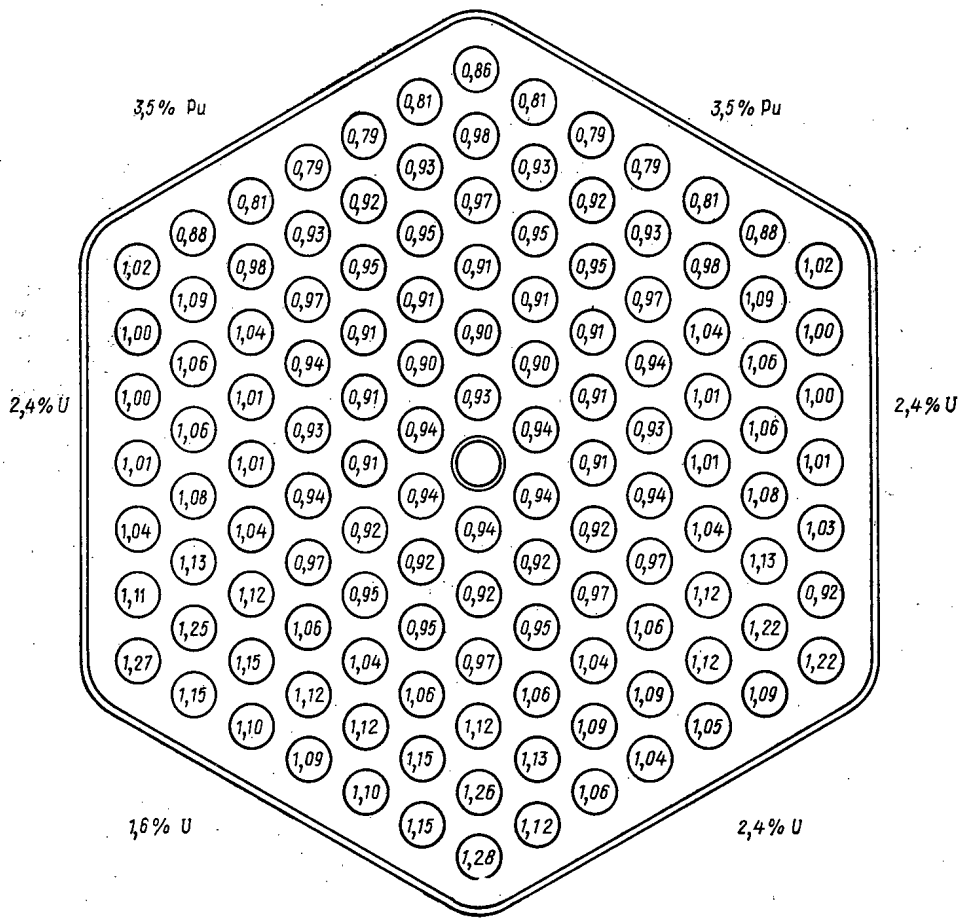

Fig. 1. Distribution of energy evolution in a plutonium fuel assembly containing fuel with three degrees of enrichment and boron (800 ppm).

Local peaks of energy evolution and interaction between neighboring uranium fuel assemblies were studied by placing the plutonium assemblies in a position in which they were surrounded by uranium assemblies with enrichment factors of 1.6 and 2.4% and analogous plutonium assemblies (Fig. 1). In the plutonium assembly the fuel elements lying along the outer water gap contain 2.15% PuO_2 and the remainder 3.5%. The four inner fuel-element hexagons contain 4.3% PuO_2. The enrichment of the whole assembly with respect to fissile plutonium is 4.3%. The two contiguous plutonium assemblies in Fig. 1 are identical with the central assembly.

In the configuration illustrated in Fig. 1, if the plutonium assemblies are replaced by uranium with a 3.6% enrichment we shall obtain a maximum relative heat-evolution peak (equal to 1.24) in the corner adjacent to the fuel with the 1.6% enrichment. On the other hand, if the three plutonium assemblies have the same PuO_2 content, equal to 3.5%, the relative heat-evolution peak will increase to 1.59, arising from the thermal neutron flux of the uranium fuel, in which this flux is considerably higher. This peak is due to the thermalization of the neutrons in the water gap.

In view of the high level of local heat evolution it is essential to change the enrichment inside the fuel assembly. A reduction of the plutonium content in the outer elements of the fuel assembly only will lead to a considerable change of neutron flux in the fifth hexagonal ring of the fuel elements and make it essential to use a third enrichment factor.

It follows from Fig. 1 that a relative heat-evolution peak of 1.28 occurs in the fuel elements at the boundary between the plutonium and uranium fuel assemblies. In any practical construction it would even be desirable to use a fourth plutonium enrichment factor, which would require a corresponding rotation of the fuel assembly when the fuel is recharged or transposed.

When studying the general energy pattern we considered the replacement of the highly enriched uranium by plutonium fuel. In so doing we investigated possible specific changes in the use of the nuclear fuel, established the required indices of the active zone, and also determined the relative value of the fissile plutonium by comparison with ^{235}U in the lattice of the VVÉR-440 reactor.

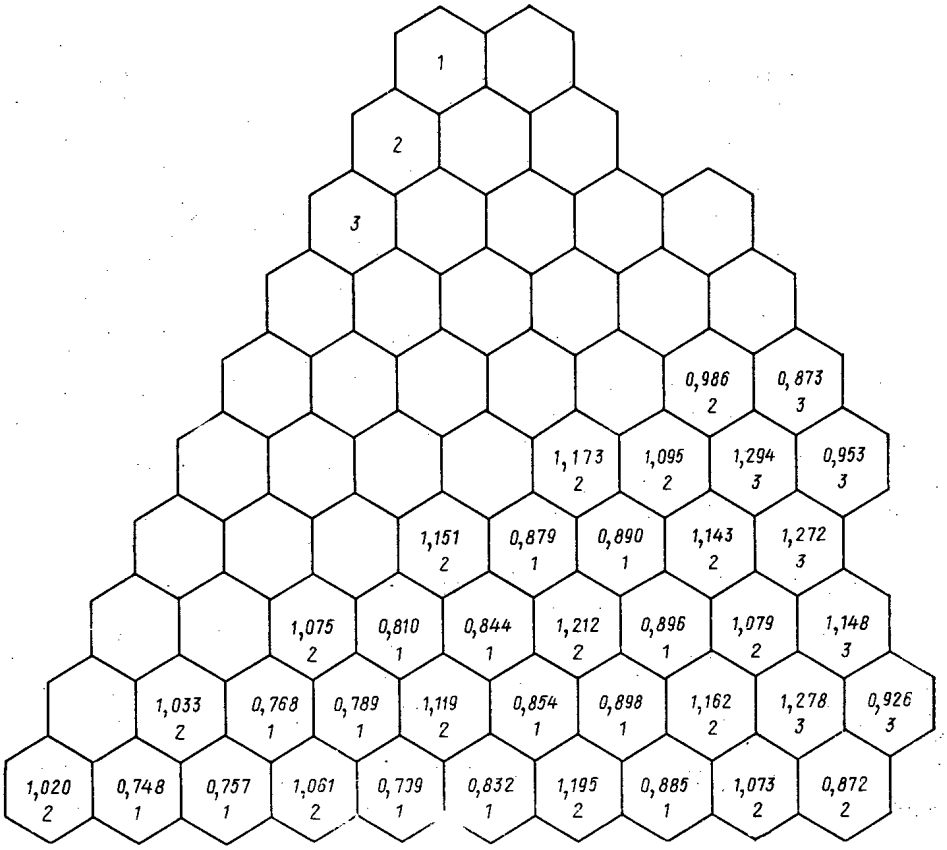

Fig. 2. Distribution of heat evolution in a group of heat-evolving assemblies (1/12 part of the total symmetry) containing uranium and plutonium fuel and boron (800 ppm) K_{eff} = 0.98824: 1) 1.41 wt. % ^{235}U; 2) 2.14 wt. % fissile Pu; 3) 3.40 wt. % fissile Pu; the numbers in the cells represent the relative energy distribution.

Plutonium fuel gives a greater depth of burnup than uranium. Certain changes must therefore be made in the order of using the nuclear fuel. We shall consider an "open" commercial situation in which there are no restrictions on the use of the plutonium loaded into the reactors. (The opposite situation is that of a closed fuel cycle in which the consumption of plutonium is limited by its production.) It was found that the active zone of the VVÉR-440 offered great possibilities in the breeding of plutonium. Figure 2 illustrates a lattice in which all the fuel assemblies except those in which the lowest uranium enrichment is employed are replaced by plutonium-containing versions. Economy in separation processes suggests replacing the highly enriched uranium by plutonium, but at the same time flexibility and the high cost of making plutonium assemblies dictates the use of poorly enriched uranium in the active zone.

The general distribution of energy evolution is shown in Fig. 2, from which we see that an acceptable distribution of heat evolution may be obtained in the active zone in the manner indicated. The radial nonuniformity coefficient is 1.294, which is usually an acceptable figure for a PWR reactor.

CONCLUSIONS

Our study has been limited to a neutron-physical analysis of the active zone in the presence of a "fresh" charge. Allowing for the disposition of the fuel assemblies this reflects a reasonably practical situation. The difficulties associated with local peaks of energy evolution may be quite easily overcome by using different fuel enrichments inside the assembly.

Our example of the charging of the active zone with plutonium is of a hypothetical character, since there is far more plutonium in this arrangement than is required in any practical situation. The calculations show that there are no problems as regards the distribution of heat evolution with respect to the radius of the active zone.

It would be extremely desirable to pursue this investigation with due allowance for the factors involved in the burnup of the nuclear fuel. Certain experimental work will be required in this connection so as to provide confirmation of the validity of the computer calculations. The nonuniformity of the distribution of energy evolution will be smoothed as the nuclear fuel is impoverished during burnup.

Another important aspect to be studied is that of determining the "weight" of the control rods. We feel that a study of reactivity problems will reveal some more rigorous limitations than those deduced from the study of energy distribution undertaken in the present investigation.

LITERATURE CITED

1. R. Crowther et al., Trans. Amer. Nucl. Soc., 18, 297 (1974).
2. Generic Environmental Statement on the Use of Recycle Plutonium in Mixed-Oxide Fuel in LWRs, USAEC, WASH-1327 (1974).
3. D. Call and P. Lacey, Trans. Amer. Nucl. Soc., 19, 347 (1975).
4. P. Siltanen, FORM, A Multigroup Code for Calculating the Fundamental Mode Flux and Current Spectra of Fast Neutrons, Techn. Res. Center of Finland, Nucl. Engng. Laboratory, Rep. No. 6 (1973).
5. J. Saastamoinen and F. Wasastjerna, THERMOS-OTA, A Revised Version of the THERMOS Program for Thermal Lattice Calculations with the Auxiliary Programs THEPSL and THECOM, Techn. Res. Center of Finland, Nucl. Engng. Laboratory, Rep. No. 10 (1974).
6. E. Kaloinen, A Two-Dimensional Multigroup Diffusion Code for Trigonal or Hexagonal Mesh, Techn. Res. Center of Finland, Nucl. Engng. Laboratory, Rep. No. 1 (1973).

DESIGN OF SODIUM—WATER STEAM GENERATORS

P. L. Kirillov and V. M. Poplavskii

UDC 621.181.021:621.039.517.5

Various possible constructions of sodium—water steam generators have now been established, but the terminology has not yet been settled, and this causes certain difficulties when discussing design problems and also in the preparation of technical translations, as clearly revealed in the recent steam-generator seminar (Proc. Development of Sodium-Cooled Fast Breeder Reactor Steam Generators, Los Angeles, Vol. 1, 1974).

The construction of steam generators for nuclear power stations with fast reactors cooled by liquid sodium is being developed in two directions.

The first is characterized by shell constructions in which the principal characteristics are: the incorporation of shells having dimensions matching the thermal power of one reactor loop; no parallel connection of the shells; the impossibility of disconnecting any shell without infringing the technological basis of the loop. Each shell is capable of executing one or several functions such as economizer, evaporator, steam superheater, and intermediate superheater; it may combine two or even all these elements. If the shell combines all the elements, it will characterize the integral (one-shell) construction (Fig. 1a). If the shell is divided into several parts we shall have the two- or three-shell construction (Fig. 1b, c).*

The second direction is that of section-type (module) constructions with the following main characteristics: sections connected in parallel; the combination of all functional elements of the steam generators in one or several modules; the fact that the disconnection of one or even several sections does not lead to the stopping of the whole steam generator. A section may be made in one-, two-, or three-module form (Fig. 2a, b, c) and so on.

*In the captions to Figs. 1 and 2 the proposed terminology is given in four languages.

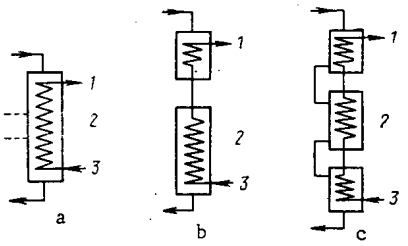

Fig. 1. Korpusnyi parogenerator	Shell-type steam generator:	Corps type generateur de vapeur:	Korpus Typ Dampferzeuger:
a) integral'nyi (odnokorpusnyi)	integral (one-shell)	type integre (un corps)	integrierter (ein Korpus)
b) dvukhkorpusnyi	two-shell	deux corps	zwei Korpusse
c) trekhkorpusnyi	three-shell	trois corps	drei Korpusse

Translated from Atomnaya Énergiya, Vol. 40, No. 4, pp. 286-288, April, 1976. Original article submitted May 4, 1975.

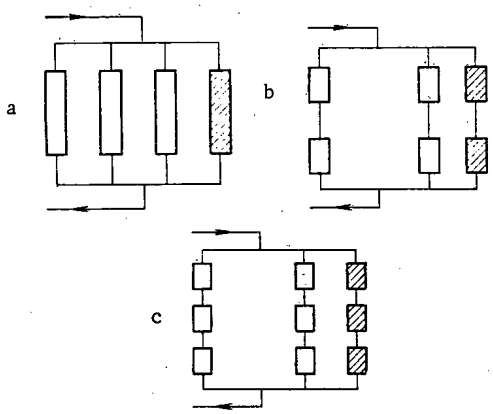

Fig. 2. Sektsionnyi (modul'nyi) parogenerator:	Section-type (module type) steam generator:	Section type generateur de vapeur:	Sektion Type Dampferzeuger:
a) integral'naya sektsiya (odnomodul'naya)	integral (one module)	integral (un module)	integrierte Sektion (ein Modul)
b) dvukhmodul'naya sektsiya	two-module	deux-modules	zwei Modul-Sektion
c) trekhmodul'naya sektsiya	three-module	trois-modules	drei Modul-Sektion

A section is a part of the steam generator comprising one or several modules capable of being disconnected simultaneously.

A module is an individual construction element, technologically perfected under workshop conditions, possessing the characteristics of a heat exchanger (shell, heat-transfer elements, inlet and outlet coolant chambers, and so forth). A module may have a specific purpose (economizer, evaporator) or combine several elements, i.e., it may constitute a combined module.

Modules may be classified by dimensions: micromodules (1 MW), low-power modules (1-10), medium (10-100), and high-power modules (over 100 MW). Shell-type steam generators have the following advantages: compactness, low specific cost, low metal requirements, inexpensive assembly, and a minimum number of instruments.

The shortcomings of shell-type steam generators include: complication of manufacturing technology due to their large size; greater time of manufacture and complexity as regards conservation, difficulty in finding defective elements under working conditions; the essential disconnection of the whole loop for repairing the steam generator when a single tube develops a fault; the impossibility of determining the consequences of leak development, and hence the impossibility of prolonging operation after the removal of a leak. There are grounds for considering that as a result of the interaction of sodium with water the material of neighboring tubes may undergo serious structural changes in the case of substantial leaks, and damage right through if small leaks occur.

The advantages of section-type (module) steam generators include: simplicity of manufacturing technology; the possibility of checking the thermohydraulic characteristics under test-bed conditions directly on full-size modules; great reliability because of the possibility of localizing any emergency within a single module should a particular tube suffer damage; the possibility of continuing work when other modules fail; the moderate cost of the module.

The disadvantages of sectioned (module-type) steam generators include: less compactness than that of shell-type systems; greater size and total amount of metal, high total cost; greater complexity (collectors, fittings, instruments); possible flow misalignment when operating with a large number of parallel channels; higher pressures when the sodium and water interact.

The development of a new type of steam-generator construction has recently been proposed; in this the sodium flows through tubes, and a vapor — liquid mixture occupies the intertube space. Such constructions are called "inverted" steam generators; their main advantage is the restriction of the area of the

emergency if a leak develops and the sodium comes into contact with water. The reaction region is taken out of the piping and into the inlet and outlet chambers; neighboring tubes remain undamaged. Another advantage is the pressure outside the tubes, which reduces the stresses in the walls at the water interface.

Shortcomings of this construction are as follows: the difficulty of finding a leak and restoring the system following the opening of the sodium space and preliminary purifications; the possibility of fissure corrosion at the points at which the tubes are fitted into the tube board; possible instability of the hydraulic characteristics of the two-phase mixture and the thermal state of the walls, owing to the low mass velocities in the intertube space.

In order to obtain experience and establish the positve and negative features of this construction, a great deal of design and experimental work will have to be carried out.

At the present time shell-type steam generators have been made in the EFFBR (USA), PFR (UK), and BOR and BN-350 installations (USSR), and sectional steam generators in the EBR-II (USA), Phenix (France), and BOR and BN-600 (USSR).

As yet, however, there is no single opinion as to the best form of sodium–water steam generator for the fast-reactor nuclear power stations of the immediate future. This is chiefly because of a lack of service experience.

British, French, and Italian specialists are largely inclined toward shell-type steam generators for high-power reactors. Soviet and United States scientists consider that section-type (module) steam generators have sufficient advantages.

Operating experience accumulated in the Soviet Union during the manufacture of the steam generators for the BOR-60 and BN-350 installations, as regards experimental construction, the development of manufacturing technology, assembly, conservation, adjustment, and practical use, has shown that the section-type steam generator will be the best for the immediate future as regards providing the greatest degree of safety together with adequate efficiency (the steam generator being kept in action during leakage). The choice of the number of sections and the number of modules in each section will have to be based on economy as well as safety and efficiency.

In order to realize the advantages of section-type construction it is essential to create an effective system of emergency protection, such as to increase the serviceability of the steam generator very substantially and reduce the danger of leaks.

There is at present a clear need to develop objective criteria for assessing the merits of various steam-generator constructions. These criteria will certainly incorporate the cost of the steam generator and its running expenses.

NATURE AND THERMAL STABILITY OF RADIATION-INDUCED DEFECTS IN ZIRCONIUM HYDRIDE

P. G. Pinchuk, V. N. Bykov,
G. A. Birzhevoi, Yu. V. Alekseev,
A. G. Vakhtin, and V. A. Solov'ev

UDC 621.039.532

The influence of gaseous elements introduced into the lattice of a metal on the character and stability of its radiation-induced defects is being widely studied at the present time [1]. It is interesting to study the nature and annealing of the defects in irradiated interstitial phases having a metalloid sublattice consisting of atoms of gaseous elements. In the present investigation we studied the nature and annealing of defects in zirconium hydride $ZrH_{1.9}$ irradiated at 50°C with an integrated flux of $3.2 \cdot 10^{21}$ neutrons/cm^2 ($1.8 \cdot 10^{20}$ neutrons/cm^2 with energies of over 1 MeV) by measuring the density d, electrical resistance ρ, microhardness H_μ, and lattice constants a and c at 25°C and also the thermal conductivity λ at 100°C (Table 1). In determining the lattice thermal conductivity $\lambda_p = \lambda - (LT/\rho)$ in which the Lorentz constant $L = 2.45 \cdot 10^{-8}$ W·Ω/deg^2, the values of ρ were reduced to a temperature of 100°C. Isochronous annealing was carried out at 50-600°C with a holding period of 1 h, and isothermal annealing at 325°C for up to 1000 min.

Results of the Investigations. Following the irradiation of the hydride, the hydrogen content C_H = H/Zr (determined by the thermal-decomposition method), the type of crystal lattice (face-centered tetragonal), and the microstructure remained constant, but the lattice constant c increased, while the lattice constant a, the degree of tetragonality, and the unit-cell volume all diminished. No vacancy pores or dislocation loops were observed on studying a $ZrH_{1.9}$ sample irradiated with $1.8 \cdot 10^{21}$ neutrons/cm^2 at 50°C under the electron microscope at a magnification of 10^5.

The curves representing the changing properties of samples irradiated with up to $3.2 \cdot 10^{21}$ neutrons/cm^2 during the annealing process (Figs. 1 and 2) were plotted from the experimental points by means of a piecewise polynomial approximation, using segments of cubic parabolas [2], while the recovery spectra of the properties (Fig. 3) were obtained by differentiating the original curves. The increment in electrical resistance found after annealing at 80°C (a single point) was anomalous and was disregarded in the analysis. The concentration of hydrogen vacancies, i.e., free tetrahedral pores (Fig. 2), was determined as $C_V^H = [(2-C_H^*)/2]\ 100\%$ where C_H^* was found from the curves relating the lattice constants a and c to the hydrogen content [3].

TABLE 1. Change in the Properties of the Hydride $ZrH_{1.9}$ as a Result of Irradiation with an Integrated Flux of $3.2 \cdot 10^{21}$ Neutrons/cm^2 at 50°C

State of sample	ρ, $\mu\Omega \cdot$cm	$\frac{\Delta\rho}{\rho}$, %	d, g/cm^2	$\frac{\Delta d}{d}$, %	H_μ, kg/mm^2	$\frac{\Delta H_\mu}{H_\mu}$, %	λ_p, W/m·deg	$\frac{\Delta\lambda_p}{\lambda_p}$, %	$\frac{c}{a}$
Original	35,5	—	5,612	—	147	—	18,6	—	0,895
Irradiated	88,2	148	5,539	—1,31	216	47	4,9	—74	1,909
Mean-square measuring error	0,5	—	0,1	—	4	—	5,5	—	0,1

Translated from Atomnaya Énergiya, Vol. 40, No. 4, pp. 289-292, April, 1976. Original article submitted July 9, 1975.

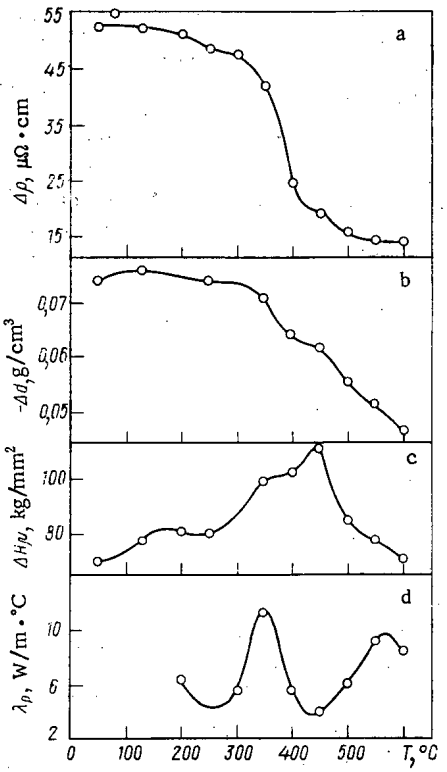

Fig. 1

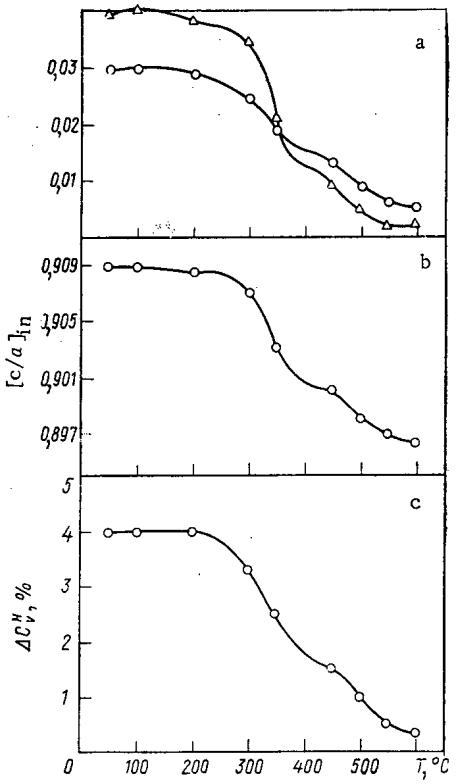

Fig. 2

Fig. 1. Change in the physical properties of the irradiated hydride during isochronous annealing for 1 h (a, b, c): a) resistivity $\Delta\rho = \rho_{irr} - \rho_{nonirr}$ at 25°C; b) hydrostatic density $\Delta d = d_{irr} - d_{nonirr}$; c) microhardness $\Delta H\mu = H\mu_{irr} - H\mu_{nonirr}$; d) phonon component of thermal conductivity at 100°C.

Fig. 2. Recovery of the changes in lattice constants, the degree of tetragonality of the irradiated sample, and the concentration of hydrogen vacancies during the isochronous annealing of the irradiated hydride for 1 h (a, b, c): a) $\Delta a = a_{irr} - a_{nonirr}$; b) $\Delta c = c_{irr} - c_{nonirr}$; ○) Δa, A; △) Δc, Å; c) $\Delta C_v^H = C_{v\,irr}^H - C_{v\,nonirr}^H$.

The curves of Figs. 1-3 exhibit three stages in the recovery of the properties in question (1-3); the corresponding temperature intervals appear in Table 2. At temperatures above 540°C we notice the beginning of the next stage. The activation energy Q characterizing the recovery of the properties was determined by a method based on combined isochronous and isothermal annealings [4] in the case of the electrical resistance, and also by reference to the recovery spectra in that of all the other properties, using the formula $Q = 2.5\ k\Delta(T_a^2/T)$ derived in [5], where T_a is the temperature of maximum recovery rate of the properties in °K; ΔT is the width of the peak at half height; and k is Boltzmann's constant.

Discussion of the Results. Since vacancy pores were formed in the hydride as a result of irradiation at 50°C, while the unit-cell volume diminished, the 1.31% swelling of the samples originally observed must have been due to the accumulation of a corresponding number of isolated zirconium vacancies or small complexes of these (≤10 Å).

It is well known that the tetrahedral pores in the metallic sublattice of zirconium hydride are the nodal points of its hydrogen sublattice. In the hydrogen-saturation of zirconium, the filling of the tetrahedral pores with hydrogen in the ε-region of the Zr — H diagram is accompanied by an increase in lattice tetragonality [3]. Irradiation reduces the tetragonality, and this may be interpreted as being due to the transition of hydrogen from the tetrahedral pores to the octahedral pores or defects in the metallic sublattice. The influence of the latter on the tetragonality cannot be discounted, although in this case the changes in a and c will take place in the same direction. The increase in the tetragonality of the hydride on annealing is equivalent to the filling of the tetrahedral pores on saturating with hydrogen. The change in the tetragonality of the hydride on irradiation appears to be mainly associated with the accumulation of defects in the hydrogen sublattice.

TABLE 2. Characteristics of Various Stages in the Recovery of $ZrH_{1.9}$ Properties

Property	Temperature range, °C	T_a, K	Q, eV	
			by method of [5]	by method of [4]
ρ	59—290	470	0,3	0,2
	290—440	650	1,30	1,53
	440—540	755	1,40	1,55
d	50—270	460	0,3	—
	270—430	645	1,28	—
	430—540	755	1,9	—
$\frac{c}{a}$	250—415	590	0,72	—
	415—540	750	1,32	—
λ_p	310—450	660	1,28	—

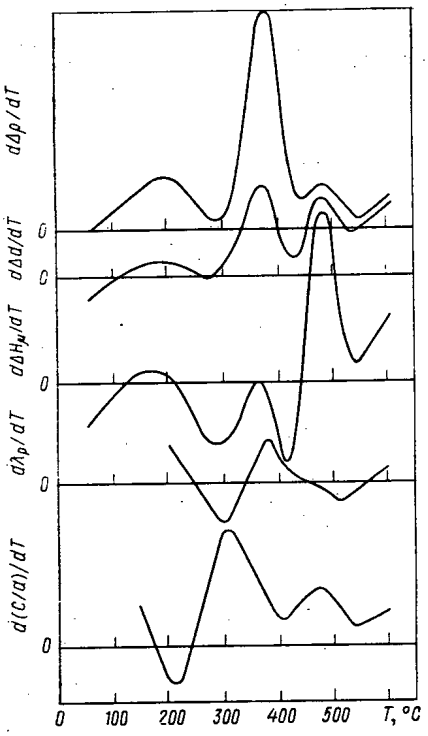

Fig. 3. Recovery spectra of the resistivity, hydrostatic density, and microhardness, the phonon component of the thermal conductivity, and the lattice tetragonality during the isochronous annealing of the irradiated hydride (relative units).

Our investigations into $ZrH_{1.9}$ samples irradiated with a dose of $6.2 \cdot 10^{21}$ neutrons/cm^2 at 480°C showed that the density, microhardness, and lattice thermal conductivity changed by −2.4, +79, and −34% respectively, while the increment in electrical resistance was +32%; the change in the tetragonality lay within the limits of experimental error. A comparison between these results and the data of Table 1 shows that defects in the metallic sublattice are responsible for the changes in density, lattice thermal conductivity, and microhardness, and also for some of the increase in electrical resistance, which is in toto due to defects in each of the sublattices.

The activation energy Q = 0.27 ± 0.05 eV at the first stage in the recovery of the properties agrees closely with the migration energy of interstitial atoms in fcc metals [6]; the activation energy at the second and third stages (1.35 ± 0.1 and 1.54 ± 0.2 eV respectively) agrees with the activation energy of zirconium self-diffusion (1.2-2.2 eV) [7, 8] and that of the diffusion of zirconium in the hydrides $ZrH_{1.6-1.7}$ (1.1-1.7 eV) [9]. A characteristic feature of zirconium is the similarity between the self-diffusion activation energy and the energy of vacancy migration, since the concentration of the latter in the metal is almost always sufficient to guarantee a diffusion process [10]. This is evidently also true of zirconium hydride, especially after irradiation. Assuming that the sequence of the annealing stages for the metal sublattice defects in the hydride is the same as in metals [5, 11], we may conclude that at the second stage the zirconium vacancies migrate, while at the third stage the complexes of defects are annealed. The slight reduction in swelling at the second stage is evidently associated with the fact that most of the migrating vacancies form cavities. The activation energy for the recovery of the lattice tetragonality at the second stage (0.72 eV) coincides with the migration energy of hydrogen [12], while the temperature corresponding to the maximum rate of recovery is in this case 55-70° lower than in the recovery of the other properties. Evidently at the second stage the recovery of the hydrogen sublattice takes place in advance of the annealing of the zirconium vacancies.

At the third stage the complex defects formed in the course of annealing (and possibly during irradiation) vanish. The recovery of the hydrogen sublattice now occurs within the same temperature range, and with the same activation energy, as the annealing of defects in the metallic sublattice. Evidently some of the displaced H atoms occur in complexes of zirconium vacancies and are released when these decompose.

After annealing at 600°C the hydrogen sublattice is completely restored (according to c/a measurements) but changes of 62% in density, 100% in microhardness, and 26% in electrical resistance remain intact.

The microhardness recovery curve of the irradiated hydride exhibits two maxima lying at 180 and 450°C; this is due to the formation of complexes during the migration of point defects similar to those formed in zirconium and Zircaloy after irradiation or quenching [13, 14]. The rise in H_μ close to 200°C is associated with the formation of defect aggregates, while the peak at 450°C is associated with the formation of prismatic dislocation loops $b = (a/3)[11\bar{2}0]$. The agreement between the microhardness peaks found in [13, 14] and in the present investigation suggests that the peak at 180°C corresponding to the first stage in the recovery of the properties is associated with the formation of aggregates of interstitial zirconium atoms, while the peak at 450°C (boundary between the second and third stages) is associated with the formation of vacancy cavities, and not dislocation loops, as in zirconium, since the reduction in swelling associated with the annealing of the vacancies is very insignificant in this region.

The face-centered $ZrH_{1.9}$ lattice with its small degree of tetragonality resembles the lattice of fcc metals, in which five stages of defect annealing are known to occur (I-V). Stage III is often explained as being due to the migration of interstitial atoms and has a maximum at $0.215T_m$; stage IV is due to the migration of vacancies at $0.29\ T_m$; stage V is due to self-diffusion beginning at $0.33T_m$ [11]. If we assume that these same values correspond to the analogous characteristic temperatures of zirconium hydride, then according to Table 2 we obtain $T_m\ ZrH_{1.9} = 2155 \pm 75$ °K which is close to T_m(Zr) = 2125 °K. This agrees with the experimental fact that the melting points of zirconium and zirconium hydride differ by only 7-8% [15].

CONCLUSIONS

1. On irradiating $ZrH_{1.9}$ with an integrated flux of $3.2 \cdot 10^{21}$ neutrons/cm^2 ($1.8 \cdot 10^{20}$ neutrons/cm^2 with energies over 1 MeV) at 50°C, zirconium vacancies accumulate, possibly together with small vacancy complexes (≤ 10 Å) and also defects in the hydrogen sublattice. The defects of the metallic sublattice cause swelling, an increase in hardness, and increased thermal and electrical resistance. The defects of the hydrogen sublattice increase the electrical resistance and reduce the lattice tetragonality.

2. The recovery of the properties on annealing the irradiated hydride at 50-540°C takes place in three stages; the first is associated with the migration of interstitial atoms, the second with vacancy migration, and the third with the annealing of complex defects.

There are two temperature ranges of complex-formation: Close to 180°C aggregates of interstitial atoms are apparently formed, and at 270-450°C vacancy cavities (voids).

3. The recovery of the hydrogen sublattice takes place in the second and third stages.

4. The melting point of zirconium hydride ($T_m = 2155 \pm 75$ °K) may be estimated by comparing the annealing temperatures of similar defects in the hydride and fcc metals.

The authors wish to thank V. I. Shcherbak for great help in the electron-microscope investigations.

LITERATURE CITED

1. D. Norris, Radiat. Effects, 15, No. 1-2, 1 (1972).
2. M. Yu. Orlov, Preprint Physical Power Institute TR-1011 [in Russian], Obninsk (1972).
3. P. Paetz and K. Lücke, Z. Metallkunde, 62, No. 9, 662 (1971).
4. C. Meechan and J. Brinkmen, Phys. Rev., 103, No. 5, 1193 (1956).
5. R. V. Baluffi et al., in: Recovery and Recrystallization of Metals [in Russian], Metallurgiya, Moscow (1966), p. 8.
6. A. C. Damask and J. G. Dienes, Point Defects in Metals, Gordon (1964).
7. V. S. Lyashenko, V. N. Bykov, and L. V. Pavlinov, Fiz. Metal. i Metalloved., 8, No. 3, 362 (1959).
8. E. V. Borisov, in: Metallurgy and Metallography [in Russian], Izd. AN SSSR (1958), p. 291.
9. G. Bentle, Amer. Ceram. Soc., 50, No. 3, 166 (1967).
10. G. Kidson, J. Phys. Chem. Solids, 26, No. 7, 1853 (1965).
11. J. Nihoul, in: Proc. Symp. IAEA Radiation Damage in Reactor Materials, Vol. 1, Vienna (1969); p. 3.
12. P. Paetz and K. Lücke, Z. Metallkunde, 62, No. 9, 657 (1971).
13. D. Lee and E. Koch, J. Nucl. Mater., 50, No. 2, 162 (1974).
14. K. Snowden and K. Veevers, Radiat. Effects, 20, No. 3, 169 (1973).
15. J. Lakner, Chem. Engng. News, 39, 39 (1961).

EMPIRICAL RELATIONSHIP BETWEEN THE SWELLING OF 0Kh16N15M3B STEEL AND IRRADIATION DOSE AND TEMPERATURE

V. N. Bykov, V. D. Dmitriev,
L. G. Kostromin, S. I. Porollo,
and V. I. Shcherbak

UDC 669.15:621.785.3

In this paper we shall present the results of an investigation into the swelling of 0Kh16N15M3B steel used for the fuel element cans in the carbide zone of the BR-5 reactor [1, 2].

For an electron-microscope study of the radiation-induced swelling of 0Kh16N15M3B steel we used fuel-element cans of both working (G-5, G-6, G-17, and G-19) and experimental (ÉP-10, ÉP-11, and ÉP-19) packs. The test samples were cut from various cross sections of the fuel-element cans and irradiated at 430-590°C with a neutron flux of $(0.7\text{-}4.35)\cdot10^{22}$ neutrons/cm^2.

Before irradiation the fuel-element cans were annealed at 950°C for 10 min. A study of the cans in nonirradiated packs made from this steel showed that this kind of heat treatment led to the development of an initial dislocation density of $(4 \pm 2)\cdot10^{10}$ cm^{-2}.

The results of an analysis of the electron micrographs obtained from the test samples are presented in Table 1, together with the condition of irradiation.

A comparison between experimental results obtained for the swelling of materials irradiated with neutrons of varying spectral characteristics is only valid if the numbers of atomic displacements Kt are counted in each particular case. Table 1 gives the values of Kt calculated on the basis of the model proposed in [3]. The neutron spectrum for the BR-5 reactor and the values of the scattering cross sections are taken from [4].

It should be noted that at the present time various research workers use a number of other models for calculating the number of displacements [5-9]. Table 2 shows the K values calculated for the center of the active zone in the BR-5 reactor by some of the most widely employed models. The K calculations carried out for various points of the active zone showed that the main difference in all these models simply amounted to a change in the absolute value of K, while the manner in which the rate of displacement varied over the radius or height of the active zone of the reactor was practically the same for all the models in question. For a relative comparison between the experimental results any of these models may therefore be used.

Experimental observations showed that the relative increase in the volume of the steel was mainly determined by the irradiation dose and temperature. As regards the effect of the rate of creation of the displacements, it was shown in [10] that a 10-times change in the neutron flux intensity had no effect on the swelling of austenitic steels.

The relationship between the volume increment of the material (as a result of porosity development) and the irradiation dose and temperature may be expressed in the following way

$$S = g(T)\, f(Kt),$$

Translated from Atomnaya Énergiya, Vol. 40, No. 4, pp. 293-295, April, 1976. Original article submitted July 16, 1975.

TABLE 1. Conditions Governing the Irradiation and Swelling of 0Kh16N15M3B Steel

No. of pack	Neutron flux · 10^{22}, neutrons/cm^2	Dose, displacements/atoms	Irradiation temp, °C	S_{exp} %	S_{calc} %
ÉP-19	0,7	6,8	430	0,07	0,09
G-17	1,8	18,0	430	0,25	0,27
G-19	2,0	19,9	430	0,30	0,3
ÉP-10	2,05	20,5	430	0,34	0,32
G-6	2,2	21,5	430	0,35	0,35
ÉP-19	0,8	8,6	440	0,10	0,12
ÉP-19	0,9	9,8	442	0,11	0,15
ÉP-19	0,9	9,8	445	0,12	0,15
ÉP-19	0,9	9,8	447	0,12	0,16
ÉP-19	0,9	9,8	450	0,13	0,16
G-19	3,05	28,4	470	0,86	0,82
ÉP-19	0,95	10,0	470	0,18	0,19
G-17	2,95	31,5	475	0,74	0,97
G-19	3,05	28,4	475	0,90	0,83
G-6	3,5	37,4	475	1,29	1,24
G-17	2,95	31,3	480	0,6	0,96
G-6	3,5	37,4	480	1,28	1,25
G-17	2,95	31,3	485	0,8	0,97
G-6	3,5	37,4	485	1,22	1,25
G-17	2,95	31,3	490	0,75	0,96
G-6	3,5	37,4	490	1,14	1,23
G-17	3,6	39,1	500	0,88	1,20
G-17	3,6	39,1	505	0,94	1,15
G-17	2,9	31,0	505	0,78	0,83
G-5	2,55	26,3	505	0,60	0,67
G-6	4,35	46,8	505	1,50	1,45
G-17	3,6	39,1	515	1,10	1,07
ÉP-19	1,35	14,7	520	0,27	0,23
G-5	1,65	15,8	520	0,34	0,25
G-5	2,95	34,3	520	0,87	0,70
G-6	3,5	32,9	520	1,16	0,75
G-6	4,35	46,8	520	0,94	1,13
G-19	3,8	43,6	520	1,40	1,27
G-17	2,90	27,3	530	0,38	0,46
G-17	3,6	39,0	530	1,10	0,80
G-6	4,35	46,8	530	1,20	1,03
ÉP-19	2,2	12,8	535	0,12	0,13
ÉP-19	1,35	14,7	535	0,15	0,16
ÉP-19	1,2	12,8	540	0,11	0,11
G-5	1,65	15,8	540	0,15	0,15
G-17	2,95	31,3	540	0,24	0,42
G-17	3,6	39,1	540	0,42	0,60
G-6	3,5	32,9	540	0,28	0,47
ÉP-10	4,15	44,4	540	0,47	0,72
ÉP-19	1,2	12,8	545	0,12	0,091
ÉP-19	1,35	14,7	545	0,13	0,11
G-17	3,6	39,1	545	0,30	0,51
G-6	4,35	46,8	545	0,67	0,66
ÉP-10	4,15	44,4	550	0,33	0,5
G-17	2,90	27,3	550	0,09	0,24
ÉP-19	1,2	12,8	555	0,09	0,06
G-17	2,90	27,3	555	0,10	0,19
ÉP-19	1,05	12,2	570	0,02	0,02
G-19	2,95	31,3	570	0,07	0,10
G-17	2,95	31,3	580	0,03	0,05
G-6	3,5	32,8	580	0,08	0,06

TABLE 2. Values of K, Kt, and α for Various Models

$K \cdot 10^7$, displacements/atom · sec	No. of displacements corresponding to a neutron flux of 10^{23} neutrons/cm^2 (E > 0,1 MeV)	α	Literature
6,1	132,3	0,92	[5]
5,6	121,2	1,00	[3]
4,3	93,0	1,30	[6]
3,9	84,3	1,44	[7]
3,1	67,1	1,81	[8]
2,8	60,6	2,00	[9]

where g(T) and f(Kt) are functions describing the swelling as a function of temperature and irradiation dose. The problem of finding the empircal dependence of S on T and Kt thus usually amounts to the determination of g(T) and f(Kt).

In the first case we may take one of the following functions:

$$\exp\left(\frac{a_1}{T}+\frac{a_2}{T}\right) \text{ [11]};$$
$$\exp\frac{a_1}{T}+\exp\frac{a_2}{T} \text{ [12]};$$
$$\exp\left(a_1+a_2T+\frac{a_3}{T}\right) \text{ [13]}; \quad (1)$$

TABLE 3. Values of ΔS, ΔS/S, σ_a

Temperature range	Number of points	ΔS	ΔS/S, %	σ_a
430—450	10	0,06	31	0,18
470—490	10	0,15	17	0,11
510—530	11	0,17	20	0,24
535—550	13	0,12	45	0,12
555—580	5	0,15	200	0,20

$$\exp\left(a_1T+\frac{a_2}{T-T_2}+\frac{a_3}{T_2-T}\right),$$

where a_1, a_2, a_3, T_1, and T_2 are parameters of the equation. In our own opinion these functions should give a better idea of the real dependence of S on the irradiation temperature than an expression in the form of polynomials [15].

For the function f(Kt) we may assume a power law of swelling, the power index in turn depending on the irradiation temperature:

$$\begin{matrix}(K,t)^{a_1+a_2/T-\theta+a_3/(T-\theta)^2} & [13,14];\\ (K,t)^{a_1+a_2T}.\end{matrix} \qquad (2)$$

These functions also correspond better to the real dose dependence of the swelling than the linear dependence of S on Kt used in [15].

The choice of functions for describing the swelling is made by a computer analysis of the experimental results indicated in Table 1. Trial of the first and second functions showed that the swelling of 0Kh16N15M3B steel in the temperature and irradiation dose range studied could be reasonably described by the equation

$$S=5.33\cdot10^{-7}(\alpha KT)^{0.19+1.63\cdot10^{-3}T}\times\exp\left(0.0235T-\frac{8.35}{T-630}-\frac{17.82\cdot10^2}{980-T}\right),$$

where T is the temperature in °K.

Since research workers are at present using a number of different models for calculating Kt, the parameter α has been introduced into the empirical equation so as to allow the use of several of these. The values of the conversion factor α corresponding to some of the models most widely used in calculating the numbers of displacements are given in Table 2.

It should be noted that for an irradiation temperature T equal to T_1 or T_2 the swelling of 0Kh16N15M3B steel becomes equal to zero. These temperatures may therefore be taken as the lower and upper limits of swelling.

In analyzing any empirical equation, its reliability and error always have to be considered. Table 3 gives the values of the relative errors (ΔS/S), the confidence intervals (ΔS) for a confidence probability of 0.9, and the mean square errors of the power index associated with the dose (σ_a) for several temperature ranges.

We see from this table that the relative error S depends very considerably on the temperature and is lowest in the range 500 ± 30°C.

Extrapolation of the experimental data to an integrated flux of 10^{23} neutrons/cm^2 (Table 2) shows that the swelling of 0Kh16N15M3B steel may extend to 7-8%.

The authors are deeply indebted to A. A. Proshkin, A. N. Tuzov, and A. G. Kostromin for help in this work.

LITERATURE CITED

1. V. N. Bykov et al., At. Énerg., 34, No. 4, 247 (1973).
2. V. N. Bykov et al., At. Énerg., 36, No. 1, 24 (1974).
3. J. Jenkins, Nucl. Sci. and Engng., 41, 155 (1970).
4. N. N. Aristarkhov, V. V. Bondarenko, and A. I. Voropaev, in: Transactions of the Physical Power Institute [in Russian], Vol. 1, (1967), p. 267.
5. G. Kinchin and R. Pease, Rep. Prog. Phys., 18, 1 (1955).
6. E. Ohmae and B. Hida, J. Nucl. Mater., 42, 85 (1972).
7. D. Dovan, Nucl. Sci. and Engng., 49, 130 (1972).
8. R. Nelson, E. Etherington, and M. Smith, UKAEA, Rep. TRG-2152 (D) (1971).
9. J. Norgett, M. Robinson, and I. Torrens, AERE, Harwell, Rep. TR-494 (1973).
10. E. Bloom and J. Stiegler, ORNL-4480, 76 (1969).

11. T. Claidson, R. Barker, and R. Fish, Nucl. Appl. and Techn., 9, 10 (1970).
12. C. Cox and F. Homan, ibid., p. 317.
13. H. Brager et al., Metal Trans., 2, 1893 (1971).
14. M. Burger, G. Clottes, and I. Leelere, Franco—Soviet Symposium, Paper No. 12, Obninsk (1972).
15. K. Bagley, I. Bramman, and G. Cawthorne, in: Proc. Europ. Conf. on Voids Formed by Irradiation of Reactor Materials, Harwell, BNES (1971), p. 29.

THE ADSORPTION OF KRYPTON AND XENON AT LOW PARTIAL PRESSURES ON INDUSTRIAL SAMPLES OF ACTIVATED CARBON

I. E. Nakhutin, D. V. Ochkin,
S. A. Tret'yak, and A. N. Dekalova

UDC 541.183:661.879

At atomic power stations abroad [1] and in the Soviet Union [2], radiochromatographic systems are used for the purification of off-gas from radioactive contaminants. The main unit of this system is the adsorber, packed with activated carbon, through which the gas flow with the radioactive contaminants is passed. As a result of dynamic adsorption and radioactive decay in the adsorber, a stationary state is established, where the concentration of radioactive gas diminishes toward the outlet of the adsorber [3, 4]. The efficiency of radiochromatographic gas purification equipment depends on the adsorptive capacity of the activated carbon for the inert gases krypton and xenon.

In [5] measurements of the equilibrium adsorption coefficients of krypton and xenon on various grades of activated carbon over a wide temperature range were reported; it was found that one of the best sorbents was SKT carbon [6].

In the present work we measured the equilibrium adsorption coefficients of krypton and xenon from air and helium on nine grades of activated carbon manufactured in the USSR over the temperature range from +20°C to −80°C.

Distribution of the inert gases between the gas phase and the adsorbent was measured in a sealed circulation apparatus by the method of radioactive tracers according to the concentration of the radioactive isotopes ^{85}Kr and ^{133}Xe. The adsorption of the carrier gas was measured by a gravimetric method with a quartz spiral spring balance. Figure 1 shows the temperature dependence of the adsorption coefficient (Γ) of xenon from helium (continuous lines) and from air (broken lines) on four grades of activated carbon. For helium the dependence of $\ln(\Gamma/T)$ on $1/T$ is linear. Gravimetric measurements revealed that the adsorption of helium on activated carbon was insignificant. The calculated values for the differential heat of adsorption of xenon are given in Table 1 (column 3).

TABLE 1. Properties of the Activated Carbons

Grade of activated carbon	Apparent density of the sample, g/cm³	Heat of adsorption of xenon from helium, kcal/mole	Specific surface area by the BET method* m²/g	Micropore volume (Dubinin method, cm³/g
SKT	0,457	—	1,09·10³	0,47
SKT-1A	0,470	—	1,12·10³	0,45
SKT-1B	0,458	—	1,05·10³	0,47
SKT-2A	0,441	8,2	1,17·10³	0,49
SKT-2B	0,498	7,4	1,04·10³	0,44
SKT-3	0,472	7,3	1,10·10³	0,47
SKT-4A	0,418	—	1,33·10³	0,55
SKT-6A	0,388	7,5	1,50·10³	0,66
ART-2	0,428	—	1,13·10³	0,49

*Brunauer — Emmett — Teller method.

Translated from Atomnaya Énergiya, Vol. 40, No. 4, pp. 295-298, April, 1976. Original article submitted June 12, 1975.

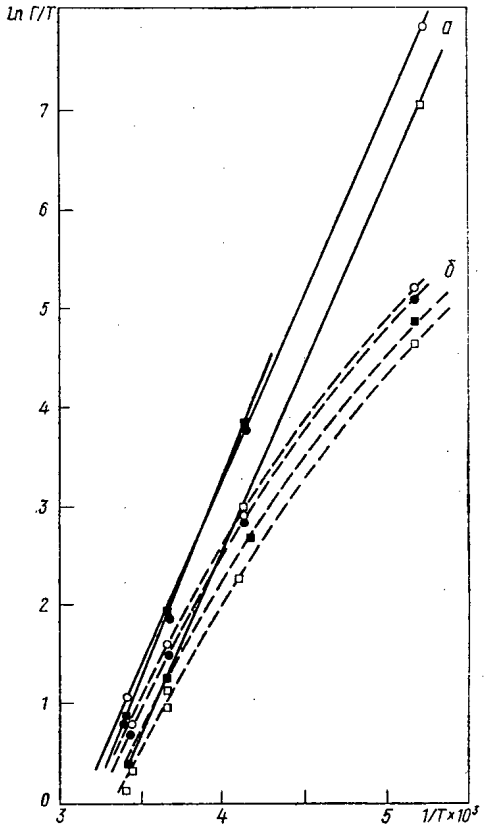

Fig. 1

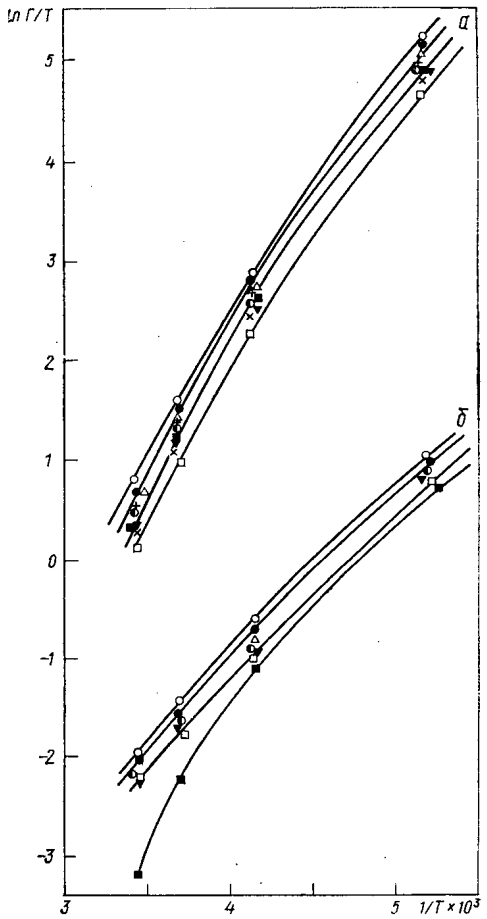

Fig. 2

Fig. 1. Temperature dependence of the reduced adsorption coefficient of xenon from (a) helium and (b) air on activated carbons of grades: ○) SKT-2B; ●) SKT-3; ■) SKT-2A; □) SKT-6A.

Fig. 2. Temperature dependence of the reduced adsorption coefficient of (a) xenon and (b) krypton from air on activated carbons of grades: ○) SKT-2B; ●) SKT-3; △) SKT-1A; +) SKT-1B; ◐) ART-2; ■) SKT-2A; ▼) SKT; ×) SKT-4A; □) SKT-6A.

Figure 1 shows that the gradient of the straight line varies slightly for various grades of activated carbon. The heat of adsorption also varies correspondingly. However, our values essentially exceed the heat of liquefaction of xenon (3.3 kcal/mole [7]). It is probable that these large values of the heat of adsorption of xenon on activated carbon correspond to low filling of the adsorption volume. Even at a temperature of −80°C the maximum quantity of adsorbed xenon in our experiments was no more than $3.8 \cdot 10^{-3}$ neutrons $\cdot cm^3/cm^3$ of carbon.

Figure 2 shows the temperature dependence of the adsorption coefficient of xenon and krypton from air on various grades of activated carbon. For air this dependence is not described by a straight line. This arises because at a different temperature a different quantity of air is adsorbed on activated carbon; this reduces the adsorptive capacity for the inert gases. Figure 3 shows the temperature dependence of the quantity of air that is adsorbed on activated carbon.

We know from [8] that the adsorption isotherms of krypton and xenon on carbonaceous adsorbents have a form similar to the Langmuir isotherm. For these, the isotherm is characterized by a steep rise with constant gradient in the low-pressure region; according to the data of [9], the linearity of the isotherm is maintained for krypton and xenon up to pressures of $4 \cdot 10^{-2}$ mm Hg.

In the adsorption of krypton and xenon from a mixture the presence of the gas macrocomponent can alter the shape of the isotherm. This especially applies to air, the adsorption of which has an appreciable value, as Fig. 3 indicates, unlike helium, which is virtually not adsorbed in this temperature range. For this reason we measured the initial section of the adsorption isotherm of xenon from a mixture with air

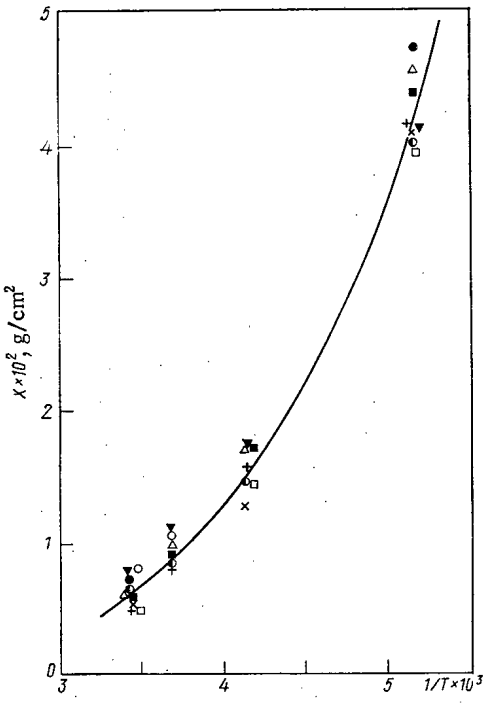

Fig. 3. Adsorption isobar of air on activated carbons of grades: ○) SKT-2B; ●) SKT-3; △) SKT-1A; +) SKT-1B; ◐) ART-2; ■) SKT-2A; ▼) SKT; ×) SKT-4A; □) SKT-6A. X is the quantity of air adsorbed on unit volume of activated carbon, 10^2 g/cm^3.

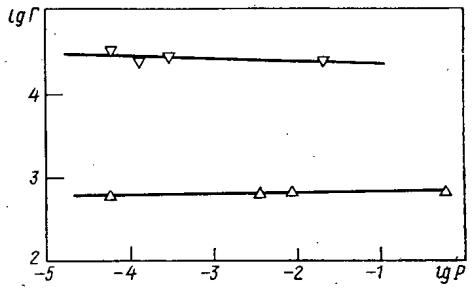

Fig. 4. Adsorption coefficient of xenon from air on activated carbon of grade SKT-2B as a function of partial pressure at ▽) 191°K and △) 294°K.

(740 mm Hg) on SKT-2B activated carbon at two temperatures. Figure 4 presents the adsorption coefficient as a function of the partial pressure of xenon. At 191°K we observed a small reduction in the adsorption coefficient as the partial pressure of xenon increased, but for practical purposes this can be ignored.

When selecting an adsorbent it is not always possible to measure its adsorptive capacity for a particular substance. Usually to compare adsorbents more general properties are used (specific surface area, micropore and transitional pore volume, pore size distribution), which are measured by standard methods, using standard substances, in particular nitrogen.

In the present work we measured the adsorption isotherms of nitrogen at its boiling point on all the samples of activated carbon, and from these results we calculated the specific surface area by the BET method [8] and the micropore volume by Dubinin's method [7] (see Table 1, columns 4 and 5).

We calculated the specific surface area by the BET method assuming monomolecular filling of the energetically uniform surface. Starting from this we could expect to observe a proportional relationship between the values of specific surface area and the adsorption for different substances. However, we did not observe this correlation (see Table 1, and Figs. 1 and 2) with the samples of activated carbon in our experiments, at least in the region of low partial pressures.

In the theory of the volume filling of pores the micropore volume is used as a parameter characterizing the adsorptive capacity of the adsorbent. As Table 1 shows, the micropore volumes of activated carbon, measured with nitrogen, and calculated from Dubinin's theory of volume filling [7, 10], also do not provide a basis for any conclusions on the cause of the adsorption of krypton and xenon at low partial pressures. Consequently the conventional properties — specific surface area and micropore volume — cannot be used to estimate the adsorptive capacity of activated carbons for krypton and xenon at low partial pressures.

It is of interest to observe that the ranking of carbons by apparent density corresponds to the ranking by adsorption coefficient. However, we find this rather difficult to explain.

LITERATURE CITED

1. F. Schumann, Report SZS-133, Berlin, East Germany (1972).
2. E. K. Yakshin et al., At. Énerg., 34, No. 4, 285 (1973).
3. I. E. Nakhutin and D. V. Ochkin, Inzh. Fiz. Zh., 9, No. 1, 112 (1965).
4. I. E. Nakhutin, D. V. Ochkin, and Yu. V. Linde, Zh. Fiz. Khim., 43, No. 7, 1811 (1969).
5. A. M. Trofimov and A. M. Pankov, Radiokhimiya, 7, No. 3, 293 (1965).
6. A. G. Cherepov, B. R. Keier, and T. G. Plachenov, in: Preparation, Structure, and Properties of Sorbents [in Russian], Vol. 1, Trudy Leningradskogo Tekhnologicheskogo Instituta im. Lensoveta, Leningrad (1971), p. 39.
7. S. J. Gregg and K. S. W. Sing, Adsorption, Surface Area, and Porosity, Academic Press, New York — London (1967).
8. S. Brunauer, The Adsorption of Gases and Vapours, Oxford University Press, London (1945).
9. K. Chackett and D. Tuck, Trans. Faraday Soc., 53, No. 12, 1652 (1957).
10. M. M. Dubinin, in: Physical Adsorption from Multicomponent Phases, Proceedings of the 2nd All-Union Conference on Theoretical Problems of Adsorption [in Russian], Nauka, Moscow (1972), p. 41.

TOTAL NEUTRON CROSS SECTION AND NEUTRON RESONANCE PARAMETERS OF ^{243}Am IN THE ENERGY RANGE 0.4-35 eV

T. S. Belanova, A. G. Kolesov,
V. A. Poruchikov, G. A. Timofeev,
S. M. Kalebin, V. S. Artamonov,
and R. N. Ivanov

UDC 621.039.556

One of the main isotopes in the production of ^{252}Cf is ^{243}Am and it is therefore necessary to know its neutron cross section with great accuracy. Information about the neutron cross section of ^{243}Am is of great scientific value in addition to its applied usefulness. It is well known that the data for the total neutron cross section and resonance parameters of this isotope were mainly obtained in 1970-1972. The present paper is the result of ^{243}Am transmission measurements by the time-of-flight method which began in 1972 at the SM-2 reactor.

The neutron burst was shaped by a selector with three synchronously revolving rotors suspended in a magnetic field [1]. A bank of helium counters served as a neutron detector. The measurements were made with a 4096-channel analyzer. The best resolution of the spectrometer over a 92-m flight path was 70 nsec/m.

Measurements and Results. The target was prepared from a stable dehydrated powder of americium oxide with a known oxygen content (AmO_2). To achieve this, the powder was heated in an oxygen atmosphere

TABLE 1. Neutron Resonance Parameters for ^{243}Am

E_0, eV	Γ, meV	$2g\Gamma_n$, meV	E_0, eV	Γ, meV	$2g\Gamma_n$, meV
0,416±0,003	39±2	0,00084±0,00005	16,56±0,07	27±7	0,174±0,005
0,977±0,004	37±2	0,0134±0,0003	17,84±0,07	35±8	0,210±0,007
1,355±0,004	56±1	0,890±0,007	18,14±0,07	27±15	0,046±0,007
1,744±0,005	39±1	0,208±0,002	19,50±0,07	27±10	0,193±0,007
3,134±0,009	47±3	0,012±0,003	19,88±0,07	40±20	0,085±0,006
3,424±0,009	45±2	0,253±0,008	20,94±0,07	29±15	0,54±0,18
3,844±0,009	22±5	0,009±0,001	21,09±0,07	16±10	0,86±0,22
5,120±0,012	63±2	0,260±0,006	21,85±0,08	27	0,14±0,02
6,551±0,015	50±3	0,794±0,044	22,01±0,08	—	—
7,063±0,017	46±3	0,072±0,011	22,59±0,09	33	1,00±0,60
7,86±0,02	36±9	1,580±0,130	22,72±0,09	19	0,65±0,50
8,39±0,02	40±2	0,010±0,002	24,39±0,09	22	0,73±0,02
8,77±0,02	46±2	0,113±0,002	25,38±0,10	40	0,14±0,02
9,32±0,02	43±2	0,133±0,002	26,30±0,10	31	0,06±0,01
10,31±0,03	47±2	0,433±0,007	26,75±0,10	—	1,16±0,03
10,87±0,04	—	0,013±0,002	27,34±0,11	—	0,43±0,02
11,27±0,04	49±2	0,267±0,003	28,73±0,12 *	—	0,97±0,12
11,68±0,05	35±4	0,094±0,002	29,29±0,12 *	—	0,68±0,15
12,12±0,06	41±3	0,152±0,003	30,12±0,13 *	—	0,49±0,20
12,87±0,06	43±4	2,20±0,20	31,06±0,13 *	—	0,7±0,15
13,15±0,06	45±5	1,00±0,08	31,49±0,13 *	—	0,12±0,05
15,12±0,07	33±15	0,070±0,007	32,43±0,14 *	—	0,88±0,15
15,39±0,07	37±6	0,36±0,08	33,19±0,14 *	—	1,9±0,2
16,20±0,07	39±3	0,518±0,009	33,92±0,14 *	—	0,8±0,1

* Area method, with $T_j = 30$ MeV.

Translated from Atomnaya Énergiya, Vol. 40, No. 4, pp. 298-303, April, 1976. Original article submitted June 23, 1975; revision submitted August 6, 1975.

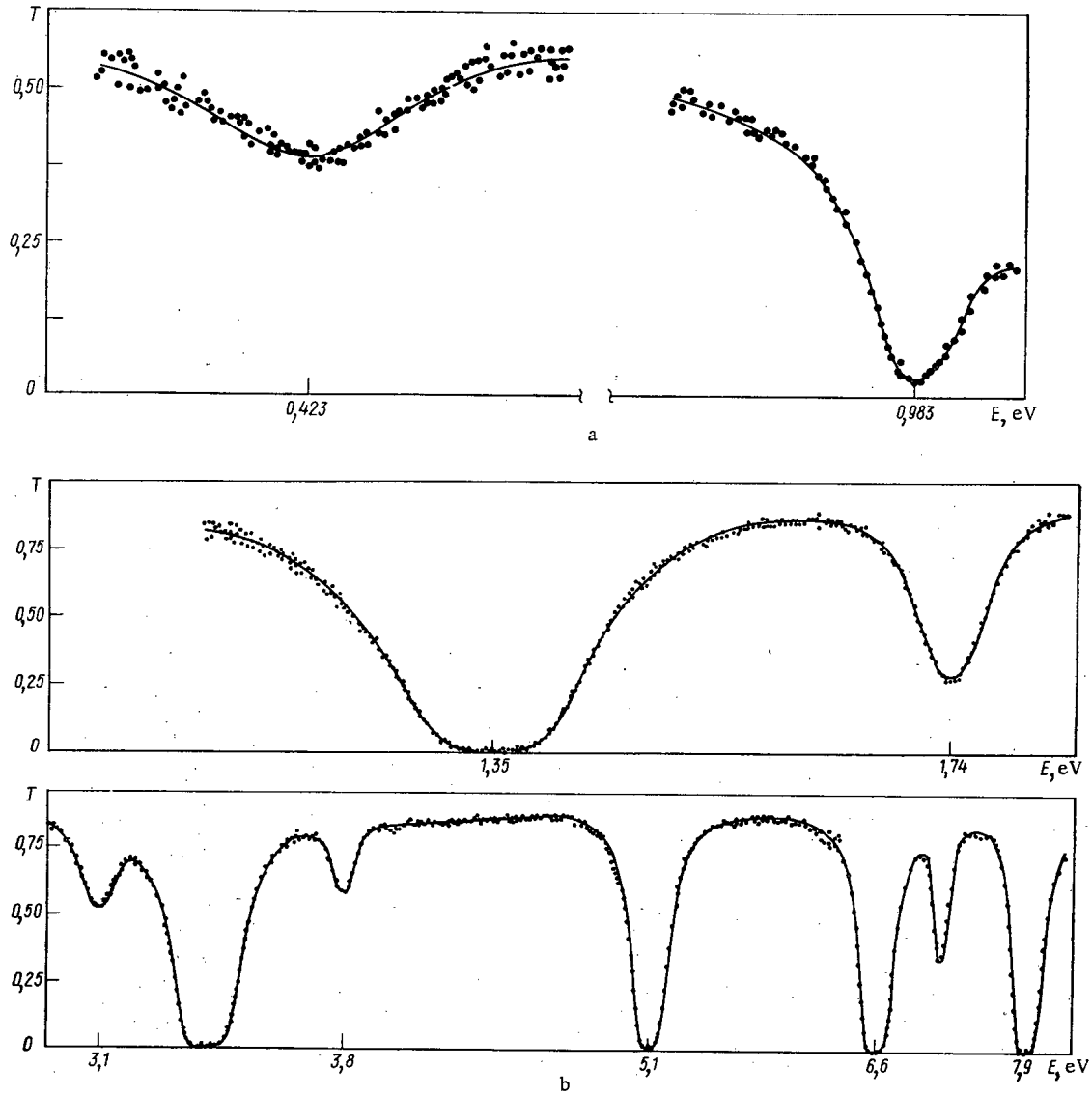

Fig. 1

for 3 h at 400°C. Following this, 266 mg of powder were poured into an aluminum capsule with a wall thickness of 1 mm, filling a volume 0.8 × 8.0 × 14.0 mm in size. The target was remotely inserted in the neutron beam in such a way that transmission could be measured for thicknesses of 0.8 and 14.0 mm, which correspond to $0.45 \cdot 10^{21}$ and $0.79 \cdot 10^{22}$ atom/cm^2. The isotopic composition of the sample was the following: ^{243}Am, 96.60%; ^{241}Am, 3.32%; ^{244}Cm, 0.08%. The sample contained 79.8% americium.

The statistical accuracy of the measurements was 0.5-1.5% and the neutron background varied from 0.7 to 4.0%. The transmission data were corrected for neutron scattering by oxygen (3% in the thick sample) and for the contribution of ^{241}Am to the transmission of ^{243}Am. Using resonance parameters obtained earlier for ^{241}Am [2], the transmission was calculated for the 3.32% content of ^{241}Am in the test sample. The energy dependence of the transmission T of ^{243}Am after the introduction of the specified corrections is shown in Fig. 1 for neutrons in the range 0.4-35 eV. Below 26 eV, the resolution of the device made it possible to calculate neutron resonance parameters by the shape method in accordance with the one-level Breit—Wigner formula; above 26 eV, the area method was used with the radiation width assumed to be 30 meV. The calculations were performed on a BÉSM-6 computer [2] with resultant determination of the resonance position E_0, the neutron width $2g\Gamma_n$, and the total width Γ (Table 1). In addition to statistical errors, the calculations took into account errors associated with the determination of the shape of the resolution function and with the distortion of ^{243}Am transmission by the ^{241}Am impurity.

There are two levels at energies of 21.0 and 22.7 eV on the transmission curve. In the process of fitting the experimental and theoretical transmission curves, it was established that these levels were

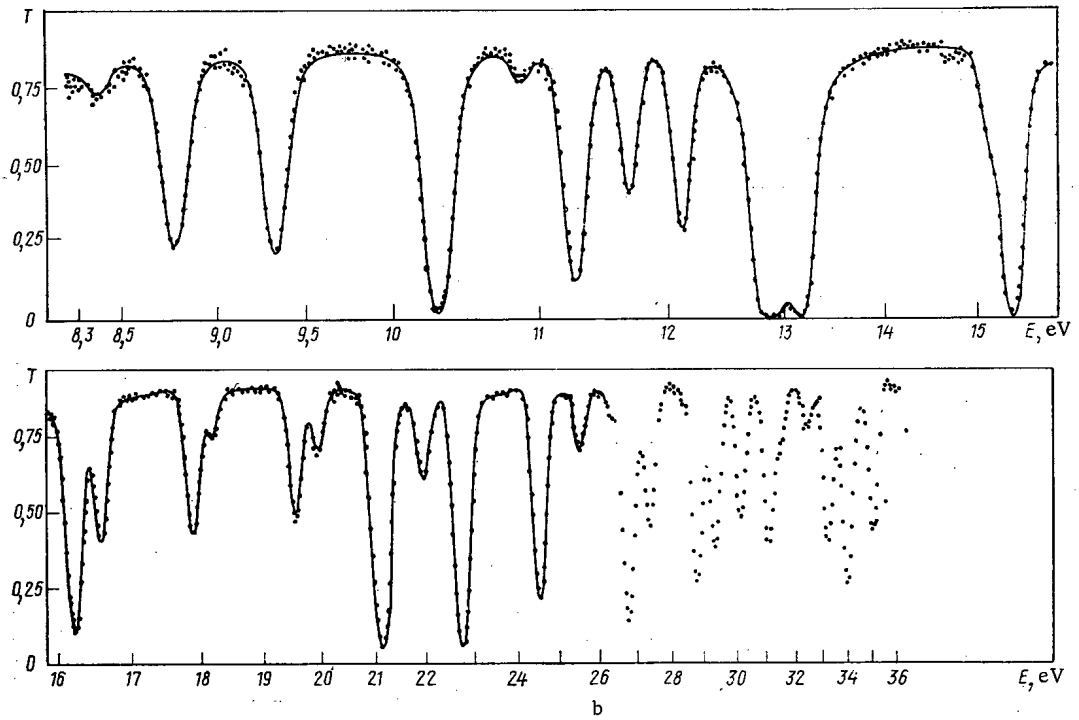

Fig. 1. Transmission of ^{243}Am: ——) theoretical calculation by shape method; •) experiment; a) to 1 eV, b) 1-8 eV, c) 8-35 eV.

TABLE 2. Values of $\bar{D}$ and S_0 Obtained for ^{243}Am

$S_0 \cdot 10^{-4}$	$\bar{D}$, eV	E_0, eV	Reference
0,84±0,25	1,37	0—15	[7]
0,96±0,10	0,67±0,06	0—50	[8]
0,89±0,19	0,71±0,10	0,4—35	this work

unresolved doublets. The first level consists of resonances at 20.94 and 21.09 eV, and the second level of resonances at 22.59 and 22.72 eV. Resonance parameters were calculated for all four levels. A similar situation was pointed out in [3]. The theoretical transmission curve shown in Fig. 1 as the solid curve was calculated from the neutron resonance parameters. The agreement of the theoretical and experimental transmission curves provides evidence for the correctness of the adjustment of ^{243}Am transmission for the ^{241}Am impurity.

The presence of a 20% admixture of inactive elements in the sample made it impossible to determine the potential scattering cross section σ_p. Such measurements are being made at the present time with a highly purified sample of ^{243}Am. It should be noted that there is no information about σ_p in published data for this isotope.

Discussion of Results. The values obtained for resonance parameters are basically in agreement with published data [3-8] although there are cases of considerable divergence of comparable quantities.

The neutron width of the level at 13.15 eV obtained in this work, while agreeing with $2g\Gamma_n = 0.79$ meV [7], is considerably lower than the values 1.33 and 1.45 meV [3, 4]. At 22.59 eV, the neutron width of 0.52 meV is two times smaller, and at 22.72 eV ($2g\Gamma_n = 1.33$ meV) [3] it is two times greater than the corresponding neutron widths obtained in the present work for these levels (see Table 1).

We did not confirm the existence of a weak level at 22.011 eV [8], which was obtained with a sample twice as "thin" as the sample used in this work. The calculated value of the total resonance integral was I = 1740 ± 150 b.

Information about resonance parameters in the energy range 0.4-35 eV made it possible to evaluate certain statistical properties of the ^{243}Am nucleus. We calculated the average level spacing $\bar{D} = 0.71 \pm 0.10$ eV, the mean reduced neutron width $2g\bar{\Gamma}_n^0 = 0.127$ meV, and the strength function $S_0 = 0.89 \pm 0.19 \cdot 10^{-4}$. The integral distribution of reduced neutron widths is given in Fig. 2. Analysis showed [9, 10] that it corresponds to a Porter — Thomas distribution with number of degrees of freedom $\nu = 1.01 \pm 0.24$. The best

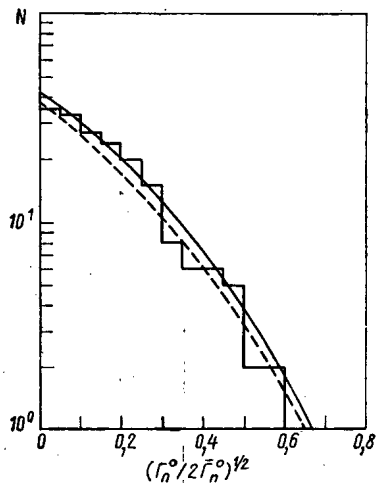

Fig. 2

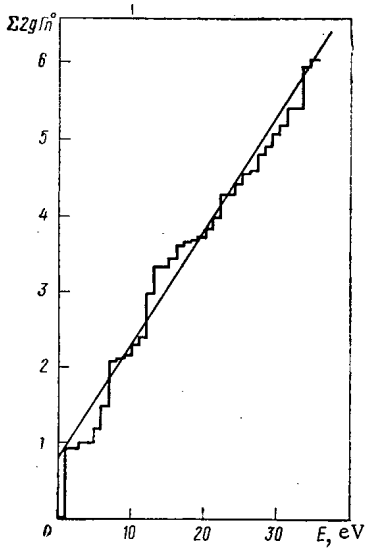

Fig. 3

Fig. 2. Integral distribution of reduced neutron widths for ^{243}Am (N is number of resonances): ——) Porter — Thomas distribution for one degree of freedom normalized to 55 levels; — — — —) same distribution normalized to 48 levels; histogram is experimental distribution.

Fig. 3. Sum of reduced neutron widths $\Sigma\, 2g\Gamma_n^0$ as a function of neutron energy. The strength function $\bar{\Gamma}_n^0/\bar{D}$ is given by the slope of the line ($S_0 = 0.96 \cdot 10^{-4}$).

agreement of this distribution with the experimental histogram (solid line in Fig. 2) was obtained for a neutron-level number n = 55 and for $2g\bar{\Gamma}_n^0 = 0.118$ meV. This indicates that one should assume the loss of seven weak levels below 35 eV. With the inclusion of these levels, $\bar{D} = 0.62$ eV and $S_0 = 0.95 \cdot 10^{-4}$, which is in good agreement with S_0 determined directly from the experimental data (including also $S_0 = 0.96 \cdot 10^{-4}$ obtained from the slope of the line in Fig. 3). Values of $\bar{D}$ and S_0 obtained by various authors are compared in Table 2.

The overestimate of the value of $\bar{D}$ in [7] is explained by the fact that a total of 12 levels was observed in the energy range 0-15 eV. Subsequent measurements showed that there were 21 resonances in the ^{243}Am nucleus in that energy range [4, 5, 8]. Figure 4 shows the distribution of spacing between neutron levels; the solid curve describes the Wigner distribution for a single system of levels [11] and the dashed curve is the superposition of two distributions, while the histogram gives the experimental distribution. It is clear from the figure that the Wigner distribution for a single system of levels fits the histogram better despite the fact that two systems of levels should be realized in the ^{243}Am nucleus. If one is not seeking deeper physical causes for this,* the existing situation may simply be the consequence of insufficient resolution of closely located levels or loss of weak resonances.

The experimental data were analyzed for long-range correlation in accordance with the Δ_3 test for an orthogonal ensemble proposed by Dyson and Mehta [12]. An experimental value $\Delta_3 = 0.54$ was determined and theoretical values $\Delta_3 = 0.77 \pm 0.22$ for two systems of levels and $\Delta_3 = 0.39 \pm 0.11$ for a single system of levels. The agreement between experimental and theoretical values of Δ_3 verifies the correctness of the Dyson — Mehta theory if a single system of levels is realized in the nucleus. In the present case, a comparison of the values of Δ_3 does not permit one to arrive at any conclusion whatever about the levels in the ^{243}Am nucleus.

Figure 5 shows the results of the σ(K) test — the correlation of the position of two levels between which there are K levels.

The authors are grateful to Yu. S. Zamyatnin and Yu. G. Abov for interest in the work and valuable

*It has been suggested [13] that there is a "repulsion" of levels with different spin values.

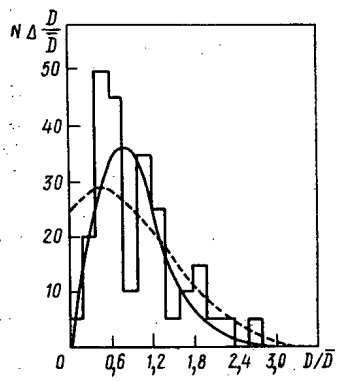

Fig. 4.

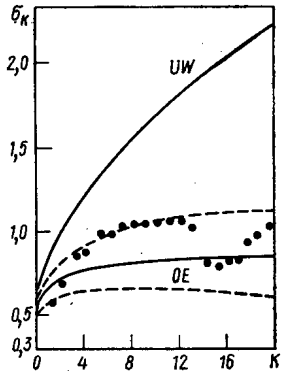

Fig. 5.

Fig. 4. Distribution of spacing between levels in ^{243}Am (N, number of resonances; D, spacing between them).

Fig. 5. Correlation $\sigma(K)$ of positions of two levels between which there are K levels for ^{243}Am: UW, DE) theoretical values of $\sigma(K)$ for uncorrelated Wigner distribution and for an orthogonal ensemble; •) experiment; — — — —) limits of statistical spread of $\sigma(K)$ for 50 levels.

discussions, and also to V. A. Safonov, S. I. Babin, S. N. Nikol'skii, T. V. Denisova, V. Ya. Gabeskiriya, V. M. Nikolaev, and G. V. Kuznetsov, who provided assistance in various stages of the work.

LITERATURE CITED

1. S. M. Kalebin et al., Proceedings Neutron Physics Conference [in Russian], Pt. II, Naukova Dumka, Kiev (1972), p. 267.
2. T. S. Belanova et al., At. Énerg., 38, No. 1, 29 (1975).
3. O. Simpson et al., Report ANCR-1060 (1972).
4. J. Berreth et al., Rep. IN-1407, USAEC (1970), p. 66.
5. O. Simpson et al., Bull. Amer. Phys. Soc., 15, 569 (1970).
6. O. Simpson et al., Rep. IN-1407, USAEC (1970), p. 72; Nucl. Sci. Engng., 55, 273 (1974).
7. R. Cote et al., Phys. Rev., 114, 505 (1959).
8. BNL-325, Third Ed. (1973).
9. C. Porter and R. Thomas, Phys. Rev., 104, 483 (1956).
10. H. Sharma and Ray. Ram, Progr. Theor. Phys., 51, 1642 (1974).
11. L. Lynn, The Theory of Neutron Resonance Reactions, Clarendon Press, Oxford (1968).
12. F. Dyson and M. Mehta, J. Mathem. Phys., 4, 701 (1963).
13. E. Wigner, in: Statistical Properties of Nuclei, J. Garg (editor), New York — London (1972), p. 7.

TOTAL NEUTRON CROSS SECTION AND NEUTRON RESONANCE PARAMETERS OF ^{241}AM IN THE ENERGY RANGE 0.004-30 eV

S. M. Kalebin, V. S. Artamonov, R. N. Ivanov, G. V. Pukolaine, T. S. Belanova, A. G. Kolesov, and V. A. Safonov

UDC 621.039.556

The energy dependence of the total neutron cross section σ_t of ^{241}Am was investigated in the energy range up to 8 eV by the time-of-flight method at the heavy-water reactor of the Institute of Theoretical and Experimental Physics. The best resolution of the spectrometer was 14 nsec/m [1]. Similar studies were made at the SM-2 reactor at NIIAR [2] for neutron energies of 8 eV and above. The measurements were made with identical neutron selectors and detectors [1, 3]. In both experiments, the same sample with thicknesses of $0.63 \cdot 10^{21}$ and $3.3 \cdot 10^{21}$ atom/cm^2 was used which contained 99.99% of the isotope ^{241}Am. The experimental conditions and the procedure for analysis of the experimental data were identical at both reactors [2].

Results of Measurements. The energy dependence of the total neutron cross section is shown in Fig. 1. Figure 2 shows the dependence of the experimentally obtained transmission T on neutron energy. The high purity of the americium sample and its monoisotopic composition made it possible to assert that all 13 levels observed in the energy range 0.004-8 eV belong to the nucleus ^{241}Am. The spectrometer resolution made it possible to calculate the parameters for these resonances by the shape method in accordance with the one-level Breit – Wigner formula. The resultant parameters were used to calculate a theoretical transmission curve which is shown in Fig. 2 as a solid curve. A negative level at 0.425 eV was introduced in order to match the theoretical value of T with the experimental value in the thermal energy region (see Fig. 2).

TABLE 1. Neutron Resonance Parameters for ^{241}Am

E_0, eV	Γ, meV	$2g\Gamma_n$, meV	E_0, eV	Γ, meV	$2g\Gamma_n$, meV
—0,425	40	$2g\Gamma_n^0 = 1,0$	14,66±0,07	44±5	2,30±0,13
0,306±0,002	45±1	0,0556±0,0004	15,66±0,07	32±12	0,215±0,012
0,573±0,004	43±1	0,0928±0,0016	16,35±0,07	44±5	1,185±0,033
1,268±0,004	41±2	0,330±0,016	16,81±0,07	31±8	0,575±0,020
1,916±0,005	46±2	0,107±0,002	17,69±0,07	40±10	0,373±0,016
2,538±0,008	41±2	0,070±0,001	18,09±0,07	—	—
2,581±0,009	38±2	0,150±0,004	19,39±0,07	37±12	0,182±0,016
3,956±0,009	28±3	0,230±0,008	20,28±0,07	—	0,050±0,010
4,947±0,010	31±5	0,176±0,005	20,84±0,08	—	0,064±0,011
5,390±0,012	38±7	0,844±0,114	21,72±0,08	—	0,067±0,012
6,100±0,013	42±14	0,116±0,005	22,74±0,09	—	0,070±0,012
6,650±0,015	—	0,05±0,03	23,08±0,09	—	0,39±0,05
7,53±0,02	—	0,07±0,04	23,33±0,09	—	0,40±0,05
8,17±0,02	42±5	0,096±0,004	24,17±0,09	—	1,27±0,08
9,11±0,02	48±3	0,358±0,006	25,05±0,10	—	—
9,84±0,03	48±3	0,370±0,007	25,60±0,10	—	1,21±0,08
10,11±0,03	—	0,025±0,004	26,50±0,10	—	—
10,39±0,03	45±4	0,294±0,007	26,67±0,10	—	—
10,99±0,04	52±4	0,382±0,008	27,52±0,10	—	—
11,58±0,05	—	0,018±0,003	27,65±0,10	—	—
12,06±0,06	—	0,007±0,003	28,31±0,11	—	0,40
12,86±0,06	44±5	0,116±0,009	28,82±0,12	—	0,35
13,80±0,06	—	0,050±0,015	29,43±0,12	—	0,61
14,32±0,06	—	0,066±0,012			

Translated from Atomnaya Énergiya, Vol. 40, No. 4, pp. 303-307, April, 1976. Original article submitted June 25, 1975; revision submitted August 6, 1975.

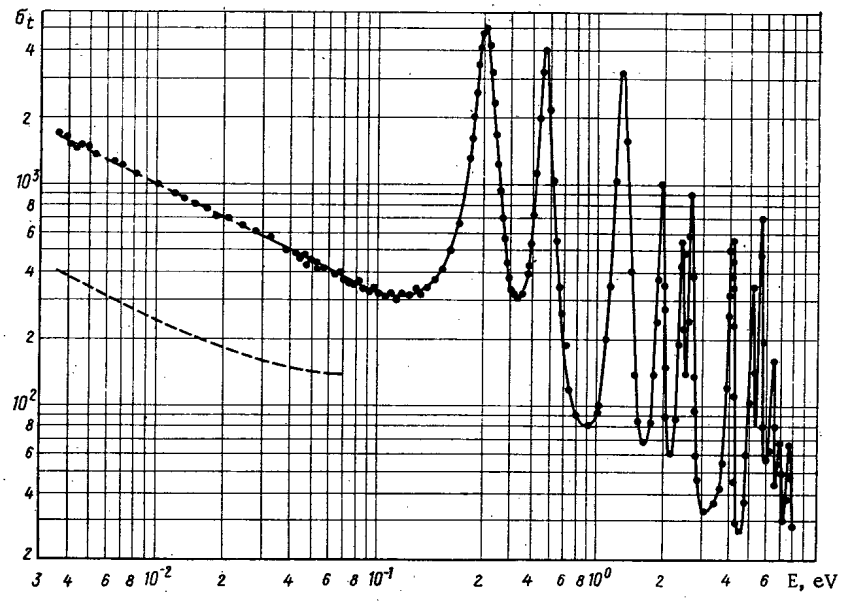

Fig. 1. Total neutron cross section of ^{241}Am from 0.004 to 8 eV; •) experimental points; ——) theoretical curve obtained from the resonance parameters in Table 1 with the inclusion of a negative level at E = 0.425 eV; — — — —) without inclusion of the negative level at 0.425 eV.

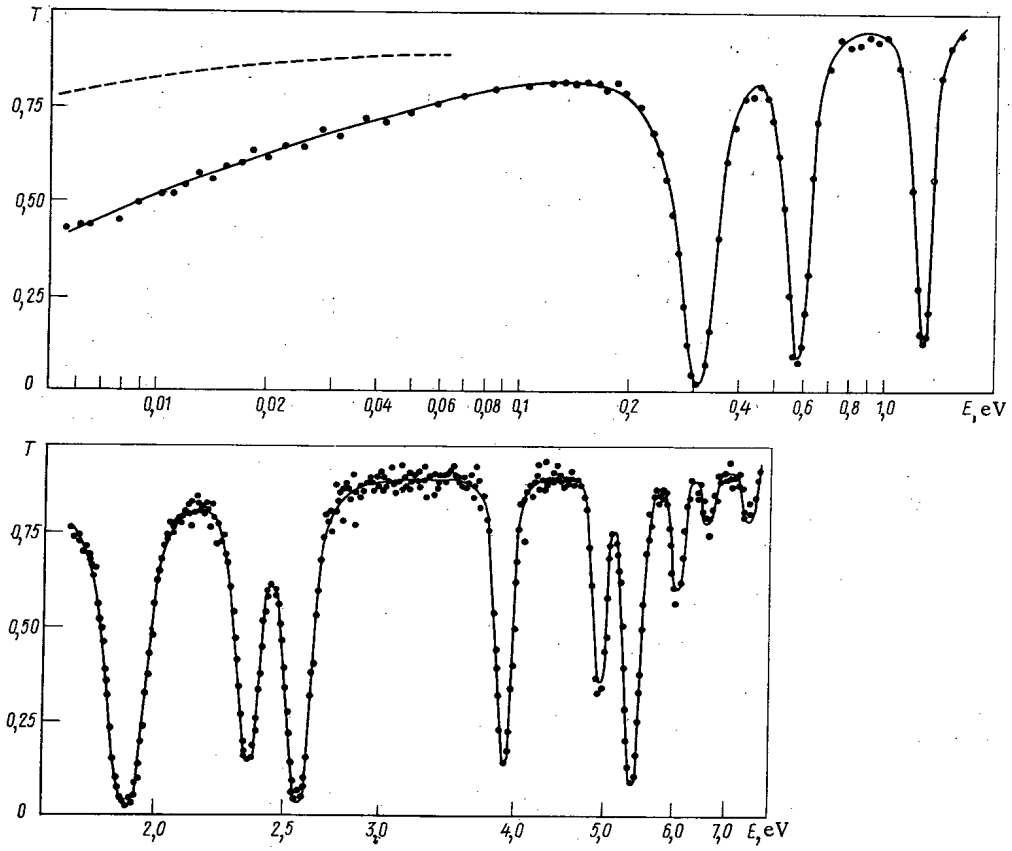

Fig. 2. Transmission of ^{241}Am in the range 0.004-8 eV: •) experiment; ——— and — — — —) theoretical calculations by the shape method respectively with and without the negative level at 0.425 eV.

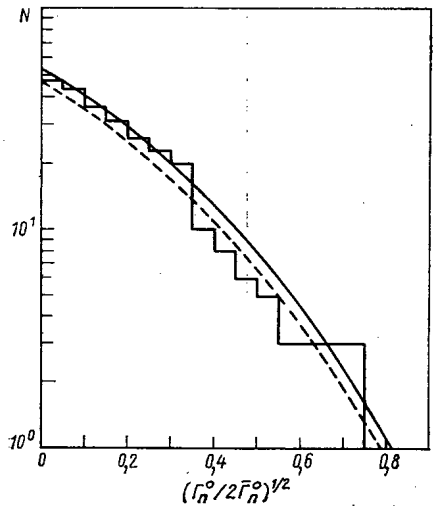

Fig. 3

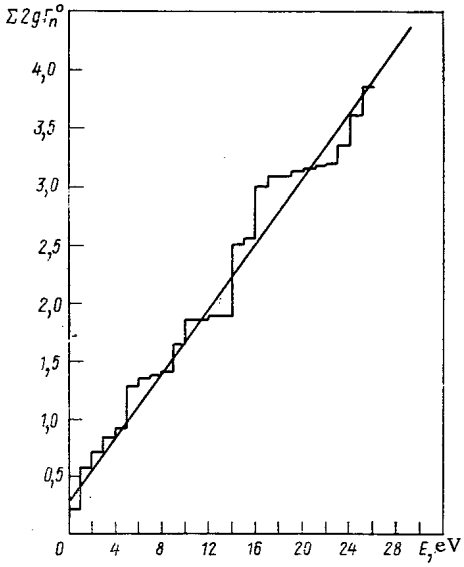

Fig. 4

Fig. 3. Integral distribution of reduced neutron widths in ^{241}Am (N, number of resonances): ——) Porter — Thomas distribution for a single degree of freedom normalized to 44 resonances; — — — —) the same distribution normalized to 38 resonances; histogram is experimental distribution.

Fig. 4. Sum of reduced neutron widths $\Sigma 2g\Gamma_n^0$ as a function of neutron energy. The strength function $\bar{\Gamma}_n^0/\bar{D}$ is given by the slope of the line ($S_0 = 0.86 \cdot 10^{-4}$).

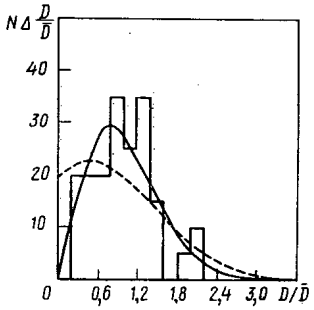

Fig. 5. Distribution of spacing between levels in ^{241}Am (N, number of resonances; D, spacing between them).

Table 1 gives the level position E_0, the values of the neutron width $2g\Gamma_n$, and the total width Γ for 45 resonances, including resonances measured previously by the authors [2]. Two levels at 2.538 and 6.65 eV were found for the first time in ^{241}Am.

Discussion of Results. The values of the resonance parameters given in Table 1 basically agree with other published data [4-9]. We point out the discrepancies.

1. A level at 1.68 eV was obtained in a study of fission of the nucleus ^{241}Am [4, 5]; data on resonance parameters for it were not presented. This level was found neither in the present work nor in other studies of the total neutron cross section of ^{241}Am [4, 6, 7].

2. Levels at 2.36 and 4.40 eV with respective neutron widths of 0.080 and 0.027 meV were given in [4, 6]. We failed to observe these levels in the present work although resonances with narrower neutron widths were recorded.

3. Strong levels at 6.78 and 7.97 eV with neutron widths of 0.23 and 0.79 meV respectively [4, 7] were also not observed. Judging from the values of $2g\Gamma_n$, these levels should appear considerably more clearly than neighboring levels which were observed (see Table 1).

4. With respect to the previously published data [2], one should add that only a single level was found at 15.66 ± 0.07 eV with $2g\Gamma_n = 0.215$ meV where, according to the data in [7], two very close levels were resolved at 15.60 ± 0.05 and 15.73 ± 0.05 eV having the respective neutron widths 0.16 ± 0.10 and 0.17 ± 0.10 meV. However, only a single resonance at 15.8 eV with $2g\Gamma_n = 0.40$ meV was observed in this energy range in [6]. Analysis of the neutron width of the level at 15.66 eV does not permit consideration of it as a double level with the parameters specified in [7].

5. The existence of a resonance at 16.02 eV, which has the high value $2g\Gamma_n = 0.14$ meV [7] and therefore should have been noted in [2], was not confirmed.

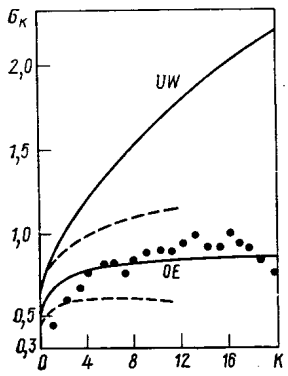

Fig. 6. Correlation $\sigma(K)$ of the positions of two levels between which there are K levels in ^{241}Am: UW, OE) theoretical values of $\sigma(K)$ for uncorrelated Wigner distribution and orthogonal ensemble; •) experiment; ———) limit of statistical spread of σ (K) for 30 levels.

What has been said above indicates that levels at the energies 2.36, 4.40, 6.78, 7.97, and 16.02 eV were erroneously assigned to the nucleus ^{241}Am. A capture cross section $\sigma_c = 624 \pm 20$ b and a total cross section $\sigma_t = 640 \pm 20$ b were measured at the thermal point. In addition, a total resonance integral I = 1650 ± 120 b was calculated, which is in good agreement with the value I = 1498 ± 120 b [4].

Information about the resonance parameters of ^{241}Am in the energy range 0.025-26 eV made it possible to evaluate certain statistical properties of this nucleus. We calculated the average level spacing $\bar{D} = 0.67 \pm 0.10$ eV, the average reduced neutron width $2g\bar{\Gamma}_n^0 = 0.102$ meV, and the strength function $S_0 = (0.76 \pm 0.18) \cdot 10^{-4}$. The integral distribution of the reduced neutron widths is shown in Fig. 3. Analysis of the distribution [10, 11] showed that it corresponded to a Porter — Thomas distribution with number of degrees of freedom $\nu = 1.07 \pm 0.23$. Best agreement of this distribution with the experimental histogram (solid line in Fig. 3) was obtained for a neutron-level number n = 44 and $2g\bar{\Gamma}_n^0 = 0.096$ meV. This indicates that one should assume the loss of six weak levels below 26 eV. With these resonances included, $\bar{D} = 0.6$ eV and $S_0 = 0.80 \cdot 10^{-4}$, which is in good agreement with S_0 determined directly from experimental data (including also $S_0 = 0.86 \cdot 10^{-4}$ obtained from the slope of the line in Fig. 4).

The distribution of spacing between neutron levels is shown in Fig. 5. The solid curve represents the Wigner distribution for a single level system, the dashed curve, the superposition of two systems of levels [12], and the histogram the experimental distribution. It is clear from the figure that the Wigner distribution for a single system of levels better describes the histogram despite the fact that two systems of levels should be realized in ^{241}Am. If one is not seeking deeper physical reasons,* this situation may simply be the consequence of insufficient resolution of closely lying levels or of loss of weak resonances, particular evidence of which is the Porter — Thomas distribution obtained.

The experimental data was analyzed for long-range correlation in accordance with the Δ_3 test for an orthogonal ensemble proposed by Dyson and Mehta [13]. We obtained the experimental value $\Delta_3 = 0.367$ and the theoretical values $\Delta_3 = 0.723 \pm 0.219$ for two systems of levels and $\Delta_3 = 0.362 \pm 0.110$ for a single system of levels. Agreement of experimental and theoretical values of Δ_3 confirms the correctness of the Dyson — Mehta theory for the case where one system of levels is realized in a nucleus.

Figure 6 presents the results of the $\sigma(K)$ test — correlation of the positions of two levels between which K levels are located.

The authors are grateful to Yu. G. Abov and Yu. S. Zamyatin for interest in the work and also to T. V. Denisova and V. A. Poruchikov who assisted in the calculations.

LITERATURE CITED

1. S. M. Kalebin et al., Yad. Fiz., 14, 22 (1971).
2. T. S. Belanova et al., At. Énerg., 38, No. 1, 29 (1975).
3. S. M. Kalebin et al., in: Proceedings Neutron Physics Conference [in Russian], Pt. II, Naukova Dumka, Kiev (1972), p. 267.
4. BNL-325, 3rd edition (1973).
5. C. Bowman et al., Phys. Rev., 137, 326 (1965).
6. R. Block, L. Slaughter, and J. Hervey, ORNL-2718 (1959), p. 26.
7. G. Slaughter, J. Hervey, and R. Block, ORNL-3085 (1961), p. 42.
8. H. Derrien, in: Proceedings Neutron Physics Conference [in Russian], Pt II, Izd. ONTI FÉI, Obninsk (1974), p. 246.
9. B. Leonard and E. Seppi, Bull. Amer. Phys. Soc., 4, 31 (1959).
10. C. Porter and R. Thomas, Phys. Rev., 104, 483 (1956).
11. H. Sharma and Ray. Ram, Prog. Theor. Phys., 51, 1642 (1974).

*It has been suggested [14] that there is a "repulsion" of levels with different values of spin.

12. L. Lynn, The Theory of Neutron Resonance Reactions, Clarendon Press, Oxford (1968).
13. F. Dyson and M. Mehta, J. Mathem. Phys., 4, 701 (1963).
14. E. Wigner, in: Statistical Properties of Nuclei, J. Garg (editor), New York—London (1972), p. 7.

THE PULSED ÉLIT-1B ELECTRON ACCELERATOR

Yu. G. Bamburov, S. B. Vasserman,
V. M. Dolgushin, V. F. Kutsenko,
N. G. Khavin, and B. I. Yastreva

UDC 621.384.658

The ÉLIT-1B electron accelerator (Fig. 1) is one of the pulsed high-voltage accelerators which were developed in the last few years by the Institute of Nuclear Physics of the Siberian Branch of the Academy of Sciences of the USSR and which make use of a tesla transformer [1]. The ÉLIT-1 accelerator [2], which was built in 1966 in the Institute, was the prototype.

When compared with the ÉLIT-1, the basic dimensions of the accelerator were maintained yet all the basic parameters of the ÉLIT-1B (electron energy, pulse current, average current, and average power) were substantially increased by improving the design of the apparatus, the electrical supply system, the vacuum system, etc. This affects mainly the average power which was increased by one order of magnitude.

Particular attention was paid to the problems related to the reliability which, in turn, is dictated by the requirements to be fulfilled by industrial accelerators. It was found by long-term testing that the crucial components of the accelerator, viz., the high-voltage winding of the transformer and the accelerating tube, work at least 1000 h without defects. The service life of the cathode of the electron gun was 400-500 h.

The combination of high pulse power and high average power of the electron beam, the compactness of the accelerator, the simplicity of its design, and its reliable operation make it possible to use the ÉLIT-1B accelerator for various industrial applications. The international conference which was held in April 1974 in Vienna and which was concerned with the sterilization of medical materials by irradiation [3] and, in addition, the achievements of various organizations irradiating medical materials, which were exhibited as documents on the stand of the Institute of Nuclear Physics, have shown that this accelerator is very promising for the sterilization of medical materials by an electron beam.

The basic parameters of the accelerator are as follows: accelerated electron energy up to 1.4 MeV; pulse current up to 50 A; pulse power up to 60 MW; pulse duration between 30 nsec and 2.5 μsec; and pulse repetition frequency up to 100 Hz. During long-term operation, the average beam current can reach 4.5 mA; in forced operation, the beam current can be increased to 6.5 mA. The beam parameters can be adjusted within wide limits. The accelerator was tested under various conditions, among them long-term operation (1000 h) at an electron energy of 1.1-1.2 MeV, a pulse repetition frequency of 100 Hz, and an average beam power of 4-5 kW.

Fig. 1. The ÉLIT-1B accelerator.

The Electrical Circuit. Figure 2 shows a simplified scheme of the accelerator. The primary circuit (L_1C_1) and the secondary circuit (L_2C_2) of the tesla transformer have a resonance frequency of 60 kHz and a coupling coefficient of almost 0.6 at which the maximum voltage in the secondary circuit is reached during

Translated from Atomnaya Énergiya, Vol. 40, No. 4, pp. 308-311, April, 1976. Original article submitted May 26, 1975; revision submitted October 6, 1975.

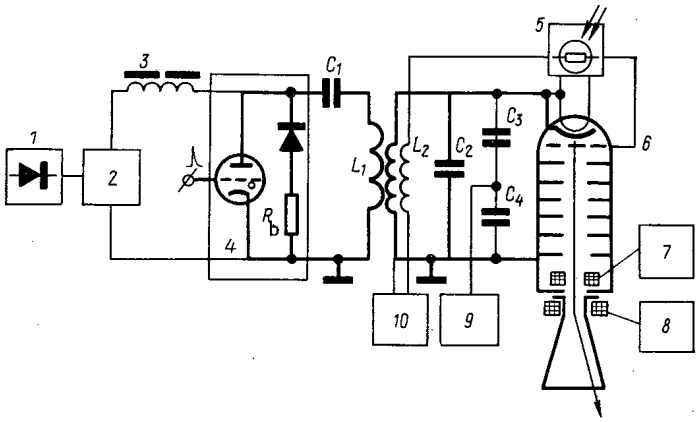

Fig. 2. Structural electrical scheme: 1) voltage regulator; 2) rectifier; 3) choke; 4) commutator; 5) control block of the electron gun; 6) grid of the gun; 7) supply block of the focusing lens; 8) beam-sweeping system; 9) measurement circuits and circuit for the protection from subsequent breakdowns; 10) supply block of the gun.

the second half-wave of the oscillations. The capacitor C_1 (1.1 μF) is charged to 15-25 kV. The capacitor-charging process is oscillatory. The charging apparatus comprises an RNTT 330-250 voltage regulator with thyristors, an industrial power transformer with a rectifier, and a charging choke. The oscillations which begin in the circuits when the thyratron section of the commutator is closed are terminated by the full discharge of the capacitor C_1. The forward branch of the commutator consists of two TGI1-2500/35 thyratrons connected in parallel; VCh-160 diodes (40 of them connected in series) are used in backward direction. A load resistor R_L is inserted into the diode branch of the commutator. Since energy is transferred into the secondary circuit mainly when the forward branch of the comutator is effective, the load resistor hardly influences the efficiency with which energy is transferred from the primary circuit to the secondary circuit. The strong attenuation which the load resistor causes liberates the circuit from excessive heating and improves the breakdown strength of the high-voltage circuit. For the value of the load resistor, which was used in the commutator and which is equal to the characteristic resistance of the circuits, the amplitude of the second half-wave (which is in-phase with the accelerating half-wave) of the voltage U_2 amounts to about 50% of the first half-wave. The load resistor is built of nickel–chromium wire applied as a bifilar winding on an insulating body; the resistor is cooled with running tap water.

The dissipation of the energy, which was not used for accelerating electrons, by the load resistor reduces the efficiency of the apparatus when compared with the recuperation conditions of [2] but preserves the other advantages of recuperation (small energy losses inside the accelerator and short duration of the high-voltage effect). The commutator can be easily adjusted and works reliably. The progress which industry has made in the field of powerful controllable gas-discharge tubes and semiconductor diodes makes it possible to plan the future development of reliable commutators with energy recuperation for accelerators of the type under consideration.

The control block of the electron gun is mounted inside the high-voltage electrode and has its potential. This control block provides for the heating of the gun and shapes the control pulse which is applied to the grid and has an amplitude of up to 5 kV. The pulse generator is triggered by a fraction of the high voltage, which is derived from a capacitive transducer. In order to obtain the optimum position of the control pulse on the time scale and in relation to the accelerating voltage under the various conditions of operation, the trigger pulse is passed through an adjustable delay line. The delay of the line is changed by a switch (step selector switch) which is operated by application of light pulses to the light guide shown in Fig. 3. The same switch changes the delay of a line with which the duration of the control pulses is adjusted. The corresponding light signals are introduced into the block via a second light guide.

A focusing lens and a beam-sweeping system are mounted in the exit section of the accelerator. The focusing lens is applied by a sinusoidal current pulse having an amplitude of up to 80 A and a duration of 100 μsec. The beam passes in succession through 32 positions on the foil of the exit horn. This sweep is obtained by applying current pulses with a variable amplitude to the deflecting coils mounted on the outside

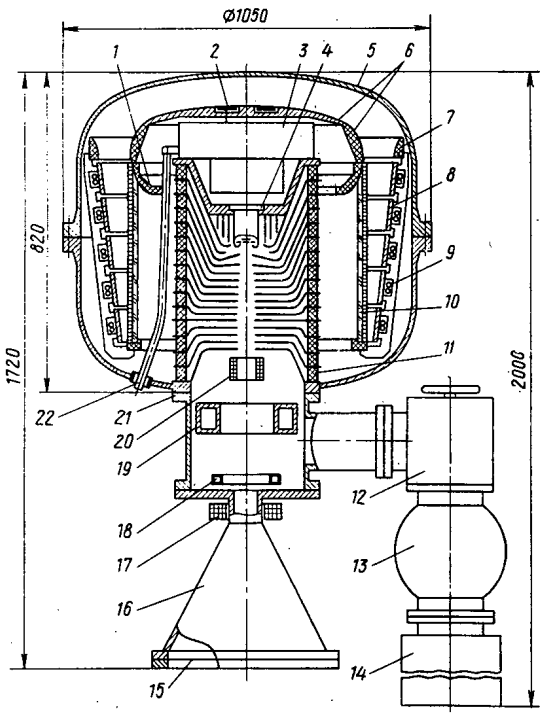

Fig. 3. Design of the accelerator: 1) shielding electrode; 2) capacitive sensor; 3) gun-control block; 4) electron gun; 5) tank; 6) high-voltage electrode; 7) electrode; 8) primary coil; 9) tubes for cooling the primary coil; 10) secondary coil; 11) accelerating tube; 12) valve; 13) nitrogen trap; 14) NORD-250 vacuum pump; 15) titanium foil; 16) exit horn; 17) sweep system; 18) Rogowski loop; 19) nitrogen trap; 20) focusing lens; 21) vacuum volume; 22) light guide (2 of them).

of the exit horn. Since the deflecting pulse is much longer than the pulses of the electron current (4 msec and 1.5 μsec), the field generated by the deflecting coils is quasi-constant. The independent amplitude adjustment of the deflecting pulses makes it possible to adjust the current distribution in the exit window so that either a uniform current density distribution over the length of the window or a current density distribution following a certain law is obtained. When the pulse repetition frequency is changed, the sequence of the beam positions on the foil remains unchanged.

In order to rule out a series of electrical breakdown events which could damage the accelerating tube, the secondary coil, and other components, a protection is provided. The protection circuit removes the pulses triggering the commutator after a first breakdown and de-energizes the circuit charging the capacitor C_1. The short front appearing on the accelerating voltage at the time of the breakdown is the signal for triggering the above circuit. The short front is derived from the capacitive divider C_3, C_4, which at the same time serves for measuring the high voltage.

The operation of the deflecting system, the focusing lens, and the commutator is synchronized by a generator of delayed pulses. The main components of the supply source are mounted in two cabinets with the dimensions 1.8 × 0.8 × 0.9 m and in two racks (power rack and control rack) with the dimensions 1.9 × 0.6 × 0.5 m.

Construction of the Accelerator. The high-voltage transformer, the accelerating tube, and the control block of the gun are mounted in a tank filled with an inert gas (SF_6) under a pressure of 10 atm (see Fig. 3).

The turns of the primary coil, which is made of copper tubing, are cooled with water. The secondary coil is electrically a single-layer coil; a second layer is required for transferring the supply voltage over two parallel leads to the control block of the electron gun. The coil is wound on a body of organic glass (Plexiglas). In order to reduce overvoltages between the turns of the coil in the case of electrical breakdown of the entire voltage, a protective electrode is provided. The accelerating tube is subdivided into sections. The insulating rings are made of Plexiglas. The insulator surface facing the vacuum is corrugated. The average electrical field strength amounts to 25 kV/cm on the insulator.

In the center of the tube, the electrodes are drawn together to face each other. The electrical field strength in the upper part of the tube reaches 100 kV/cm. The cathode of the gun is made of lanthanum hexaboride (LaB_6). The cathode has a diameter of 17 mm. An NORD-250 magnetic discharge pump with nitrogen traps is used for evacuating the accelerator tube. During operation, the vacuum in the lower part of the tube is 10^{-8} mm Hg.

The horn of the exit section has a window with a size of 40 × 6 cm made of 100-μ-thick titanium foil. The beam diameter on the foil is adjusted by a pulsed magnetic lens.

The accelerator and the exit section have a weight of 1 ton. The tank has a diameter of 0.9 m and a height of 0.85 m.

Modes of Accelerator Operation and Results of Tests. Two modes of accelerator operation are provided. In the first mode, the parameters can be varied to a very large extent, particularly as far as the pulse duration of the beam current is concerned, which can be adjusted from a panel to 30, 70, 100, 130, 160, 200, 240, 300, 500, and 1000 nsec with flanks of about 10 nsec. In the second mode of operation,

which is designated mainly for long-term operation with a high average power, the pulse duration is fixed and equal to 2.5 μsec. This mode of operation also allows the adjustment of the other parameters (except for the pulse duration). The nonmonochromaticity (the total energy spread) of the beam amounts in this case to 15%. In both modes of operation, the electron energy can be adjusted from 0.4 to 1.4 MeV, the pulse current can be adjusted from 0 to 50 A, and the frequency of the pulse repetition can be changed from single pulses to 100 Hz. The current pulses are rectangular in both modes of operation and for all pulse durations. The transition from one mode of operation to the other makes it necessary to exchange the control block of the electron gun inside the tank of the accelerator (see Fig. 1).

As indicated above, long-term tests of the accelerator were made at an average beam power of 4-5 kW. At a beam power of 5 kW and a beam energy of 1.2 MeV, electrical breakdown occurs in the tube on the average every 3-5 h of continuous operation. After that, the protective means shut off the high voltage. The accelerator is ready to be put into operation again 1-2 min later. These breakdowns do not result in irreversible changes in the accelerator. At a beam power of 4 kW and a beam energy of 1.1 MeV, there are practically no breakdown events. The average beam power can be increased to 7 kV for short time intervals (by increasing the current). The accelerator can be operated in this mode for 10 min without switching it off. The temperatures of the tube sections and of the secondary coil were monitored during long-term tests with an average beam power of 5 kW. The readings of temperature indicators working with the fusion principle did not exceed 55°C.

We indicate below the dependence of the maximum pulse current and of the accelerator power upon the electron energy at a pulse repetition frequency of 1-2 Hz and a pulse duration of 2.5 μsec:

E, MeV	0.7	0.8	0.9	1.0	1.1	1.2	1.3	1.4
I, A	38	42	48	54	56	50	40	20
P, MW	27.5	33.5	43	54	61	60	52	28

The maximum current is given by the capacity of the electron gun; when the electron energy is reduced, the current amplitude is given by the transmissivity of the tube channel; at high energies, the current is limited by the electrical breakdown strength of the tube.

We also tested a modification of the accelerator with an electron gun of greater power (cathode diameter 30 mm) and a slightly modified configuration of the electrodes in the accelerating tube. We obtained with this version a pulse current of 150 A at an energy of 1.2 MeV, a pulse duration of 2 nsec, and a pulse repetition rate of up to 50 Hz.

LITERATURE CITED

1. S. B. Vasserman et al., The Pulsed High-Voltage Electron Accelerators of the Institute of Nuclear Physics (Novosibirsk) for Industrial Applications and Experiments, 4th All-Union Conference on Accelerators of Charged Particles [in Russian], Moscow (1974).
2. E. A. Abramyan and S. B. Vasserman, At. Énerg., 23, No. 1, 44 (1967).
3. Proc. Intern. Conf. "Sterilization by Ionizing Radiation," Vienna, April 1-4 (1974).

CROSS SECTIONS OF THE INTERACTION OF PROTONS AND ELECTRONS WITH ATOMS OF HYDROGEN, CARBON, NITROGEN, AND OXYGEN

V. A. Pitkevich and V. G. Videnskii

UDC 539.124.17.125.4.04

When one wishes to obtain the statistical distribution functions of the radiation energy absorbed by the sensory volumes of biological objects with a size of ~10–100 Å, it is convenient to employ calculation methods in which both the differential and the total cross sections of the interaction of heavy charged particles and electrons with the atoms of the biological tissue are used. The information on the required cross sections of interaction is far from being complete in the published literature. The goal of the present work is to supply some of the missing information and to collect and analyze literature data.

We consider for heavy particles the energy range in which only ionization and excitation of the atoms of the medium are the important processes. For example, this energy range of the protons begins at 200 keV [1]. In the case of electrons, we consider ionization, excitation, and elastic scattering from the energy 100 eV.

Data on the cross sections of the excitation of atoms by charged particles have been compiled in [2-4]. However, the calculations were made only for some transitions and the results serve to verify the applicability of various approximations in the quantum mechanical theory. Using these approximations frequently implies considerable computational work which at times does not justify the effort. Therefore, the first Born approximation as the simplest approximation was used to obtain systematic data on the cross section of excitation of the most intensive transitions in light atoms excited by charged particles. The concept of a generalized oscillator strength of the transitions can be used in this approximation for both resolved and forbidden transitions. The single-electron approximation was used in [5] to calculate the generalized oscillator strength of several atoms ranging from helium to sodium. When the usual expression for the transition probabilities in the Born approximation is used [6], the following formula for the excitation cross section is obtained:

$$\sigma_{0\to n}=\frac{4\pi a_0^2}{E\Delta E_n}\int\limits_{k^2(\Delta E_n/2E)^2}^{4k^2} f_{0\to n}(K^2)\,\frac{dK^2}{K^2}, \qquad (1)$$

where $\sigma_{0\to n}$ denotes the cross section of the excitation of a transition, cm^2; a_0 denotes the radius of the first Born orbit, cm; E denotes the energy of the incoming particle, Rydberg units; ΔE_n denotes the energy of the excitation of the transition, Rydberg units; k denotes the wave number of the incoming particle, a.u.; K denotes the momentum transferred from the incoming particle to the atom, a.u.; and $f_{0\to n}$ denotes the generalized oscillator strength of the transition.

TABLE 1. Energy (eV) of the Transitions of Highest Intensity

Atom	Transition								
	$2S-2P$	$2P-3S$	$2P-4S$	$2P-5S$	$2P-3P$	$2P-4P$	$2P-5P$	$2P-3d$	$2P-4d$
C	13,12	7,48	9,68	—	8,84	10,08	10,53	9,83	10,43
N	10,93	10,3	12,9	10,6	12,0	13,3	—	13,0	13,7
O	15,65	9,52	11,9	12,7	11,0	12,4	—	12,1	12,76

Translated from Atomnaya Énergiya, Vol. 40, No. 4, pp. 311-317, April, 1976. Original article submitted June 9, 1975.

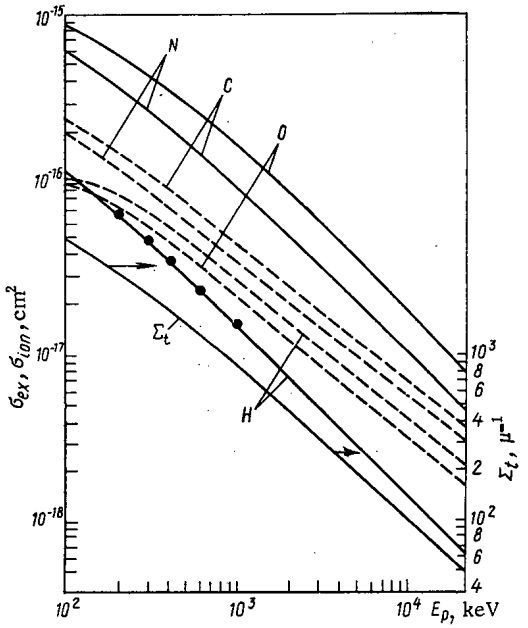

Fig. 1

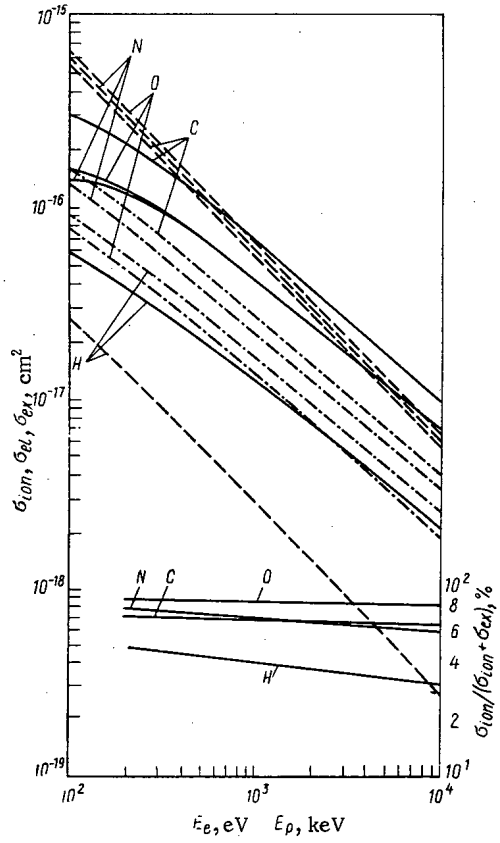

Fig. 2

Fig. 1. Cross sections of the inelastic interactions of protons with atoms of tissue-equivalent matter: ——) cross sections which were calculated for ionization with the theory of binary collisions; — — —) cross sections of the excitation of transitions of highest intensity in H, C, N, and O atoms; the cross sections were calculated from the generalized oscillator strengths of the transitions.

Fig. 2. Cross sections of the interaction of electrons with H, C, N, and O atoms: ——, — — —, and —·—·—) cross sections of ionization, elastic scattering, and excitation, respectively.

We have considered these transitions in atoms of carbon, nitrogen, and oxygen, which render the greatest contribution to the cross section of excitation. The energies of these transitions were taken from [7] and are listed in Table 1. In the case of electrons, $E = E_e/Ry$ in Eq. (1); in the case of protons, $E = m/M(E_p/Ry)$.

When the cross sections of the excitation of hydrogen were calculated, the rigorous formulas were used in the first Born approximation [6]. After some simple yet laborious transformations of the formulas for the matrix elements of the transitions, we obtain for the hydrogen atom:

$$\sigma_{1S\to 2S} = \frac{4.617\cdot 10^{-11}}{E}\int_a^b \frac{dx}{(9+4x)^6}; \tag{2}$$

$$\sigma_{1S\to 2P} = \frac{1.039\cdot 10^{-10}}{E}\int_a^b \frac{dx}{x(9+4x)^6}; \tag{3}$$

$$\sigma_{1S\to 3P} = \frac{5.259\cdot 10^{-10}}{E}\int_a^b \frac{(16+27x)^2\,dx}{(16+9x)^8\,x}; \tag{4}$$

$$\sigma_{1S\to 4P} = \frac{4.155\cdot 10^{-9}}{E}\int_a^b \frac{(768x^2+928x+275)^2\,dx}{x(25+16x)^{10}}. \tag{5}$$

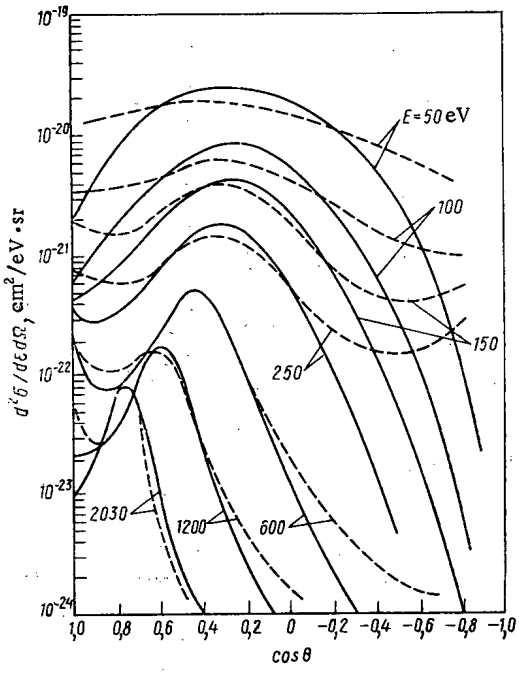

Fig. 3

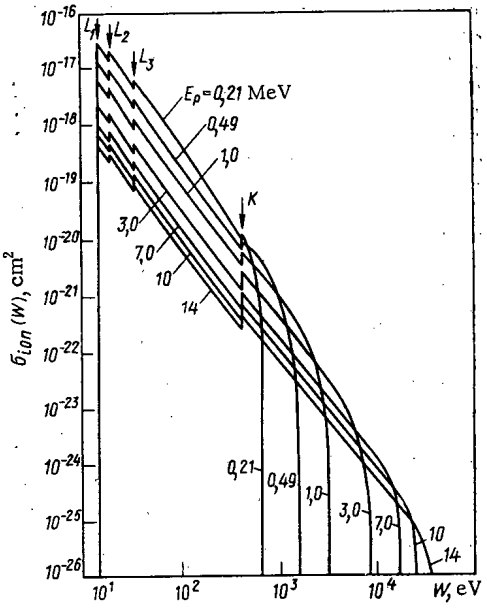

Fig. 4

Fig. 3. Angular distributions of the outgoing electrons in ionizing collisons of 1.7 MeV protons with nitrogen atoms: the cosine of the electron exit angle is plotted to the abscissa; the double differential cross section is plotted to the ordinate; ——) calculations based on the theory of binary collisions; the interaction of the proton with the outgoing electron was brought into account; — — —) experimental results of [13].

Fig. 4. Differential ionization cross sections over the transferred energy W of $^{14}N_7$ atoms; protons of various energies (the calculations were made in an approximation given by the theory of binary collisions).

The cross section of excitation is expressed in cm^2; E denotes the energy of the electrons or heavy charged particles and is expressed in Rydberg units [calculated as in Eq. (1)]; $a = E(\Delta E_n/2E)^2$; and b = 4E. The energies of the transitions whose excitation cross sections were determined with Eqs. (2)-(5) are 10.2, 10.2, 12.09, and 12.75 eV, respectively.

The total excitation cross section σ_t of a particular atom is equal to the sum of the partial cross sections. The average energy of excitation is determined with the formula

$$\overline{\Delta E} = \sum_n \Delta E_n (\sigma_{0\to n}/\sigma_t). \quad (6)$$

The average excitation energy of the atoms of hydrogen, carbon, nitrogen, and oxygen in the energy interval of the incoming particles under consideration is practically constant and equal to 10.6, 11.8, 11.1, and 13.4 eV, respectively. Figure 1 shows as an example the results of calculations which were made for the cross sections of excitation of these atoms by protons with energies between 100 keV and 20 MeV. Figure 2 shows the results of calculations of the cross sections of excitation of light atoms by electrons with energies between 100 eV and 10 keV (dash—dot lines).

TABLE 2. Ionization Potentials, Effective Number of Electrons, and Average Electron Energies for all Subshells of Carbon, Nitrogen, Oxygen, and Hydrogen Atoms

Atom	J_i, eV				N_i				$\overline{E}_i$, eV			
	L_1	L_2	L_3	K	L_1	L_2	L_3	K	L_1	L_2	L_3	K
$^{12}C_6$	11,26	16,6	24,96	307	2	4/3	2/3	2	35,9	37,0	37,0	441,5
$^{14}N_7$	14,54	19,7	33,8	420	3	5/4	3/4	2	42,8	44,0	44,0	610,1
$^{16}O_8$	13,6	28,5	40,0	562	4	4/3	2/3	2	70,3	71,9	71,9	805,8
$^{1}H_1$	—	—	—	13,6	—	—	—	1	—	—	—	13,6

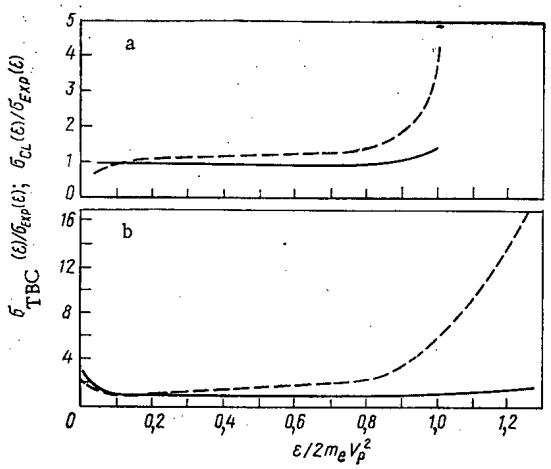

Fig. 5

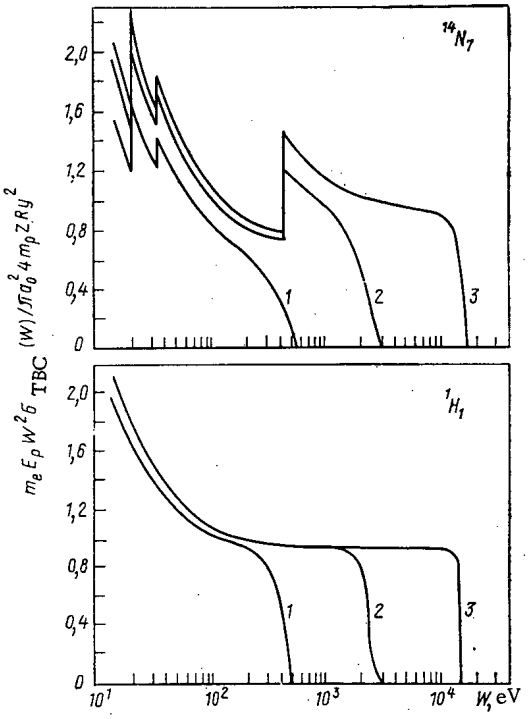

Fig. 6

Fig. 5. Comparison of the differential cross sections of the ionization of $^{14}N_7$ atoms by protons with the experimental data of [13]; the differential cross sections were calculated with the theory of binary collisions and in the approximation of scattering at free electrons. The kinetic energy of the electron emitted in the ionization event is plotted to the abscissa in units of the maximum energy; ——) ratio of the cross sections calculated with the theory of binary collisions to the experimental cross sections and is plotted to the ordinate; — — — —) ratio of the classical cross section to the experimental cross section and is plotted to the ordinate.

Fig. 6. Comparison of the differential cross section of the ionization of nitrogen and hydrogen atoms by protons with the energies 1) 0.2, 2) 1.0, and 3) 7.0 MeV; the differential cross sections were calculated with the theory of binary collisions and with the approximation of scattering at free electrons (the discontinuities correspond to the binding energies of the atomic electrons).

When one wishes to model the form of the interaction of a heavy charged particle with atoms, the energy transferred in the interaction, the kinetic energy, and the exit angle of the secondary electron, one must know the total cross section and the double differential cross section (of the energy and of the exit angle) of ionization. Measurements of the double differential cross section of ionization of several light atoms by protons and electrons were reported in [8-13]. However, the experimental data on the double differential cross section are incomplete because they neither comprise a large energy range nor many types of incoming particles. Therefore, in order to calculate the double differential cross section, the differential cross section of the transferred energy and the total cross sections of ionization, the theory of binary collisions was used [14-18]. The essence of the theory of binary collisions is that the inelastic interaction of a charged particle with an atom is considered as classical scattering at one of the electrons of the atom; the electron has a momentum and an energy which are given by its state in the atom. This approximation provides a formula for the scattering cross section which depends upon the particle parameters before and after the collision. This cross section is then averaged over the probability distribution of the momentum vector of the atomic electron and its energy, both obtained by quantum mechanical methods. When the shell structure of light atoms is properly brought into account, the differential ionization cross sections over the transferred energy are in good agreement with the corresponding experimental cross sections [19]. An acceptable agreement is obtained only at the maximum of the double differential cross section for the angular distributions of the outgoing electrons of ionization. The theoretical cross sections are several dozen times smaller than the experimental cross sections at both small and large exit angles. At small angles, the discrepancy is partially explained by the fact that for comparable

velocities of the outgoing electron and, say, the proton, the proton captures the electron in the interaction region and, at a certain distance from the atom, the electron is emitted in the direction of motion of the incoming particle. This effect is disregarded in the theory of binary collisions. The authors of [20] have attempted to include into their considerations the interaction of the incoming proton with the outgoing electron in the case of the hydrogen atom which was considered within the framework of quantum mechanics. The result was a coefficient which depends upon the velocity vectors of both the proton and the electron and with which the double differential cross section must be multiplied in the first Born approximation in order to obtain better agreement with the experimental results. The correction can be applied to the angular distributions of the outgoing electrons of ionization when the considerations are concerned with atoms of hydrogen, carbon, nitrogen, and oxygen; the distribution is to be calculated with the theory of binary collisions. It was then possible to significantly improve the agreement with the experimental results at small angles. For angles exceeding 90°, the calculated cross sections are much smaller than the experimental cross sections and at the present time there exists no theoretical explanation of this fact. But the calculated cross sections can be used, because at large exit angles the experimental cross sections are 1.5-2 orders of magnitude smaller than the cross sections at the maximum.

When we use a hydrogen-like velocity distribution of the atomic electrons for each subshell of light atoms, we can derive a final formula for the double differential cross section of ionization of the i-th subshell:

$$\frac{d^2\sigma_i}{d\varepsilon\, d\Omega}=\frac{64a_0^2}{\pi(\varepsilon+J_i)}\frac{\Phi_i\alpha_i^{7/2}N_i}{(\varepsilon+J_i)^2_{\mathrm{Ry}}}\times\frac{2\pi\gamma(\theta)}{1-e^{-2\pi\gamma(\theta)}}\int\limits_{y_1(\theta)}^{y_2(\theta)} f(y;\,\alpha_i,\,\Phi_i,\,\cos\theta)\times \times\varphi(y;\,\alpha_i,\,\Phi_i,\,\cos\theta)\,dy; \tag{7}$$

$$f(y;\,\alpha_i,\,\Phi_i,\,\cos\theta)=\frac{y^7(\alpha_i+y^2)^{1/2}}{(\alpha_i^2+y^2)^4}\times \times[\alpha_i^2+(\alpha_i+\Phi_i^2)y^2-2\alpha_i^{1/2}\Phi_i y\times(\alpha_i+y^2)^{1/2}\cos\theta]^{-3/2}; \tag{8}$$

$$\varphi(y;\,\alpha_i,\,\Phi_i,\,\cos\theta)=\frac{\alpha_i+y^2}{y^2}\sin^2\theta- -\frac{1}{2}\left[1-\left(1+\frac{m_e}{m_p}\right)\frac{\alpha_i^{1/2}(\alpha_i+y^2)^{1/2}}{y\Phi_i}\cos\theta+\frac{m_e}{m_p}\frac{\alpha_i(\alpha_i+y^2)}{y^2\Phi_i^2}\right]; \tag{9}$$

$$\gamma(\theta)=(v_p^2-2v_pK\cos\theta+K^2)^{1/2}-v_p^{-1}, \tag{10}$$

where v_p denotes the velocity of the incoming particle, a.u.; K denotes the velocity of the outgoing electron, a.u.; θ denotes the exit angle of the electron relative to the proton trajectory; ε denotes the kinetic energy of the outgoing electron; J_i denotes the binding energy of the electrons in the i-th subshell; N_i denotes the number of electrons in the i-th subshell (the number is calculated from the multiplicity of the levels of the atom); $\overline{E}_i$ denotes the average energy of the electrons in the i-th subshell; $(\varepsilon + J_i)_{\mathrm{Ry}}$ denotes the energy transferred, Rydberg units; and

$$\Phi_i=\frac{v_p}{q_i};\quad \alpha_i=\frac{\varepsilon+J_i}{\overline{E}_i};\quad q_i=\left(\frac{2E_i}{m_e}\right)^{1/2}. \tag{11}$$

The limits of integration are selected with proper regard for the energy and momentum conservation laws; the limits of integration are:

1. $\cos\theta \geqslant 0$:
   a) if $\beta_i \geqslant \cos\theta$, then $0 \leqslant y \leqslant y_{2,i}$;
   b) if $\beta_i < \cos\theta$, then $y_{1,i} \leqslant y \leqslant y_{2,i}$.
2. $\cos\theta < 0$:
   a) if $\beta_i \geqslant |\cos\theta|$, then $0 \leqslant y \leqslant -y_{1,i}$;
   b) if $\beta_i < |\cos\theta|$, then $d^2\sigma/d\varepsilon\, d\Omega = 0$.

We have

$$y_{1,i}=\frac{C_i}{A_i+B_i};\quad y_{2,i}=\left|\frac{C_i}{A_i-B_i}\right|;$$

$$\beta_i=\left(1-\frac{m_e}{m_p}\frac{\alpha_i}{\Phi_i^2}\right)^{1/2}; \tag{12}$$

$$A_i=\left(1-\frac{m_e}{m_p}\right)\left(\Phi_i^2-\frac{m_e}{m_p}\alpha_i\right)^{1/2}; \tag{13}$$

$$B_i=\Phi_i|\cos\theta|\left[\left(1-\frac{m_v}{m_p}\right)^2+\frac{4\Phi_i^2}{\alpha_i}\sin^2\theta\right]^{1/2}; \tag{14}$$

$$C_i = 2\left(\frac{m_e}{m_p}\alpha_i - \Phi_i^2 \sin^2\theta\right). \quad (15)$$

The binding energies of the electrons and their effective number were calculated from tables of the energy levels of atoms [21]. The average energies of the electrons were calculated with the method described in [22]. The values of these parameters are listed in Table 2.

In order to make a comparison with the experimental results, the angular distributions of the electrons were calculated for nitrogen atoms at a proton energy of 1.7 MeV. The comparison is illustrated in Fig. 3. The experimental cross sections were taken from [13]. For electrons with an energy >200 eV and exit angles < 90°, the greatest discrepancy does not exceed 100%. For angles >90°, the calculated cross sections are much smaller than the experimental cross sections, as indicated above. It must be noted that, unless corrections for the interaction of the outgoing proton with the electron knocked off by the proton are introduced, the calculated cross sections differ from the experimental cross sections several dozen times at small angles.

Thus, this simple method of calculating the double differential cross section for complicated atoms allows an improved determination of the angular distribution of the electrons which are emitted in the ionization of an atom. The simplicity and the rather good agreement with the experimental results at angles < 90° are the advantages of this calculation method over the quantum mechanical method which has been worked out only for hydrogen and helium atoms.

After integrating over the exit angle of the electron, one can obtain the differential ionization cross section as a function of the transmitted energy. The calculations were made for hydrogen, carbon, nitrogen, and oxygen atoms and for protons with energies between 0.21 and 14 MeV (step width of the energy 140 keV); the calculations were also made for α particles with energies between 2 and 5.6 MeV. Figure 4 shows as an example the results of calculations for nitrogen and for protons of various energies; it follows from the curves that the differential ionization cross section in dependence of the transmitted energy is characterized by discontinuities at energies which are equal to the binding energies of the electrons in the atoms. Figure 5 shows the ratio of the differential ionization cross section as a function of the kinetic energy of the emitted electrons (nitrogen atoms), as calculated by the theory of binary collisions and in the approximation of scattering of free electrons, to the experimental cross section of [13]. The proton energy is a) 1.0 and b) 0.2 MeV. It follows from the figure that the classical cross section is distinguished from the experimental cross section particularly at high kinetic energies of the electrons, i.e., at energies close to the maximum energy. The cross sections calculated with the theory of binary collisions are in good agreement with the experimental cross sections except for very small and very high energies of electron emission. For low kinetic energies of the outgoing electrons, one could not expect a good agreement with the experiments, because the experiments were made on molecular nitrogen and this detail was disregarded. The fact that the classical cross sections are closer to the experimental cross sections at low energies must be considered a matter of chance, because the cross sections calculated with the theory of binary collisions are in better agreement with the experimental data. For the purpose of estimating the classical differential cross sections of ionization, Fig. 6 shows the ratio σ_{TBC}/σ_{CL} for protons bombarding hydrogen and nitrogen. It follows from the figure that the cross section of scattering at free electrons can be used only at very high energies of the outgoing particles (in excess of 7 MeV in the case of hydrogen and in excess of 10-15 MeV in the case of nitrogen) and for outgoing particle energies which are much greater than the energy of the atomic bonds.

We used the differential cross sections to calculate the total ionization cross sections, the atomic stopping power, etc. The agreement with the experiments is not worse than 25%. Figure 1 shows the total cross sections of the ionization of light atoms by protons of various energies. The symbol (•) indicates the experimental cross sections taken from [23] for hydrogen. The same figure (right scale) depicts the dependence of the total macroscopical cross section of inelastic interactions of protons with tissue-equivalent matter upon the proton energy.

The total cross sections of the ionization of hydrogen, nitrogen, and oxygen atoms by electrons can be calculated with the semi-empirical formulas of [24]; one can use the results of [25] in the case of carbon atoms. The results of [25] can also be used to calculate the differential ionization cross sections as functions of the transmitted energy in the case of electron-induced ionization of atoms. The calculated differential cross sections of the ionization of atoms by electrons can be described by the approximation formula

$$\frac{d\sigma}{dW}=\begin{cases}\frac{C}{E_e W_0^k}; & J\leqslant W\leqslant W_0;\\ \frac{C}{E_e W^k}; & W\leqslant W\leqslant W_{\max};\end{cases}\qquad K=2.2\pm 0.1; \tag{16}$$

where J denotes the ionization potential of the atoms; W denotes the energy transmitted; $W_0 = E_0 + J$; and E_0 is equal to 15, 20, and 25 eV for carbon, nitrogen, and oxygen atoms, respectively. The constant C can be determined from the condition

$$\sigma_t = \int_J^{W_{\max}} (d\sigma/dW)\, dW. \tag{17}$$

The following formula can be employed in the case of hydrogen [26]:

$$\frac{d\sigma}{dW}=\frac{C}{E_e}\left(\frac{1}{W_{\text{Ry}}^2}+\frac{4}{3}\frac{1}{W_{\text{Ry}}^3}\right). \tag{18}$$

The total cross sections and the angular distributions of electrons in the elastic scattering were calculated with the tables of [6] which were obtained in the first Born approximation and with Hartree – Fock wave functions. Figure 2 shows the dependence of the total ionization cross sections and of the cross section of elastic scattering upon the electron energy for hydrogen, nitrogen, and oxygen atoms. The results can be extrapolated to high energies of the electrons. The lower part of the figure shows how the contribution of the cross section of ionization of light atoms by protons to the total interaction cross section depends upon the energy of the protons.

Thus, the results make it possible to model, with acceptable accuracy, the transfer and absorption of the energy of ionizing radiation in biological objects which, in a first approximation, can be considered a mixture of noninteracting atoms.

LITERATURE CITED

1. Collection of the Reports of the Symposium on Miscellaneous Problems of Dosimetry [in Russian], Gosatomizdat, Moscow (1962).
2. L. A. Vainshtein, I. I. Sobel'man, and E. A. Yukov, Cross Sections of the Excitation of Atoms and Ions by Electrons [in Russian], Nauka, Moscow (1973).
3. P. Kazaks, P. Ganas, and A. Green, Phys. Rev. A, 6, No. 6, 2169 (1972).
4. M. Seaton, Rev. Mod. Phys., 30, 979 (1958).
5. E. McGuire, Rep. SC-RR-70-406, New Mexico (1971).
6. N. F. Mott and H. S. Massey, Theory of Atomic Collisions, Oxford Univ. Press (1965).
7. A. R. Striganov and N. S. Sventitskii, Tables of the Spectral Lines of Neutral and Ionized Atoms [in Russian], Atomizdat, Moscow (1966).
8. J. Grooks and M. Rudd, Phys. Rev. A, 3, 1628 (1971).
9. W. Glass, L. Toburen, and N. Wilson, in: Proc. 3rd Symposium on Microdosimetry, Stresa (Italy), Oct. 18-22 (1971), EURATOM, pp. 71-88.
10. C. Kuyatt and T. Jorgenson, Phys. Rev., 130, 1444 (1963).
11. N. Stolterfoht, Z. Phys., 248, 81 (1971).
12. N. Stolterfoht and W. Jacobi, in: Proc. 3rd Symposium on Microdosimetry, Stresa (Italy), Oct. 18-22 (1971), EURATOM, 4810 d-f-e, pp. 95-104.
13. L. Toburen, Phys. Rev. A, 3, No. 1, 216 (1971).
14. M. Gryzinski, Phys. Rev., 138A, No. 2, 336 (1965).
15. J. Garcia, Phys. Rev., 159, No. 1, 39 (1967).
16. E. Gerjuoy, Phys. Rev., 148, No. 1, 54 (1966).
17. R. Stabler, Phys. Rev., 133A, No. 5, 1268 (1964).
18. L. Vriens, Proc. Phys. Soc., 90, No. 4, 935 (1967).
19. V. G. Videnskii and V. A. Pitkevich, in: Problems of Microdosimetry, Trans. of the 2nd All-Union Conference on Microdosimetry [in Russian], Atomizdat, Moscow (1974), p. 28.
20. A. Salin, J. Phys. B (London), 2, No. 2, 631 (1969).
21. C. Moor, Atomic Energy Levels, 1 (1949).
22. B. Robinson, Phys. Rev., 140A, No. 3, 764 (1965).
23. J. Hooper et al., Phys. Rev., 121, No. 4, 1123 (1961).
24. W. Lotz, Z. Phys., 206, 205 (1967).

25. K. Omidvar, H. Kyle, and E. Sullivan, Phys. Rev. A, 5, No. 3, 1174 (1972).
26. L. Vriens and T. Bonsen, J. Phys. B (London), 1, No. 2, 1123 (1968).

PULSED NEUTRON SOURCES FOR MEASUREMENT OF NUCLEAR CONSTANTS

S. I. Sukhoruchkin

UDC 621.039.556

The increased demand for nuclear data is due to their wide application in various branches of science and technology. The separate types of nuclear data (neutron cross sections and nuclear spectroscopic information, mainly at low levels) supplement one another in a certain sense. Over a wide range of fields, reliable results can be obtained effectively only by the combined use of these types of data [1-3]. In addition there are areas in which nuclear data obtained from pulsed neutron sources are decisive. Table 1 lists the basic types of pulsed neutron sources being used or built (planned) in the Soviet Union and abroad. Sometimes the following very crude classification of pulsed neutron sources is used: Sources with a neutron moderator are one type (usually their operating neutron range extends from thermal energies to several hundred keV); sources without a moderator, which produce only fast neutrons, are the other (third column of Table 1). Pulsed sources can also be grouped according to another parameter, e.g., their cost. Then to the first group of unique and expensive, usually multipurpose, machines, we assign meson factories and synchrocyclotrons (Nos. 2 and 6 of Table 1) and underground nuclear explosions. Linear accelerators, isochronous cyclotrons, and pulsed reactors may be assigned to the second group (Nos. 3, 4, and 5). These machines may be built in the majority of developed countries. As a rule, they have a multipurpose profile (as a supplement for nuclear studies and photonuclear studies; low-and intermediate-energy charged-particle physics research; research in solid-state physics). Finally, the third and relatively inexpensive group includes mechanical choppers for neutron beams from steady-state reactors (No. 1) and electrostatic accelerators. Many nuclear constants for reactor design are needed at such high accuracy and resolution that these constants may be measured only on machines belonging to the first two groups. Record-breaking parameters are not necessary to solve a number of other problems and in this regard many other countries can participate in applied research on neutron physics (and nuclear spectroscopy) using pulsed sources. We now consider the basic types of apparatus and the work done with them in somewhat more detail.

TABLE 1. Basic Types of Pulsed Sources

No.	Source type	Moderator	Installation sites	
			USSR	foreign
1	Mechanical chopper on a steady state reactor	No	NIIAR, ITÉF	Brookhaven (USA), Kiel University (FRG) [4]
2	Synchrotron with vertical ejection	Yes	LNPI [5]	Columbia University (USA)
3	Isochronous synchrotron with vertical ejection	No	IYaI AN SSSR [6]	Karlsruhe (FRG) [7]
4	Pulsed reactor	Yes	JINR [8, 9]	Ispra (Italy, planned)
5	Linear electron accelerator	»	IAÉ [9]	Saclay (France), Gilly (Belgium), San Diego, Washington, Oak Ridge, Livermore, Troy (USA) [4]
6	Electrostatic accelerator	No	IAÉ [10], FÉI [11]	Argonne National Laboratory (USA), and others

Translated from Atomnaya Énergiya, Vol. 40, No. 4, pp. 318-331, April, 1976. Original article submitted December 2, 1974; revision submitted October 24, 1975.

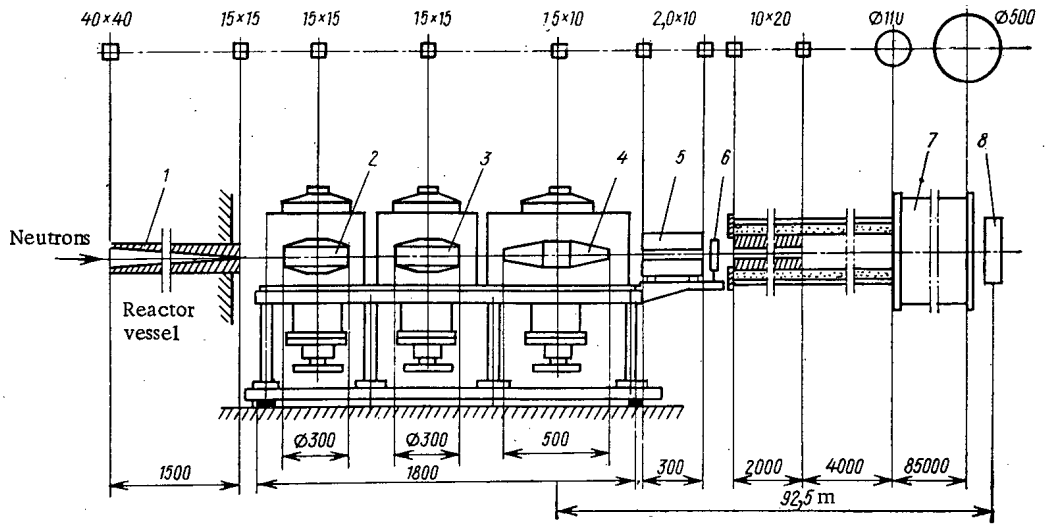

Fig. 1. A three-rotor mechanical chopper on the SM-2 reactor: 1) iron collimator; 2-4) rotors; 5) Plexiglas collimator; 6) sample; 7) evacuated neutron drift tube; 8) detector.

Mechanical Choppers on Steady-State Reactors

Historically, mechanical choppers on neutron beams from reactors were one of the first types of neutron velocity selectors or, as they are most often called, time-of-flight spectrometers. A modern chopper is a very complicated device, since its design must include a high-speed rotor (to obtain a short time interval over which the slits of the chopper overlap and the chopper becomes transparent to neutrons) with sufficient mass (to completely eliminate neutrons from the beam when the slits of the stationary collimator and the rotating rotor do not overlap). An overall view of a highly sophisticated neutron chopper is given in Fig. 1 [12]. The incident neutron beam from the powerful SM-2 research reactor passes through a collimator and is aimed at three synchronously rotating rotors. The last of the rotors has a diameter of 500 mm and a rectangular slit 1.5 mm wide, which forms a pulsed beam of neutrons lasting about 5 μsec (for a rotor speed of about 7000 rpm). The two rotating collimators in front of the main rotor sharply reduce the background level in the apparatus and make it possible to achieve optimal conditions for precision measurements. The three choppers are made to rotate synchronously by suspending the rotors in a magnetic field and using a special synchronization system. Kalebin et al. believe that with this apparatus it is possible to achieve a resolution of about 3 nsec/m over a flight path of 100 m and the area of the rotor slit may be reduced to about 1 mm^2. It is thus possible to measure the transmission of fissioned and active samples with masses of about 10 mg at neutron energies of up to several keV. Similar measurements on other types of spectrometer undergo intensity losses, have larger backgrounds, require careful collimation, etc. Use of the SM-2 reactor, which has a large concentration of uranium in the reaction zone and uses intermediate energy neutrons, makes it possible to obtain a high intensity of neutrons in the resonance energy region. It was noted in [12] that time-of-flight studies of total cross sections on this spectrometer will expand the range of isotopes examined since milligram amounts of material are sufficient for high resolution measurements. Because of this it is also possible to study very uncommon natural elements, as well as rare radioactive isotopes and so on. A similar apparatus mounted on the beam from the heavy-water reactor at the ITEF (Inst. of Theoretical and Experimental Physics) permits analogous measurements in the thermal neutron region and in the adjacent region up to energies of 100-200 eV. Other mechanical choppers are described in [4, 13]. The chopper on the VVR-M reactor at the IYaI AN USSR (Institute of Nuclear Physics at the Academy of Sciences of the Ukrainian SSR) [13] has been used mostly to measure the total and scattering cross sections of rare-earth isotopes. The chopper at the Brookhaven laboratory has been used as a neutron source in a long series of experiments on resonance neutron-capture γ spectra. Analogous work has been done in the USSR on the IBR-30 pulsed reactor at the JINR (Joint Institute for Nuclear Research). Thus, selectors with mechanical choppers are mainly used at present for specific measurements of total cross sections of small quantities of rare and highly radioactive elements (wastes, transuranium elements, etc.).

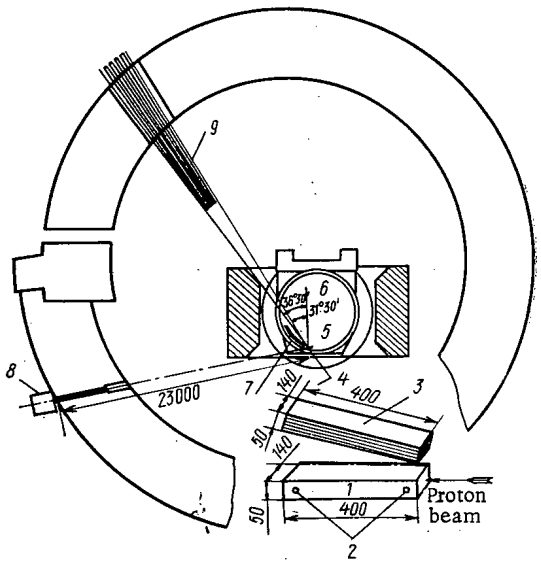

Fig. 2. The system for vertical ejection of protons in the neutron spectrometer at LIYaF: 1) lead target; 2) thermistor; 3) polyethylene moderator; 4) target (neutron source); 5) accelerated protons; 6) accelerator chamber; 7) pulsed deflector; 8) zone for mounting pulsed detectors; 9) neutron guides.

GNEIS Synchrocyclotron Spectrometer

Pulsed cyclotrons have been used in neutron spectroscopy as long as mechanical selectors. In this case a method is used to simultaneously eject all charged-particle orbits moving in the magnetic field of a circular accelerator. This method, proposed at Columbia University, permitted a sharp increase in the resolving power of spectrometers with pulsed accelerators [14], synchrocyclotrons [15, 5], and isochronous cyclotrons [7]. Figure 2 [5] is a schematic of the vertical ejection system for protons on the Gatchinskii neutron spectrometer (GNEIS) on the 1-GeV synchrocyclotron at LNPI (Leningrad Nuclear Physics Institute). Table 2 lists the basic parameters of this spectrometer (here $\tilde{N}_n$ and N_n are the average and instantaneous neutron intensities; M is the "quality factor" of the spectrometer; and, the remaining notation is customary) and analogous parameters for the Columbia synchrocyclotron and other machines. It is clear that in terms of instantaneous intensity and "quality factor" the synchrocyclotrons are roughly equivalent. The high neutron intensity in them is due to the large number of neutrons formed during collisions of high-energy protons with the target. The neutrons formed in the target (see Fig. 2) are slowed down in a hydrogen-containing block mounted above the target outside the meridional plane of the undeflected beam, and are directed into neutron guides 40–200 m in length. The computed parameters of the spectrometer (Table 3; here $\Delta\tau$ is the width of the neutron burst including moderation of neutrons, and ΔE and ΔE_0 are the energy resolution including and neglecting moderation, respectively) may be compared with the Doppler broadening of the resonance line due to thermal motion of the atoms in the material. It is clear that for energies below 1 keV the energy resolution is so great that it is desirable to cool the target to reduce the Doppler broadening (even for $A \approx 220$). The effect of uncertainty in the moderation time of the neutrons decreases sharply with increasing energy; hence, this kind of spectrometer may be used most efficiently at energies of 1-100 keV since as the energy is reduced $\Delta\tau$ is increased and the initial burst (about 20 nsec) of prompt neutrons is not used. At higher energies it is convenient to use even shorter (of order 1 nsec) neutron bursts, e.g., from isochronous cyclotrons (see Table 2). Measurement of the total neutron cross sections with a boron plate detector, of γ spectra with germanium detectors, and of fission cross sections with a fission chamber and semiconductor detectors [15] are, in a certain sense, standard for spectrometers working at neutron energies from 100 eV up to several hundred keV. The construction during the 1960's of a series of linear accelerators changed the earlier monopoly of mechanical selectors and cyclotrons. At present only synchrotrons with charged-particle energies of order 1 GeV (e.g., GNEIS) are operating in which powerful and relatively short neutron bursts are obtained due to the high energy of the protons which goes into knocking out a large number of neutrons from the collisionally excited target nuclei. These machines are mostly used to measure the total cross sections of stable isotopes with record-breaking energy resolution.

TABLE 2. Parameters of the GNEIS Spectrometer and Some Other Machines [5]

Accelerator	E, MeV	I_{av}, μA	$\bar{N}_n$, sec^{-1}	f, Hz	τ, nsec	M	N_n
GNEIS	1000	0,5—1,0	10^{14}	40—50	20	$5 \cdot 10^{29}$	10^{20}
Columbia synchrocyclotron	400	0,5	$2{,}4 \cdot 10^{13}$	60	25	$4 \cdot 10^{28}$	$1{,}6 \cdot 10^{19}$
Harwell synchrocyclotron*	150	1,0	10^{13}	200	10	10^{29}	$5 \cdot 10^{18}$
Karlsruhe isochronous cyclotron	50	100	$6 \cdot 10^{14}$	20 000	1	$1{,}2 \cdot 10^{31}$	$6 \cdot 10^{17}$

*At present $I \approx 10$ μA and $\tau = 3.5$ nsec have been achieved.

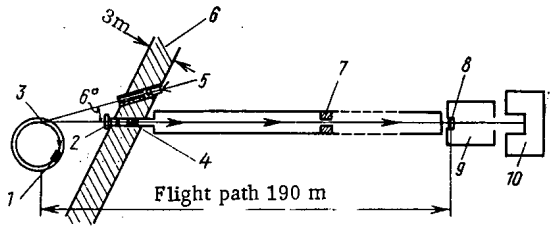

Fig. 3

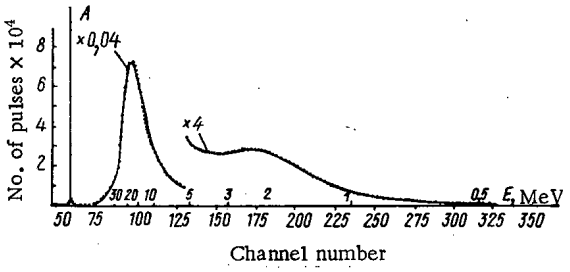

Fig. 4

Fig. 3. Diagram of an experiment to measure total cross sections on an isochronous cyclotron [7]: 1) deflecting plates in the cyclotron; 2) sample; 3) target; 4) iron collimator; 5) monitor; 6) concrete shield; 7) carbon collimator; 8) detector; 9) detector holder; 10) dump.

Fig. 4. Spectrum of neutrons from an isochronous cyclotron [7] (A is a burst of γ radiation).

TABLE 3. Dependence of the Energy Resolution of the GNEIS Spectrometer on the Neutron Energy [5]

E, eV	$\Delta\tau$, nsec	ΔE, eV	Doppler broadening for nuclei with A = 220	ΔE_0, eV
1	635	$4{,}4\cdot10^{-4}$	$2{,}2\cdot10^{-2}$	$1{,}38\cdot10^{-5}$
10	216	$4{,}8\cdot10^{-3}$	$7\cdot10^{-2}$	$4{,}35\cdot10^{-2}$
100	87	$2{,}75\cdot10^{-2}$	0,22	$1{,}38\cdot10^{-2}$
1 000	40	0,87	0,7	$4{,}35\cdot10^{-1}$
10 000	23	13,7	2,24	13,8
100 000	22	$4{,}35\cdot10^{2}$	7,1	$4{,}35\cdot10^{2}$

Isochronous Cyclotron

As the embodiment of the idea of obtaining a short neutron burst from the simultaneous ejection of all the charged particles circulating in a spiral, the isochronous cyclotron, because of its specific properties (small acceleration phase angle), has made it possible to obtain very short pulses with a high repetition rate and to use these two advantageous characteristics to study cross sections in the previously little-known neutron energy range above 0.5 to 1 MeV. The 70-MeV isochronous cyclotron presently being built in Kiev [6, 16] will be used for many purposes, including as a pulsed source in a neutron spectrometer.

Figure 3 shows the experimental arrangement used to measure total cross sections with a spectrometer on the isochronous cyclotron at Karlsruhe [7]. When there is no sample present the neutron spectrum at the detector has the form of a curve with two maxima (Fig. 4), the first of which ($E \approx 18$ MeV) is produced by the deuteron-stripping reaction and the second ($E \approx 1$ MeV) by knocking off of neutrons and fissioning of nuclei in the interior uranium target of the cyclotron. The use of a threshold detector (recoil protons) made it possible to eliminate the problem of recycle neutrons, that is neutrons from the previous pulse cycle. The neutron pulse usually lasts about 1.5 nsec, the repetition rate may be varied between 20 and 200 Hz, and the energy resolution is 0.01 nsec/m or about 30 eV at an energy of 300 keV. The special value of such record resolution is in measuring the cross sections of reactor structural materials, especially iron, sodium, and so on. The results of a measurement of another important constant. the inelastic

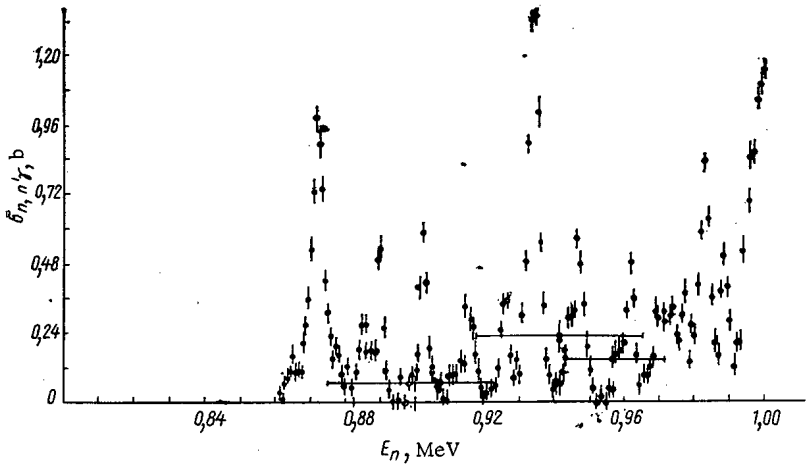

Fig. 5. New data on the inelastic scattering of neutrons on ^{56}Fe for E_γ = 846 keV: ——) previously published data; •) data from [7].

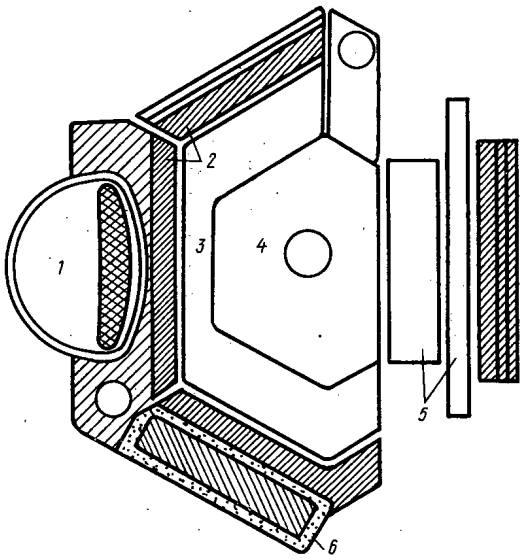

Fig. 6

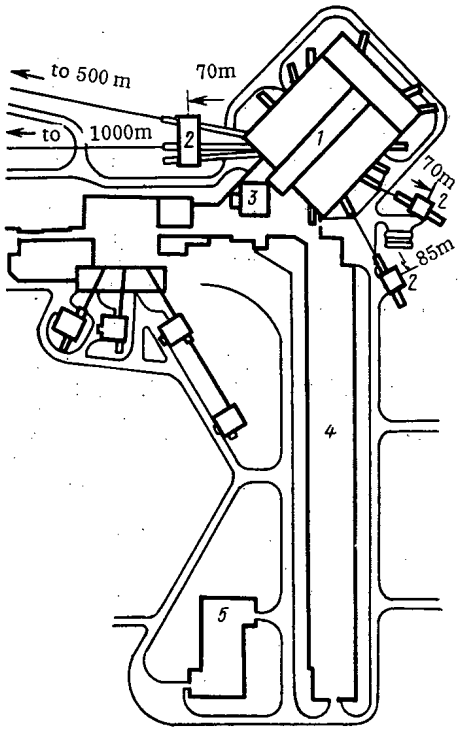

Fig. 7

Fig. 6. Diagram of the moderators in IBR-2: 1) liquid hydrogen moderator; 2) water moderators; 3) fixed reflectors and controls; 4) core; 5) moveable reflectors; 6) hot moderator.

Fig. 7. Layout of the IBR-2 and IBR-30 complexes: 1) reactor building; 2) experimental pavilions; 3) reactor control building; 4) accelerator building; 5) data processing and computer center; 6) IBR-30 building (on the 500- and 1000-m beams, pavilions other than those shown are spaced at 250 m).

neutron-scattering cross section for iron, are shown in Fig. 5. Here a fine resonance structure which was completely absent in previous measurements of this cross section (earlier data are indicated by horizontal lines) is quite clear. In measuring this cross section the detection apparatus was so arranged that the detector itself was protected from incident fast neutrons by an annular collimator. The high energy resolution obtainable from a spectrometer with a flight path of 195 m can be efficiently used only with a correspondingly very fast electronic circuit for recording and analyzing the detector pulses. Thus, the time-delay analyzer consisted of two 28,000-channel fast ADC's with channel widths of 1 nsec and the data was processed by an one-line computer. This made it possible to accept up to 100,000 pulses per second and, e.g., to measure the transmission of samples with a 1% error over 15-20 h. Considering the large volume of nuclear data in the fast and MeV energy ranges which may be obtained on a spectrometer with such an efficient neutron source, it is practical to use even such complicated equipment.

In conclusion, we note that on the U-240 isochronous cyclotron at Kiev there are three independent flight paths of length 180-200 m (with stations at 30-40 and 90-100 m). For work at flight distances of up to 50 m it is proposed that time — amplitude converters be used. The expected count rates at different flight distances for several types of detector are given in [6], as well as the energy resolution of this (still being built) spectrometer: For neutrons of about 1 MeV energy, the resolution will be about 140 eV, and at energies of 0.4 MeV, about 25 eV. This, certainly, is a very high resolution and the estimates of the count rate given in [6] show that the luminosity of this spectrometer is sufficiently large for a wide range of investigations.

Nuclear Explosions as Neutron Sources

Measurements of cross sections of highly radioactive materials have been successfully made using nuclear explosions since such measurements are difficult under laboratory conditions due to the high background from the sample, e.g., in measuring the spontaneous fission cross section of the isotope ^{244}Cm, or

TABLE 4. Parameters of Pulsed Reactors at the JINR

Reactor operating characteristic	IBR-30	IBR-2
Average power, kW	25	4000
Pulse frequency, sec^{-1}	4-100	5-50
Average neutron yield, sec^{-1}	$1.3 \cdot 10^{15}$	$1.8 \cdot 10^{17}$
Neutron lifetime, sec	$1.6 \cdot 10^{-8}$	$4.2 \cdot 10^{-8}$
Power between pulses, kW	1.2	220
Peak pulse power, MW	120	8000
Neutron yield	$5.6 \cdot 10^{18}$	$3.6 \cdot 10^{20}$
Half width of pulse, μsec	70	90
Linear accelerator for booster	LUÉ-40	LUÉ-30
Energy of electrons from linear electron accelerator, MeV	40	30
Electron current in pulse, A	0.2	250
Duration of current pulse, μsec	1.6	0.5
Frequency of accelerator pulses, sec^{-1}	100	50
Average power achieved, kW (at a frequency of 100 sec^{-1} with τ = 3 μsec)	2.5	—

the capture cross section of the fission product ^{147}Pm [4, 17, 18]. The cross sections for another spontaneously fissioning isotope, ^{252}Cf, were also measured with the aid of a nuclear explosion — the background from its natural decay was very small. The neutron source in these measurements was an underground nuclear explosion of relatively low yield having a total neutron yield of 10^{23}-10^{24}. The fission spectrum may be accompanied by thermonuclear neutrons. A moderator is usually used to increase the number of low-energy neutrons. During the explosion the moderator (located several tens of centimeters from the center) is heated to a temperature of about 25 eV and gains a velocity of about 5 cm/μsec. This displaces the Maxwellian peak in the spectrum of the emitted neutrons to 50 eV so that there are practically no neutrons with energies below 10-20 eV in this spectrum. The high neutron flux even at distances of 100-200 m from the point of explosion makes it possible to measure the capture cross section of samples with masses of tenths of a gram, despite the fact that the intrinsic radioactivity may be several thousand curies. The single shot nature of the experiment makes it difficult to make the sequential measurements with and without a filter normally made to refine the background measurement and to make various preliminary and control measurements. Therefore, the actually attainable measurement accuracy is usually 15-20%, and where measurements with other neutron sources are possible (for example, for determining total cross sections, γ spectra, etc.) it is scarcely appropriate to use explosions. The domain of application of the explosion technique, as indicated above, is small cross sections and, especially, the cross sections for highly radioactive substances.

Pulsed Reactors at JINR

The pulsed reactor IBR-30 (operational since 1969) and the pulsed reactor IBR-2 (under construction) are powerful neutron sources which use a chain fission reaction (as in the above-mentioned explosion method) to produce rare, but intense, bursts of neutrons. However, here the chain reaction is interrupted by mechanical removal of part of the core (in IBR-30) or the reflector (in IBR-2), and between pulses heat is removed. Figure 6 is a diagram showing the position of the basic components of the pulsed reactor IBR-2 [9]. Criticality is produced by two moveable reflectors located next to the core. The tungsten target of a linear induction accelerator (LIU-30), operating in the so-called booster regime, is located in the center of the core. In this regime the reactor, being in a subcritical state, is used to multiply the neutrons generated by the electron beam from the linear accelerator and the neutron burst lasts several microseconds. In the other operating regime, where the critical state is reached, the burst lasts 60-100 μsec. The basic parameters of reactors at the JINR are given in Table 4. We note that the maximum neutron intensity obtained from a pulsed reactor (about 10^{19} neutrons/sec) is sufficient to produce a larger neutron flux than that from high-power steady-state reactors (about 10^{15} neutrons/$cm^2 \cdot sec$). A large cycle of nuclear and solid-state physics experiments [8] were done on the IBR-30 reactor as well as a set of measurements of reactor constants (such as the radiative widths of ^{238}U, the Doppler effect in thick samples of

TABLE 5. Parameters of Spectrometers with Linear Electron Accelerators Used to Measure Nuclear Constants

Country, city, institute	Electron energy, MeV	Current, A	No. and length of flight paths	Pulse length, nsec	Basic types of measurements made
USSR, IAÉ	60	1	8; 25—290	50—5500	Total cross sections, capture and fission cross sections
France, Saclay	60	—	6; 13—200	50	Total cross sections and fission cross sections of cooled samples
England, Harwell	136	6	10; 5—300	5—5000	Capture cross sections, standard cross sections, fission cross sections
Belgium, Gilly	65	4	4; 8—100 м	20	Total cross sections, fission cross sections, etc.
USA, Oak Ridge	140	15	11; 20—200	2—25	Simultaneous measurements of fission and capture cross sections. α, ν, etc
USA, Washington	100	—	3; до 200	от 5	Measurements are planned
USA, Livermore	140	10	7; 4—250	от 15	Fission cross sections, total scattering cross sections, etc.
USA, Troy	100	6—20	4; 10—250	5—200	Capture cross sections ν, total cross sections, etc.

uranium, the capture and fission cross sections of ^{235}U and ^{239}Pu, etc.). In evaluating the prospects for work on the new pulsed reactor IBR-2, Yu. Yazvitskii noted [9] that the JINR pulsed reactors cannot compete with particle accelerators in high-resolution neutron spectroscopy. For example, the pulse length for the linear accelerator at the IAÉ (Institute of Atomic Energy) is 0.1 μsec as opposed to 3 μsec for IBR-2. However, the neutron yield per pulse of IBR-2 is $2 \cdot 10^{16}$ sec^{-1} and at a pulsed reactor the conditions will be favorable for work on the analysis of reaction products where the resolution requirements are lower and the first priority is neutron intensity (as in α and γ spectra from neutron resonances, etc.). At the same time, 14 neutron guides with individual gates were used, including one 1000 m in length, which makes it possible to make several measurements at once. Figure 7 shows the arrangement of the IBR-2 installation at the LNF site at the JINR [9].

Another type of multiplier target was used on the neutron spectrometer at Karlsruhe. There a stationary plutonium booster target with a constant neutron multiplication factor was used. This target, together with a linear electron accelerator, ensured a pulse duration of 0.1 μsec which made it possible to obtain an order of magnitude advantage in intensity over ordinary electron accelerators (with the same currents) and to make efficient measurements in the energy region to 1 keV.

Linear Electron Accelerator and Electrostatic Generator

We now consider the most accessible pulsed neutron sources, the linear electron accelerator and the electrostatic generator. In the first, the neutrons are obtained by stopping 30-100-MeV electrons in high Z and A targets. The linear accelerator at the IAÉ, for instance, accelerates electrons to 60 MeV. A number of modern accelerators (at Oak Ridge, Livermore, Washington) have higher energies, up to

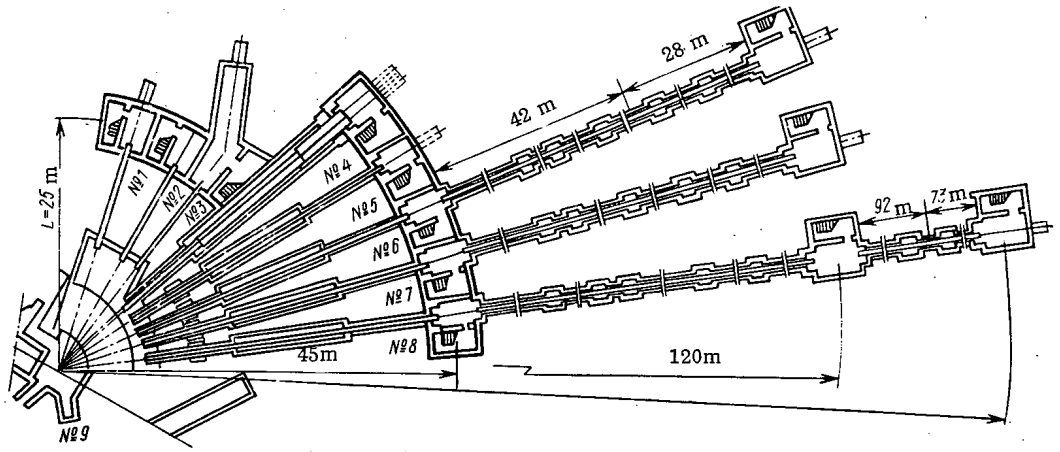

Fig. 8. Location of neutron flight paths on the linear accelerator at the IAÉ [19].

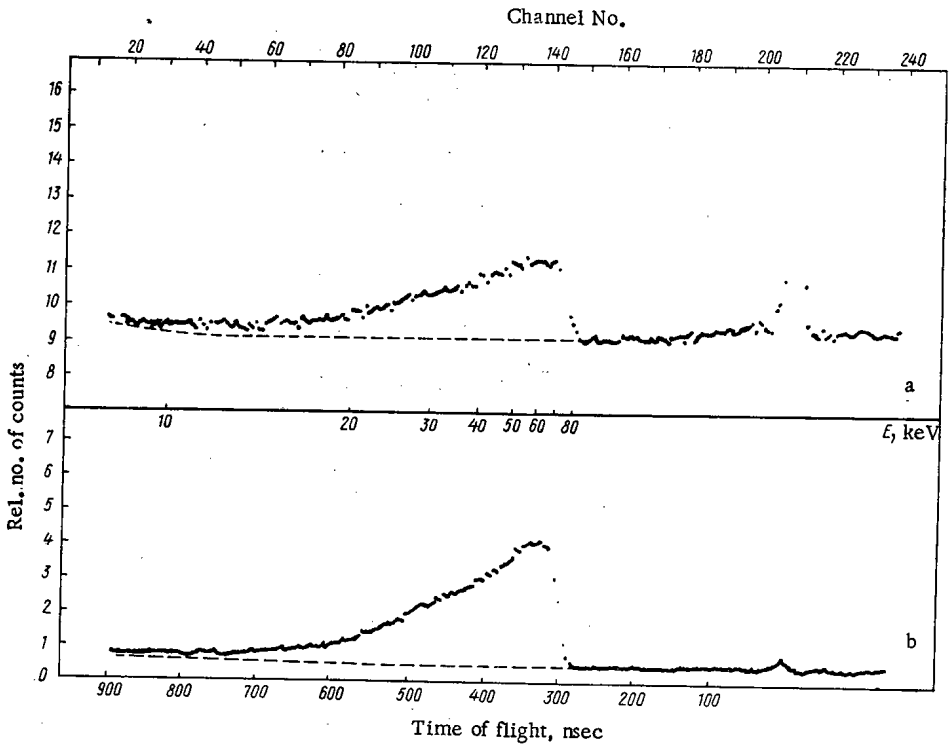

Fig. 9. Radiative (a) and fission (b) effects during measurement of the ratio α ($\alpha = \sigma_c/\sigma_t$) on a pulsed electrostatic accelerator at FÉI [11, 20].

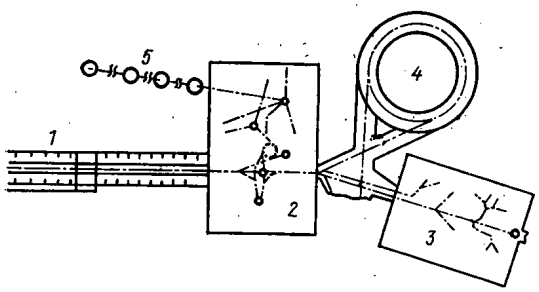

Fig. 10. Diagram of the positions of the accelerator and the experimental apparatus at a meson factory [25]: 1) linear accelerator; 2) housing for neutrals; 3) housing for mesons; 4) storage unit-stretcher; 5) experimental zones for neutron studies.

100-140 MeV, which provide somewhat larger neutron yields (see Table 1). Table 5 shows the parameters of those neutron spectrometers with linear electron accelerators which are most systematically used for measuring nuclear constants. There are, in addition, a number of accelerators operating in Japan, Brazil, and other countries. Ordinarily, for best utilization of operating time the accelerator is equipped with a large number of neutron guides with independent gates and several parallel experiments are done simultaneously. Figure 8 shows the fan-shaped arrangement of these neutron flight paths on the spectrometer with the linear accelerator at the IAÉ. On the separate paths independent measurements may be made of the cross sections for capture, fission, and scattering, the total cross section, γ spectra, and a number of other constants. The great flexibility of the electron accelerator should be noted; it is possible to change the frequency and duration of the neutron pulses from it with ease, and the use of an external target (as opposed to the case of the synchrocyclotron and phasotron) makes it possible to reduce the γ-radiation background accompanying the neutron pulse by means of shadow shielding. Thus, if it is desirable to use proton accelerators with energies of 0.5-1 GeV (cf. above) to achieve record-breaking parameters (e.g., to obtain maximum energy resolution), then it is most appropriate to use electron accelerators, which are very convenient, as multipurpose neutron sources for studies in both the resonance region of neutron energies and at high energies. They can support a broad front of work, and provide a wide range of energies and measured cross sections with relative ease, cheapness, and safety.

Because of their availability and universality of application in wide-ranging and varied branches of nuclear physics, electrostatic generators have become very widespread. Practically every institute and major nuclear laboratory (IAÉ, FÉI, LNF, JINR, KhFTI, RIAN, IYsI AN SSSR, etc.) have one or another modification of it, and several institutes have entire complexes of such apparatus. The principal operating

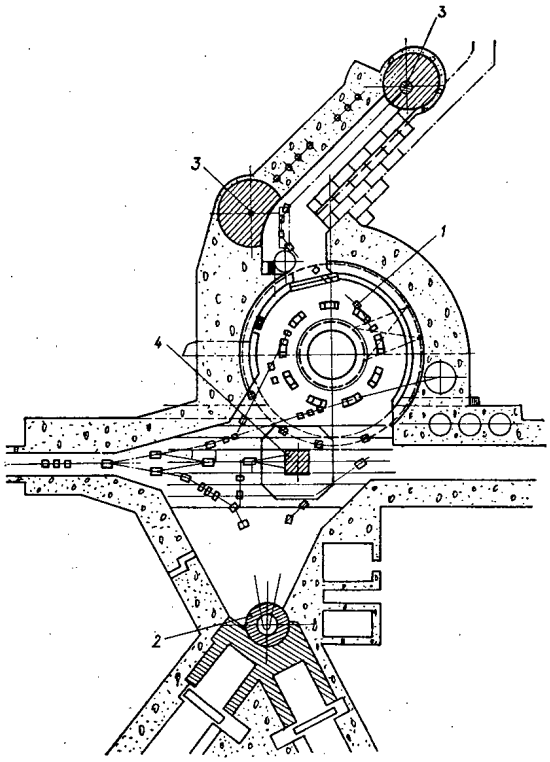

Fig. 11. A diagram of the storage ring switching operation for obtaining intense neutron pulses at a meson factory [25]: 1) storage unit-buncher; 2) superconducting meson trap; 3) neutron targets; 4) proton beam trap.

TABLE 6. Comparison of Various Neutron Generation Processes [26]

Particles	Energy	Target	$\bar{n}$, neutrons/sec·MW	$\bar{I}$, mA	Q, kW/cm^3	θ	E, MeV(γ)/neutron
e	100 MeV	^{238}U	$5\cdot10^{15}$	400	600	0,1	>1000
p	600 MeV	^{238}U	10^{17}	1	1,5	1 nsec	1
p	600 MeV	A-200	$1,7\cdot10^{17}$	1,6	2,4	1 nsec	0,3
p	150 MeV	A-200	$4\cdot10^{16}$	16	75	0,1 nsec	0,3
	Pressure	^{239}Pu	$6\cdot10^{16}$	—	—	0,1— 5 μsec	5

regime of electrostatic accelerators is not, as a rule, associated with pulsed neutron production, but neutron time-of-flight methods are provided for on several of them. An example of the use of pulsed electrostatic generators is the measurement of the α ($\alpha = \sigma_c/\sigma_f$) constant of ^{239}Pu at the FÉI [20] and IAÉ [21]. In both cases neutrons from the reaction ^{7}Li(pn) were used and the time spectra of two effects (fission and capture) in the sample, located some distance (l) from the neutron source, were recorded simultaneously. The flight path and time resolution were 1.125 m and 20 nsec (at FÉI) and 0.37 m and 8 nsec (IAÉ). Figure 9 shows experimental spectra from the first experiment [11]. On the upper curve (a), corresponding to the radiative effect, there is a distinct pulse from prompt γ radiation, and the dashed line denotes the extrapolated background for both measured effects. In the range of 70-20 keV the use of the time-of-flight technique made it possible to correctly account for background and measure the constant α (in both experiments) with an error of 15%. Another important application of the time-of-flight technique is measurement of the elastic and inelastic scattering cross sections at, e.g., FÉI [22] and the Argonne National Laboratory in the USA [23, 24]. In the latter case the source was a dynamitron operating in the pulsed mode, and the scattered neutrons are detected at once at a large number of angles and at various distances from the target. Pulsed electrostatic generators have also been used to measure the total neutron cross sections and a large number of other nuclear constants; however, as a rule, it is difficult for a number of experimental groups to operate simultaneously on these machines, and in this they differ from the majority of the other sources where there are several independent directions and many experiments may be run at once. At the same time, the simplicity, reliability, and relative cheapness of the electrostatic generator itself makes a spectrometer using it very convenient for small laboratories. In addition, the generator may always be used for other nuclear research unrelated to neutron physics.

TABLE 7. Comparison of the Operating Regimes of a Meson Factory (with proton-beam switching) with Other Machines [26]

Machine	Pulse duration, nsec	Frequency, Hz	Neutron yield, neut/sec
MF -600	100 000	10	$1{,}5\cdot10^{16}$
IBR -2	90 000	5—50	$2{,}4\cdot10^{17}$
MF-600	24	100	$3{,}6\cdot10^{13}$
	24	1 440	$3\cdot10^{14}$
MF-600	1	200 000	$1{,}5\cdot10^{14}$
Isochronous cyclotron	1	200 000	$2\cdot10^{14}$

Meson Factory

Proton linear accelerators with energies of 0.6-0.8 GeV ("meson factories") [25, 26, 27] permit use of pulsed proton beams to generate neutrons. In this case the heat delivered to the target and construction elements per emitted neutron is roughly 30 times less than for a 100-MeV electron. Table 6 [26] shows the average neutron intensity ($\bar{n}$) from heavy targets irradiated by electrons and protons (heat release 1 MW) and the average currents of accelerated particles corresponding to an intensity of 10^{17} neutrons/sec. Also given there for these average currents are the specific heat release (Q) in materials of average atomic weight (perpendicular cross-sectional area 10 cm^2) and the characteristic pulse durations (θ) and total γ energy accompanying the emission of a single neutron (for comparison we give the corresponding characteristics for fission of ^{239}Pu). Since the average number of neutrons obtained from a 600-MeV proton is about 25 for uranium and about 10 for lead, and the fraction of delayed neutrons is less than 1% (for lead, 0.1%), a very effective neutron selector may be based on a meson factory. It is possible to use switching of the proton beam from the accelerator to produce favorable conditions (in terms of pulse repetition rate and burst duration) for neutron cross-section measurements; i.e., it is possible to create regimes close to the operating regimes of such sources of slow, resonance, and fast neutrons as the IBR-2, linear accelerator, and phasotron described above, which are specialized machines for these three energy ranges. The possible regimes of a meson factory (MF-600) are compared in Table 7. It is clear that it is inferior to these specialized machines in neutron intensity by not more than an order of magnitude. A diagram illustrating the cutting off of a small part of the proton beam from the meson factory is shown in Fig. 10. If negative hydrogen ions are accelerated in the meson factory, a charge-exchange target is used to strip these accelerated ions, and the protons are collected in the storage ring, then it is possible to obtain short and very intense neutron bursts by using system for removing the protons from the ring in a single orbit. An arrangement for such switching of the 600-MeV proton accelerator designed for the institute of Nuclear Studies of the Academy of Sciences of the USSR (IYaI AN SSSR) was described in [26]. Figure 10 shows a diagram of the positions of the accelerator and experimental equipment at the meson factory at the IYaI AN SSSR, and Fig. 11 shows the locations of the storage unit-buncher and the neutron targets. The principal components of the experiment are the neutral housing with the storage unit-buncher, the meson housing, the structure for stopping the beam, and the system of tunnels for separations. The storage ring-buncher is meant to form small bursts of protons and appropriately short neutron pulses from neutron targets. It is a rigidly focussing magnetic ring with injection and extraction systems, RF resonators for stabilizing the beam burst during storage, and elements of diagnostic systems mounted in straight sections. Protons are accumulated in the ring during multiple-orbit charge-exchange injection of negative hydrogen ions from the linear accelerator. It is planned to accumulate up to about $3\cdot10^{13}$ protons per injection cycle. Two identical extraction systems are intended to eject the accumulated particles into the meson trap and onto neutron targets. A nonmultiplying neutron target in this system serves as a pulsed source for resonance and fast-neutron studies. The target is a dense packing of rods (of depleted uranium in zirconium shells) with water cooling. In the first stage there will be a regime with a repetition rate of 100 Hz and an average

TABLE 8. Comparative Characteristics of Some Neutron Spectrometers

Name and location	Energy and type of particle, MeV	Repetition rate, Hz	Beam current, mA	Pulse duration, τ, nsec	Av. intensity, $\bar{N}$, neutrons/$cm^2\cdot$sec	Source quality, $\bar{N}/\tau^2$
Linear accelerator, IAÉ	60; *e*	900	—	20—50	$5\cdot10^{13}$	$1{,}2\cdot10^{28}$
		150	—	to 15 000	$2{,}5\cdot10^{6}$	$1{,}1\cdot10^{26}$
IBR-30, JINR	40; *e*	100	—	70 000	$1{,}5\cdot10^{15}$	$3\cdot10^{23}$
		100	—	3 000	$3\cdot10^{14}$	$3{,}3\cdot10^{25}$
IBR-2, JINR	30; *e*	50	—	3 000	10^{16}	$1{,}1\cdot10^{27}$
		50	—	500	$1{,}8\cdot10^{14}$	$7{,}3\cdot10^{26}$
Linear accelerator, Oak Ridge	140; *e*	1000	500	2	$2{,}7\cdot10^{13}$	$7\cdot10^{30}$
		1000	500	16	$2{,}7\cdot10^{14}$	10^{30}
Columbia synchrocyclotron	500; *p*	600	$2\cdot10^{-3}$	20	10^{14}	$2{,}5\cdot10^{29}$
GNEIS, LNPI	10 000; *p*	50	$5\cdot10^{-4}$	10	$5\cdot10^{13}$	$5\cdot10^{29}$
Isochronous cyclotron, Karlsruhe	50; *d*	20 000	0,1	1	$1{,}2\cdot10^{13}$	$1{,}2\cdot10^{31}$

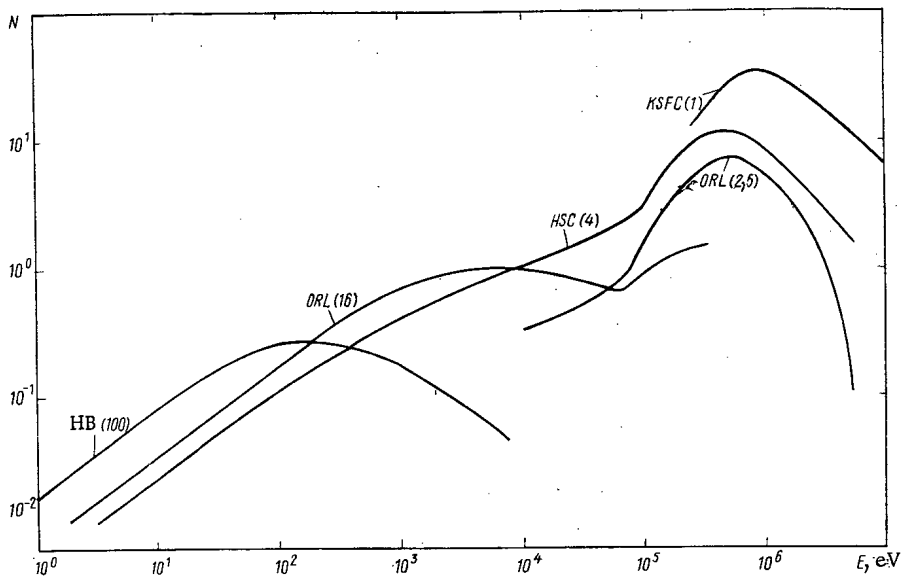

Fig. 12. Comparison of the neutron fluxes from four pulsed sources. The curves were obtained for optimum operating conditions, i.e., for different pulse repetition rates and flight path distances [23]. The duration of the neutron pulse in nanoseconds is given in parentheses (N is the number of neutrons at the detector in energy interval ΔE per $cm^2 \cdot sec$.

proton current of 50-100 μA, which corresponds to an average intensity of up to about 10^{16} neutrons/sec. In later stages it is planned to increase the average current to 500 μA and the repetition rates to 400 Hz as well as to include the possibility of sending bursts of protons of length about 200 nsec into a booster, or neutron multiplier for slow-neutron studies. Use of a multiplier with sodium cooling and plutonium oxide fuel will make it possible to generate neutron pulses of duration 4-16 μsec with repetition rates of 25-100 Hz and average intensities of up to $2 \cdot 10^{18}$ neutrons/sec. The peak flux of thermal neutrons in a light-water moderator reaches $2 \cdot 10^{17}$ neutrons/$cm^2 \cdot$sec, and the time-averaged thermal neutron flux in a heavy-water moderator is about 10^{15} neutrons/$cm^2 \cdot$sec with an average thermal power in the target of up to about 50 MW. More detailed data on this design are given in [25, 26].

The constant development of new methods of accelerating protons leads one to hope that soon the level of intense neutron pulses obtained mainly from linear electron accelerators will be exceeded. The meson factory and the Columbia synchrocyclotron are examples of ways to produce record-breaking neutron pulse intensities using proton, rather than electron, beams. This type of accelerator offers the hope of obtaining the record-breaking energy resolution in spectrometers needed, for example, to sharply increase the number of measured resonance parameters, to increase the accuracy of nuclear physics data, and to set up physical experiments which are technically impossible at present.

According to an estimate by A. M. Weinberg [28], in the year 2000 there will be about 500 working reactors in the USA alone and breeder reactors will provide a substantial part of the electric energy and heat used. Thus, the large demand for accuracy in nuclear data is not exaggerated since there would be a substantial economic loss (even on a national scale) from inaccurate determination of the parameters of large-power reactors [29]. Undoubtedly, the engineering and scientific search for more intense neutron sources will continue and other more effective machines than those described above will be proposed. The comparative characteristics of most types of neutron spectrometers are given in Table 8, where the quantity $(\bar{N}/\tau^2)$, sometimes called the "source quality," is also given. This parameter is of significance only in comparing machines of a single type or spectrometers working in the same energy range since it is useless to compare specialized spectrometers, e.g., for resonance neutrons (such spectrometers have to have a neutron moderator) with those at energies of several MeV (without moderators) as their functions are different. The problem posed by the technology of prospective reactor design of measuring a large number of nuclear constants can be solved only on a number of machines. Different types of neutron spectrometers can be compared not only in their "source quality," but also in the useful neutron flux (at the detector) for a given energy resolution, $\Delta E/E$. For example, in [7] such a comparison was made for $\Delta E/E = 8.8 \cdot 10^{-4}$

of the Karlsruhe isochronous cyclotron (KSFC), the Oak Ridge linear accelerator (ORL), and the synchrocyclotron (HSC) and booster (HB) at Harwell. From Fig. 12 [7] it is clear that the powerful linear accelerator in the energy range 100-10,000 eV and the isochronous cyclotron in the range 0.3-10 MeV have the optimal parameters (greatest flux).

In [30] the energy regions of most efficient operation of various pulsed neutron sources were distributed as follows: from thermal to 1 eV — pulsed reactors; from 1 to 200 eV — various multiplying targets (booster and installations such as IBR-2); from 200 eV to 200 keV — linear electron (and proton, obviously) accelerators and synchrocyclotrons; from 0.2 to 2 MeV — electrostatic accelerators; and, above 2 MeV — isochronous cyclotrons.

In this review we have not discussed such well-known steady-state neutron sources as beams from thermal reactors and neutron beams obtained from charged-particle reactions. We must, however, discuss the use of neutron beams filtered by scandium and iron materials which have minima in the total cross sections at certain energies (about 2 keV and 25 keV, respectively). The spectra of neutrons passing through such filters were studied in [31, 32]. At Brookhaven (USA) a similar method was used to produce a beam of neutrons for investigating the spectra of γ rays produced by radiative capture of 25-keV neutrons. To better isolate the neutrons filtered by the scandium from the background it was proposed to mount an appropriate resonance scatterer in a through channel of the reactor. According to calculations and measurements made at the National Bureau of Standards (USA) [33] the amount of neutrons of other energies in this apparatus is less than 1%. Thus, it is possible to use filtered reactor beams for measurements on almost monochromatic neutrons. Important features of these measurements are the high neutron fluxes and the stability in time (permitting uniform loading of the detectors).

An interesting example of specialization in pulsed sources are the spectrometers based on the slowing-down time of neutrons in lead. The first spectrometer of this type [34] has been operating for a long time at the FIAN (Institute of Physics of the Academy of Sciences, USSR) and recently [35] the insertion of a large lead cube (1.8 m on a side, with a mass of 75 tons) in a 100-MeV linear electron accelerator complex was described (the spectrometer at the FIAN uses a less intense source of neutrons). The neutron fluxes from a slowing-down-time spectrometer are many orders of magnitude larger than those used in time-of-flight experiments. An estimate shows that even for a short flight path (5 m) the neutron flux is 10-20 thousand times less than from a spectrometer with a lead cube. In order to verify the high luminosity of this apparatus the subthreshold fission cross sections at the first resonances of ^{238}U were measured. Despite the fact that the width of the fission band is 10-30 neV (1 neV = 10^{-9} eV), the first neutron resonances were reliably resolved. Measurements of the reaction $^{145}Nd(n\alpha)$ led to establishment of the partial width of the neutron resonances as on the order of several μeV (1 μeV = 10^{-6} eV) although the mass of the samples was several milligrams. Thus, the slowing-down-time spectrometer can very successfully exceed other machines, including a spectrometer using a nuclear explosion in which the useful energy range begins only from about 20 eV [35].

CONCLUSION

The neutron laboratories at Soviet institutes have many kinds of intense sources which make it possible to do a large number of independent measurements of cross sections and constants needed to solve scientific and applied problems. It is important that neutron spectrometers be planned and built in time for specializing in different research areas important to practical applications. This will shorten the time from the appearance of a need for a nuclear constant to completion of the corresponding research.

LITERATURE CITED

1. G. B. Yan'kov et al., in: Proceedings of the Conf. "Neutron Physics," [in Russian], Pt. 1, Izd. FÉI, Obninsk (1974), p. 30.
2. E. Steinnes, in: Proc. IAEA Symp. "Nuclear Data in Science and Technology," Paris, March 12-16, 1973, Vol. II, p. 265.
3. S. I. Sukhoruchkin, At. Énerg., 28, No. 1, 38 (1970); 31, No. 3, 245 (1971).
4. M. Moore, in: Proc. 3rd Conf. on Neutron Cross Sections and Technology, Knoxville (1971), p. 628.
5. N. K. Abrosimov et al., in: Proc. of the Conf. "Neutron Physics" [in Russian], Pt. II, Naukova Dumka, Kiev (1972), p. 188.
6. D. A. Bazavov et al., see [1], Part IV, p. 197.

7. S. Cierjacks, see [1], Part II, p. 307.
8. I. M. Frank, JINR Preprint R3-5754 (1971).
9. V. D. Anan'ev, et al., JINR Preprint 13-4392 (1969).
10. P. E. Vorotnikov et al., in: Applied Nuclear Spectroscopy [in Russian], Atomizdat, Moscow (1970), p. 305.
11. V. N. Kononov, et al., see [5], Pt. I, p. 301.
12. S. M. Kalebin et al., ibid., Pt. II, p. 267, 276.
13. V. P. Vertebnyi et al., ibid., Pt. I, p. 232.
14. K. G. Ignat'ev et al., Pribory i Tekh. Eksperim., No. 4, 25 (1959).
15. W. Havens, in: Intense Neutron Sources, USAEC, Conf. 660925 (1966), p. 565.
16. D. A. Bazazov et al., see [1], Pt. IV, p. 190.
17. B. Diven, see [15], p. 539.
18. B. Diven, Ann. Rev. Nucl. Sci., 20, 79 (1970).
19. V. F. Gerasimov et al., see [5], p. 201.
20. V. N. Kononov et al., ibid., Pt. I, p. 293.
21. P. E. Vorotnikov et al., see [1], Pt. IV, p. 42.
22. B. V. Zhuravlev et al., see [5], Pt. I, p. 219.
23. H. Jackson, Rep. to US Nuclear Data Committee (Meeting at NBS, 24-26 Oct. 1972), INDC (USA)-54 "u," p. 8.
24. S. Cierjacks, in: Proc. IAEA Symp. "Nuclear Data for Reactors — 1970," Helsinki, 15-19 June 1970, Vol. II, p. 219.
25. I. Ya. Barit et al., IYaI AN SSSR Preprint P-0003, Moscow (1975).
26. Yu. Ya. Stavisskii, Preprint FÉI-389, Obninsk (1973).
27. M. Moore, Report LASL LA-DC-72-960 (1972).
28. D. Horen and A. Weinberg, see [2], Vol. I, p. 3.
29. V. V. Orlov, At. Énerg., 31, No. 3, 195 (1971).
30. A. Michandon et al., see [15], p. 789.
31. V. G. Dvukhsherstinov et al., At. Énerg., 33, No. 1, 577 (1972).
32. V. G. Dvukhsherstinov, et al., see [5], Pt. I, p. 318.
33. E. McGarry and I. Schroder, in: Proc. Conf. on Nuclear Cross Sections and Technology, Washington, March 3-7, 1975, Report BB-18.
34. A. Bergamann et al., Proc. I Intern. Conf., Geneva (1955), Vol. 4, p. 135.
35. R. Block et al., see [33], Report BB-10.

DEPOSITED ARTICLES

ASYMPTOTIC NEUTRON DISTRIBUTION IN A NONMULTIPLYING TWO-ZONE CYLINDRICAL MEDIUM

A. L. Polyachenko

UDC 539.125.5.33

The two problems of the stationary and nonstationary one-velocity diffusion of neutrons in a nonmultiplying two-zone cylindrical medium are considered. The asymptotic flux distributions are found explicitly; these admit a simple interpretation and can be used to determine the neutron characteristics of the system from experimental data. The subscript i = 1 refers to the material inside a cylinder of radius R and i = 2 to the external medium; α = T refers to thermal and α = E to epithermal neutrons, ρ and z are cylindrical coordinates and the z axis is along the axis of the system, t is the time after a pulse, $D_{\alpha i}$, $\Sigma_{\alpha i}$, and $\varphi_{\alpha i}$ are the group values of the diffusion coefficient, the capture cross section, and the neutron flux in the α-th group in the i-th medium, and $\Phi_{\alpha 2}$ is the flux in the uniform infinite external medium calculated in the same approximation as $\varphi_{\alpha i}$.

For a pulsed neutron source the solution is obtained for an arbitrary distribution of the slowing-down density. By using a number of theorems of analyticity formulated but not proved in this paper it is shown that there are four types of solutions corresponding to the four combinations of signs of the quantities $\Sigma_{T2} - \Sigma_{T1}$ and $D_{T2} - D_{T1}$. At a time $t > t_{ac}$ there remain two types of asymptotic solutions:

1. Weak Absorption ($\Sigma_{T2} < \Sigma_{T1}$):

$$\varphi_{Ti}^{-} = A^{-} G_{Ti}^{-}(\rho) \exp\left(-\Sigma_{T2} v_T t - \frac{z^2}{4(\Lambda_{\parallel}^{-} + D_{T2} t)}\right) \times (\Lambda_{\perp} + D_{T2} t)^{-1} (\Lambda_{\parallel}^{-} - D_{T2} t)^{-1/2}.$$

2. Strong absorption ($\Sigma_{T2} > \Sigma_{T1}$):

$$\varphi_{Ti}^{+} = A^{+} G_{Ti}^{+}(\rho) \exp\left(-\Sigma_{\text{eff}} v_T t - \frac{z^2}{4(\Lambda_{\parallel}^{+} + D_{\text{eff}} t)}\right) \times (\Lambda_{\parallel}^{+} + D_{\text{eff}} t)^{-1/2}.$$

The functions $G^{\pm}$ and the effective parameters Σ_{eff}, D_{eff}, $\Lambda_{\parallel}^{\pm}$, and $\Lambda_{\perp}$ are evaluated explicitly. Thus

$$\Sigma_{\text{eff}} = \Sigma_1 + \Psi(\Sigma_{T2} - \Sigma_{T1};\ D_{T1}\Omega;\ \gamma_T);$$

$$\Psi(u; v; \gamma_\alpha) = \frac{u + v - \sqrt{(u-v)^2 + 4\gamma_\alpha uv}}{2(1-\gamma_\alpha)};$$

$$\gamma_\alpha(\sigma_\alpha) = 2\frac{D_{\alpha 1}}{D_{\alpha 2}}\left[\frac{K_0(R\sqrt{(\Sigma_{\alpha 2} - \sigma_\alpha)/D_{\alpha 2}})}{K_1(R\sqrt{(\Sigma_{\alpha 2} - \sigma_\alpha)/D_{\alpha 2}})}\right]^2;$$

$$\sigma_T = \Sigma_{T1};\ \sigma_E = \Sigma_{E1} D_{E2}/D_{E1};\ \Omega = (2.405/R)^2.$$

In the first case a measurement of $\varphi_T(t, z)$ in the inner zone permits the determination of the diffusion parameter Σ_{T2} and D_{T2} of the outer zone, but not in the second case except for small R when $\Sigma_{\text{eff}} \to \Sigma_{T2}$ and $D_{\text{eff}} \to D_{T2}$, which was confirmed experimentally.

For a steady point neutron source inside the cylinder the asymptotic z distribution of epithermal neutrons is determined by the sign of the difference $\mu_{E2} - \mu_{E1}$, where $\mu_{\alpha i}^2 = \Sigma_{\alpha i}/D_{\alpha i}$:

1. Weak slowing down ($\mu_{E2} < \mu_{E1}$)

$$\varphi_{Ei}^{-} = B^{-} G_{Ei}^{-}(\rho) \frac{1}{z} \exp(-\mu_{E2} z) \sim \Phi_{E2}(z).$$

2. Strong slowing down ($\mu_{E2} > \mu_{E1}$)

Translated from Atomnaya Énergiya, Vol. 40, No. 4, p. 332, April, 1976. Original article submitted May 21, 1975; abstract submitted October 1, 1975.

$$\varphi_{Ei}^{+}=B^{+}G_{Ei}^{+}(\rho)\exp(-\mu_{\text{eff}}z);$$

$$\mu_{\text{eff}}=\sqrt{\mu_{E1}^{2}+\Psi(\mu_{E2}^{2}-\mu_{E1}^{2};\ \Omega;\ \gamma_{E})}.$$

The asymptotic behavior of the stationary thermal neutron flux calculated in the two-group approximation is determined by which of the quantities $\mu_{\alpha i}$ is the smaller; accordingly there are four types of solutions. Thus for nuclear geophysics the characteristic case is $\mu_{E2} = \min \mu_{\alpha i}$, for which $\varphi_{T1,\ ac} \sim (1/z)\exp(-\mu_{E2}z) \sim \Phi_{T2}(z) \sim \Phi_{E2}(z)$. The result obtained in the few-group approximation

$$\varphi_{E1}(z) \sim \varphi_{T1}(z) \sim \Phi_{E2}(z);\ z > z_{ac};\ \mu_{E2} = \min$$

is confirmed by a numerical calculation in the six-group removal-diffusion model. The measurement of the dependence of φ_{E1} and φ_{T1} on z permits the determination of the asymptotic neutron relaxation length in the outer zone of the system.

The transient forms of the distributions have been obtained explicitly for both problems in the regions $t \lesssim t_{ac}$ and $z \lesssim z_{ac}$, which include the rapidly decreasing harmonics in addition to $\varphi_{\overline{ac}}$; these enable us to estimate the limiting values of t_{ac} and z_{ac}.

A comparison of the analytic properties of the spectra of the solutions, the structure of the solutions for arbitrary values of t and z, and the asymptotic behavior of the nonstationary and stationary problems shows that for a steady source the z coordinate plays the role of the time t for a pulsed source.

NEUTRON IMPORTANCE FUNCTION IN HETEROGENEOUS REACTORS

V. A. Dulin

UDC 621.039.51.12:539.125.52

We present a deviation of the multigroup equation for the neutron importance function relative to asymptotic power in an integral formulation. The equation describes the spatial and energy distributions of the importance φ_n^{+i} of neutrons in a heterogeneous reactor [1] in the usual notation.

$$\sum_{\text{trn}}^{i} \Delta x_n \varphi_n^{+i} = \sum_{m=1}^{M} \sum_{k=1}^{G} P_{m\to n}^{i} \Delta x_m W_m^{i\to k} \varphi_m^{+k}.$$

It is not the same as the adjoint of the equation for a heterogeneous neutron flux in integral form.

In the transition to a homogeneous reactor it describes the homogeneous neutron importance.

The spatial distribution over a cell of the neutron importance averaged over the fission spectrum was calculated and measured in the BFS-26 and BFS-30 zero-power heterogeneous critical slab reactors [2].

The measurements were performed by displacing a miniature ^{252}Cf source of spontaneous fission neutrons perpendicular to the layers of material and recording the relative level of the asymptotic power. The measured and calculated results shown in Fig. 1 are in good agreement.

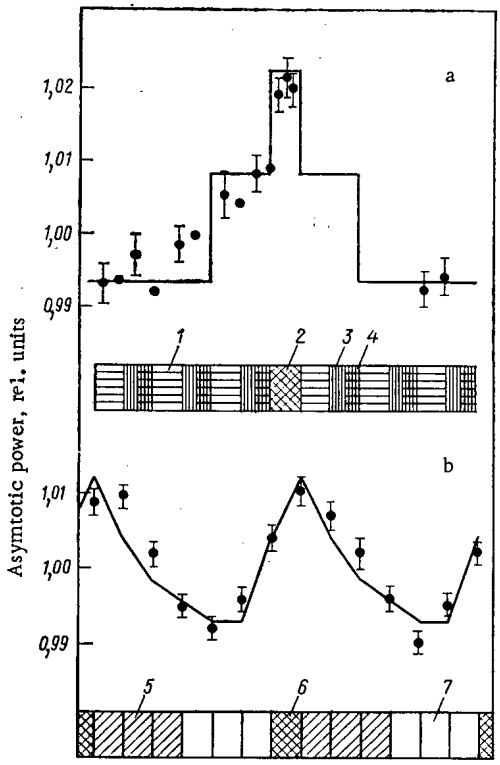

Fig. 1. Variation of asymptotic power in the displacement of a ^{252}Cf neutron source normal to the layers in the heterogeneous fast critical assemblies a) BFS-26 and b) BFS-30: 1) C; 2) ^{235}U — Al; 3) Al; 4) steel; 5) $^{238}UO_2$; 6) ^{235}U — Al; 7) Na.

Translated from Atomnaya Énergiya, Vol. 40, No. 4, p. 333, April, 1976. Original article submitted January 24, 1975; abstract submitted November 20, 1975.

LITERATURE CITED

1. F. Storrer et al., Nucl. Sci. and Engng., 24, 153 (1966).
2. V. A. Dulin et al., in: Proc. of IAEA Symp. on Fast-Reactor Physics, Tokyo, Oct. (1973), p. I, Rep. A-26.

LETTERS

IN-CORE SYSTEM FOR AUTOMATIC POWER CONTROL OF IRT-M REACTOR

L. G. Andreev, Yu. I. Kanderov,
M. G. Mitel'man, N. D. Rozenblyum,
V. P. Chernyshevich, and Yu. M. Shipovskikh

UDC 621.039.562:621.039.55

This paper gives developmental results for an in-core system of automatic power control for the IRT-M reactor and a determination of the metrologic characteristics of the system of in-core detectors with inertial correctors as compared to extra-core standard ionization chambers. Direct-charge detectors (DCD) with rhodium emitters, which are used in the in-reactor monitoring system (IMS) of the IRT-M reactor, were used as sensors for the automatic power control system. The IMS system consists of six DCD sets arranged along a diameter of the core and each set consists of five commerical type-DPZ-1P DCD positioned along the height of the core [1].

The DCD is presently the most promising of the in-reactor detectors of energy release for application in any reactor [2]. Activation DCD are inertial because of the decay time of the induced isotope, but the use of simple correctional devices makes it possible to measure neutron flux density with practically no inertia [3]. The transfer function W(p) of the correctional device must satisfy the condition

$$H(p)\,W(p) = K,$$

where K is the static transfer factor of the DCD-corrector unit; H(p) is the DCD transfer function; p = d/dt.

A DCD with rhodium emitter has a great advantage over other types of activation and Compton detectors because of high sensitivity which provides a favorable signal-to-background ratio.

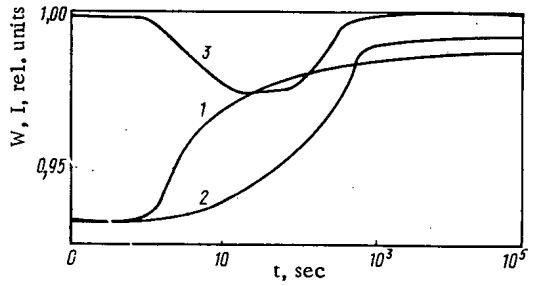

Fig. 1

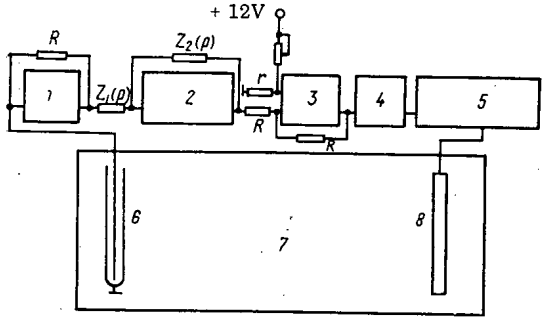

Fig. 2

Fig. 1. Contribution to reactor energy release from decay of fission products and transient responses of DCD-corrector and reactor-DCD-corrector units.

Fig. 2. Block diagram of automatic power control system for IRT-M reactor: 1) constant-current amplifier; 2) corrector; 3) power sensor; 4) power-control amplifier; 5) motor amplifier with servodrive; 6) direct-charge detector; 7) reactor; 8) automatic control rod.

Translated from Atomnaya Énergiya, Vol. 40, No. 4, pp. 335-337, April, 1976. Original article submitted December 30, 1975; revision submitted May 19, 1975.

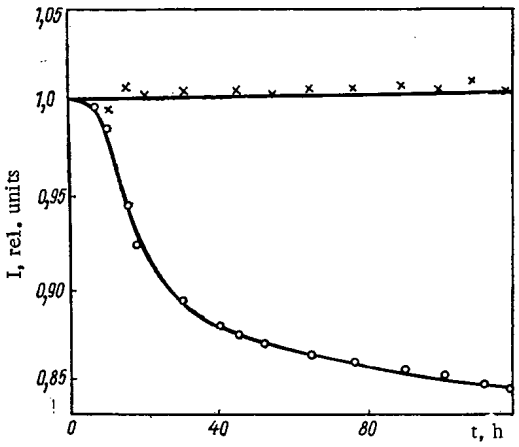

Fig. 3. Comparison of IC and DCD current over a weekly operating cycle of IRT-M reactor: ×) total DCD current; ○) IC current.

In the construction of an automatic control system, it is necessary to take into account the inertial nature of energy release associated with the delay of heat release from the decay of fission products. The time dependence of relative energy release [4] for a stable number of fissions is given by curve 1 in Fig. 1, which indicates that the power of the reactor increases for a considerable length of time after the reactor reaches a stable operating mode because of the decay of fission products; the increase amounts to 7%. For noninertial measurement of reactor power, therefore, a corrector is required with a transfer function S(p) satisfying the condition D(p)S(p) = K where D(p) is the transfer function of the reactor. This paper gives an approximation based on the similarity between the decay law for the isotope ^{104m}Rh and the law for variation of energy release after a step change in neutron flux density. Curve 2 gives the transient response of a rhodium DCD with an inertial corrector which corrects for the inertial characteristics caused by the formation of ^{104}Rh.

The transient response of the reactor-DCD-corrector unit, where the DCD with corrector serves as a detector of energy release, is given by curve 3 and differs from the ideal by no more than 3%.

A block diagram of the system developed for automatic reactor power control is shown in Fig. 2. A constant-current preamplifier amplifies the DCD current and matches the input potential of the inertial corrector to the DCD. Power sensors were assembled from K2UT402 microcircuits. A KSP-4 recorder and N-700 loop oscillograph were used to monitor power. A comparison of readings, normalized at the

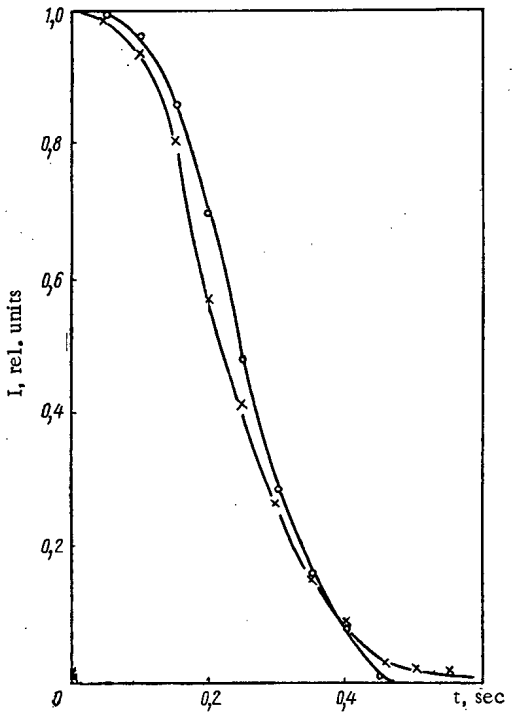

Fig. 4

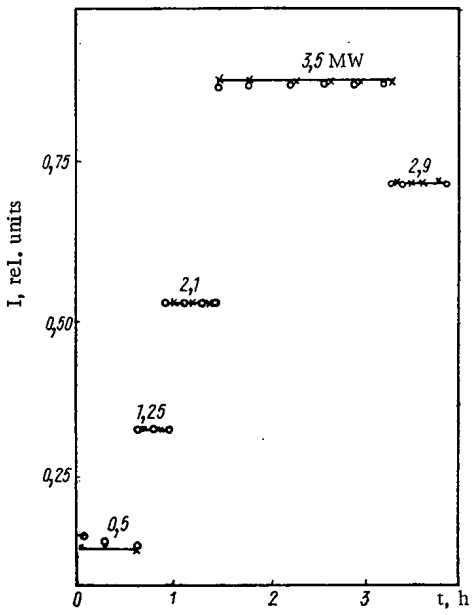

Fig. 5

Fig. 4. Readings from IC (○) and DCD-corrector unit (×) when rods of safety and control systems were dropped into the core.

Fig. 5. Readings from IC (○) and DCD-corrector unit (×) during control of reactor power by DCD-corrector.

maximum, from an in-core DCD and from an external KNK-53 ionization chamber (IC) used operationally for power determination in a stable operating mode of the reactor is shown in Fig. 3 which indicates that for constant reactor thermal power, the readings of the IC varied by 17% over 120 h of operation while the readings of the DCD remained practically constant. The actual change in the IC sensitivity as a sensor for power control was associated with shifting of compensating rods; it is therefore preferable to use in-core DCD as power sensors. The time characteristics of the DCD-inertial corrector unit and of an ionization chamber were compared. For this purpose, the safety and compensating rods were dropped into the reactor core and the readings from DCD-corrector and IC displayed on the loop oscillograph. Results of the measurements, normalized at the maximum, are shown in Fig. 4. Analysis of transient processes during rapid introduction of negative reactivity showed that the inertia of the DCD-corrector unit was no worse than the IC inertia in the relative signal range 0.05-1.0. IC inertia, which is determined by the time constant with the capacity of connecting wires and the load resistance included along with neutron transit time to the IC, is $(1\text{-}10)\cdot 10^{-3}$ sec. The discrepancy between DCD and IC readings at relative signal values < 0.05 is explained by the inertia of energy release not measured by the IC. The equipment was tested in the automatic power control mode (see Fig. 2). In this case, the total current readings from DCD and IC were compared. The time dependence of DCD and IC readings is shown in Fig. 5 for different thermal powers of the reactor and indicates that regulation was effective in the power range 0.5-3.5 MW.

The authors are grateful to B. K. Ignatov for discussion of the work and continued interest in it and to V. M. Vertogradskii for help in some of the experiments.

LITERATURE CITED

1. Direct-Charge Detectors, Technical Specifications TU16-538, 243-74 [in Russian].
2. M. G. Mitel'man et al., in: Metrology of Neutron Radiation at Reactors and Accelerators [in Russian], Vol. 1, Izd. Standartov, Moscow (1972), p. 115.
3. N. D. Rozenblyum et al., in: Dosimetry of Intense Fluxes of Ionizing Radiation [in Russian], Fan, Tashkent (1969), p. 130.
4. A. M. Weinberg and E. P. Wigner, Physical Theory of Neutron Chain Reactors, Univ. of Chicago Press (1958).

DETERMINATION OF IRRADIATION TEMPERATURE FROM MEASUREMENT OF LATTICE CONSTANT OF RADIATION VOIDS

Y. V. Konobeev

UDC 621.039.531:669.45

A method was proposed [1] for the determination of irradiation temperature in those parts of a fast-neutron reactor in which the placement of thermocouples or other temperature indicators was impossible for one reason or another. The method was based on the high sensitivity to irradiation temperature of the lattice constant of the body-centered cubic (bcc) lattice of voids in molybdenum and other heat-resistant metals produced, as is well known, in these materials after irradiation by neutron fluxes of 10^{22} neutrons/cm^2 ($E > 0.1$ MeV) and measured by transmission electron microscopy. The following relation between the void lattice constant a_L and the absolute irradiation temperature T was proposed [1]:

$$a_L = \alpha T;\ \alpha = 0.32\ ^\circ\text{K}. \tag{1}$$

A comparison between values of a_L calculated from Eq. (1) and experimental values (Table 1) demonstrates the poor description of experimental data for molybdenum irradiated in a reactor at elevated temperatures. Somewhat better agreement with experiment can be obtained if one uses the relation $N_V \sim \exp(-\beta T)$ [2] to describe the temperature behavior of void concentration in irradiated metals and considers that N_V and a_L are connected through the relation $N_V = 2/a_L^3$ for a bcc lattice. Table 1 gives values of a_L calculated from the relation

$$a_L = 54.57 \exp\left(\frac{T}{530.79}\right),\ \text{Å}, \tag{2}$$

which was arrived at by least-square analysis of the experimental data. For $T_{irr} = 1000^\circ$C, the calculated value of a_L differs from the experimental value by an amount which considerably exceeds the error in measurement of a_L (Table 1).

The purpose of this report is to show that existing data for a_L in molybdenum are well described by the relation

TABLE 1. Experimental and Calculated Values of Void Lattice Constant in Molybdenum Irradiated by Fast Neutrons

T_{irr}, °C	Reactor	Void lattice constant, Å			
		experimental a_L, Å	calculated from Eq.		
			(1)	(2)	(3)
430	EBR-11	220 [2]	225	205	221
580	EBR-11	270 [2]	272	272	268
585	EBR-11	265 [3]	275	274	270
640	DFR	300 [4]	292	304	293
680	EBR-11	320 [2]	305	328	312
800	EBR-11	390—410 [2]	343	412	390
900	EBR-11	470 [2]	375	497	491
1000	EBR-11	660 [2]	407	600	664

Translated from Atomnaya Énergiya, Vol. 40, No. 4, pp. 337-338, April, 1976. Original article submitted July 16, 1975.

$$a_L = 121\ \text{Å}\ \frac{1558\ ^\circ\text{K}}{1558\ ^\circ\text{K} - T}. \quad (3)$$

The critical temperature $T_c = 1558^\circ\text{K} = 0.52T_f$ coincides with the upper temperature limit for the existence of vacancy porosity in heat-resistant metals. Equation (3) may indicate the existence of a special phase transition associated with the formation of a spatial void lattice. According to Eq. (3), the void concentration should depend on irradiation temperature in the following manner,

$$N_v \sim \left(\frac{T_c - T}{T_c}\right)^3 \quad (4)$$

and reach a maximum value of $1.1 \cdot 10^{18}$ cm^{-3} for molybdenum when $T \to 0$. For further verification of Eqs. (2) and (3), there is particular interest in data for a_L at elevated temperatures in the range from 0.44 T_f to 0.52 T_f.

LITERATURE CITED

1. J. Moteff and V. Sikka, Trans. Amer. Nucl. Soc., 16, 97 (1973).
2. V. Sikka and J. Moteff, J. Nucl. Mater., 54, 325 (1974).
3. F. Wiffen, in: Proc. AEC Symp. Radiation-Induced Voids in Metals, New York, June 9-11, 1971, p. 386.
4. B. Eyre and A. Bartlett, J. Nuc. Mater., 47, 143 (1973).

SLOWING DOWN OF RESONANCE NEUTRONS IN MATTER

D. A. Kozhevnikov

UDC 539.125.5.174.162.3:539.125.5.162.3

Penetration of a Neutron Pulse through Resonances in the Scattering and Absorption Cross Sections. In neutron slowing-down theory an analytic expression for the Green's function of the nonstationary transport equation has been obtained in only three cases: a) $\sigma_s(E) = \text{const}$, $\sigma_a(E) = \text{const}$; b) $\sigma_s(E) = \text{const}$, $\sigma_a(E) \sim 1/v$; c) $\sigma_s \sim 1/v$, $\sigma_a \sim 1/v$ [1]. The last case has no practical application. The most interesting problem is the study of the nonstationary neutron distribution in matter, taking account of the resonance structure of the interaction cross sections. In the present paper we give an analytic solution of this general problem based on the use of the "causal" form of the central limit theorem.

The energy — time neutron distribution function in matter of arbitrary composition for an arbitrary energy dependence of the interaction cross sections is found by solving the generalized Weinberg — Wigner — Corngold — Orlov equation* by the method of spectral approximations and has the following integral representation [3]:

$$\psi_0(t, u) = \frac{1}{2\pi i}\int_{\sigma-i\infty}^{\sigma+i\infty} \psi_0(s, u)\, e^{st}\, ds, \tag{1}$$

where

$$\psi_0(s, u) = \frac{\psi_0(u)\,\psi_0(s, u^+)\, e^{-A(s,u)}}{[1+s\tau(u)]\,[1-\delta\xi_1(s, u)]}; \tag{2}$$

$$\psi_0(u) = \frac{h(u^+)}{\bar{\xi}(u)} \exp\left[-\int_{u^+}^{u} g(u')\,\frac{du'}{\bar{\xi}(u')}\right]; \tag{3}$$

$$\delta\xi_1(s, u) = \frac{1}{\bar{\xi}(u)}[\xi_1(s, u) - \xi_1(u)]; \tag{2a}$$

$$A(s, u) = \int_{u^+}^{u} \frac{sh(u')\,\tau(u') + g(u')\,[1+s\tau(u')]\,\delta\xi_1(s, u)}{[1+s\tau(u')]\,[1-\delta\xi_1(s, u^1)]} \times \frac{du'}{\bar{\xi}(u')}; \tag{2b}$$

u^+ is the initial lethargy, $h(u) = 1 - g(u)$ is the total scattering probability, $\tau(u)$ is the mean free time, $\psi_0(s, u^+)$ is the transform of the Green's function of the nonstationary one-velocity transport equation, and the quantities $\bar{\xi}(u)$, $\xi_1(u)$, and $\xi_1(s, u)$ are defined by Eqs. (8), (9), and (19) respectively of [3].

To take account of the resonance structure of the cross sections we divide the slowing-down interval $[u^+, u]$ into a sufficiently large number N of appropriate subintervals $[u_{k-1}, u_k]$, $1 \le k \le N$, $u_N \equiv u$ such that in each of them the scattering and absorption cross sections can be considered constant. Then

$$A(s, u) = \sum_{k=1}^{N} A_k(s),$$

and we can write (2) in the form

*This equation is one of the exact noncanonical forms of the transport equation [2].

Translated from Atomnaya Énergiya, Vol. 40, No. 4, pp. 338-339, April, 1976. Original article submitted January 8, 1975; revision submitted November 11, 1975.

$$\psi_0(s, u) = \psi_0(u) \prod_{k=0}^{N+1} f_k(s), \tag{4}$$

where $f_0(s) = \psi_0(s, u^+)$; $f_k(s) = e^{-A_k(s)}$, $1 \leqslant k \leqslant N$;

$$f_{N+1}(s) = \{[1 + s\tau(u)][1 - \delta\xi_1(s, u)]\}^{-1}.$$

Consequently

$$\psi_0(t, u) = \frac{\psi_0(u)}{2\pi i} \int_{\sigma - i\infty}^{\sigma + i\infty} \prod_{k=0}^{N+1} f_k(s)\, e^{st}\, ds = \psi_0(u) \int_0^\infty dt_0 f_0(t_0) \ldots \int_0^\infty dt_{N+1} f_{N+1}(t - t_0 - \ldots - t_{N+1}). \tag{5}$$

When the following conditions are satisfied:

1) The third time moment of $\psi_0(t, u)$ is finite and smaller than the arbitrary constant C, $\overline{t^3} < C$; 2) the sum of the variances $d_k[t]$

$$\left[d_k[t] = \int_0^\infty (t - \langle t \rangle_k)^2 f_k(t)\, dt \Big/ \int_0^\infty f_k(t)\, dt,\ 0 \leqslant K \leqslant N+1 \right]$$

has the property $D[t] = \sum_{k=0}^{N+1} d_k[t] \to \infty$ as $u \to \infty$; as a consequence of the central limit theorem for "causal" functions [$\psi_0(t < 0, u) = 0$] the multiple convolution (5) converges to the Γ distribution [4]*

$$\psi_0(t, u) = \psi_0(u) \frac{\alpha(\alpha t)^\varkappa e^{-\alpha t}}{\Gamma(\varkappa + 1)} H(t) \tag{6}$$

with the parameters $\alpha \equiv \alpha(u) = \langle t \rangle / D[t]$, $\langle t \rangle \equiv \langle t(u) \rangle = \sum_{k=0}^{N+1} \langle t_k \rangle$, $\varkappa = (\langle t^2 \rangle / D[t]) - 1 \equiv \varkappa(u)$; H(x) is the Heaviside function. The quantities $\langle t \rangle$ and $D[t]$ are calculated directly:

$$\langle t \rangle = \left[-\sum_{k=0}^{N+1} \frac{f_k'(s)}{f_k(s)} \right]_{s=0} = \tau(u^+) + \sum_{k=1}^{N} \langle t \rangle_k + \theta(u_N); \tag{7}$$

$$D[t] = \left\{ \sum_{k=0}^{N+1} \frac{f_k''(s)}{f_k(s)} + \left[\sum_{k=0}^{N+1} \frac{f_k'(s)}{f_k(s)} \right]^2 \right\}_{s=0} = \tau^2(u^+) + \sum_{k=1}^{N} d_k[t] + \overline{\theta}^2(u_N). \tag{8}$$

The result (6) was predicted by M. V. Maslennikov [6] in a general formulation. Equations (7) and (8) express the additivity property of the integral characteristics of the distribution function with respect to the partitioning of the slowing-down interval $[u^+, u_N]$. The terms θ and $\overline{\theta}^2$ correspond to the contribution of the last path. If we let $N \to \infty$ and replace the sums by integrals Eqs. (7) and (8) go over respectively into Eqs. (35) and (43) of [3]; i.e. in general

$$\varkappa = \frac{\langle t(u) \rangle^2}{D[t(u)]} - 1; \quad \alpha = \frac{\langle t(u) \rangle}{D[t(u)]}; \tag{9}$$

$$t_{\max}(u) = \frac{\varkappa(u)}{\alpha(u)} \equiv \langle t(u) \rangle - \alpha^{-1}(u). \tag{10}$$

Thus for a moderator of arbitrary composition and energy-dependent cross sections the time distribution of moderated neutrons is described by the gamma distribution (6) with parameters determined by the integral characteristics – the total slowing-down time $\langle t(u) \rangle$ and the variance $D[t(u)]$; the position of the maximum coincides with the slowing-down time proper $t_0(u)$.

Conditions 1) and 2) impose unessential restrictions on the type of energy dependence of the total interaction cross section. That is, distribution (6) does not hold if the mean free time does not depend on the neutron energy.

LITERATURE CITED

1. M. Williams, Thermalization and Slowing Down of Neutrons, McGraw-Hill, New York (1962).
2. D. A. Kozhevnikov and Sh. K. Nasibullaev, Dokl. Akad. Nauk SSSR, 205, No. 6, 1320 (1972).
3. D. A. Kozhevnikov and V. S. Khavkin, At. Énerg. 27, No. 2, 143 (1969).
4. A. Papoulis, Integral Transforms and Applications, Pergamon, New York (1964).
5. C. Cyros, Nukleonik, 8, No. 8, 461 (1966).
6. M. V. Maslennikov, Zh. Vychisl. Matem. i Matem. Fiz., No. 6, 1136 (1961).

*The effectiveness of the use of the central limit theorem in transport theory was first noted by Cyros [5].

MEASUREMENT OF α IN THE RESONANCE REGION

Yu. V. Ryabov

UDC 539.173.4

The experimental determination of the ratio of the radiative capture and fission cross sections $\alpha(E_n) = \sigma_c(E_n)/\sigma_f(E_n)$ for the transuranium isotopes over a wide range of neutron energies is of considerable interest for reactor engineering and nuclear physics.

The methods which have been used to measure $\alpha(E_n)$ [1-7] cannot ensure the required accuracy (3-5%) [8] because of uncertainties in the separation of capture gamma rays from the total gamma spectrum, the possible dependence of the capture and fission gamma spectra on the quantum characteristics of the compound nucleus with the determination, as a minimum, of two normalization constants in the calibration of $\alpha(E_n)$ etc. [9]. These shortcomings are characteristic of the most widely used method of measuring $\alpha(E_n)$ in which low-efficiency detectors are used to measure prompt fission neutrons and capture and fission gamma rays.

In the present paper we present an improvement of the method for measuring $\alpha(E_n)$ and show that the new experimental arrangement avoids some uncertainties and increases the accuracy and reliability of the results.

Method of Measurement. At the present time two methods are used to measure $\alpha(E_n)$. In the first method [2-5] gamma photons are recorded with high efficiency by a large liquid scintillation detector which decreases the sensitivity of the method to variations of the gamma spectrum and variations of the number of prompt fission neutrons. However, the total background of such a detector is high and can lead to appreciable uncertainties, which decrease the accuracy. Moreover an arrangement of this type is expensive and complicated to operate. In the second method [1, 6], which is considered in the present paper, the capture and fission gamma rays (gamma channel) and the prompt fission neutrons (fission channel) are recorded by small scintillation detectors with relatively low efficiency (~1%). In this case after taking account of the total background the expression for calculating $\alpha(E_n)$ in the thin-sample approximation has the form [1]

$$\alpha(E_n)=\frac{A\left[\frac{n_\gamma(E_n)}{n_f(E_n)}\right]-1}{B-\left[\frac{n_\gamma(E_n)}{n_f(E_n)}\right]C}, \tag{1}$$

where

$$A=\frac{\sum_\nu [1-(1-\varepsilon_{nf})^\nu]\,P(\nu)}{\int_{E_1}^{E_2}\varepsilon_\gamma^f(E)\,\nu_\gamma^f(E)\,dE};\quad B=\frac{\int_{E_1}^{E_2}\varepsilon_\gamma^c(E)\,\nu_\gamma^c(E)\,dE}{\int_{E_1}^{E_2}\varepsilon_\gamma^f(E)\,\nu_\gamma^f(E)\,dE};\quad C=\frac{\int_{E_a}^{E_b}\varepsilon_\gamma^{cf}(E)\,\nu_\gamma^c(E)\,dE}{\int_{E_1}^{E_2}\varepsilon_\gamma^f(E)\,\nu_\gamma^f(E)\,dE}.$$

Here $n_f(E_n)$ is the rate of counting prompt fission neutrons (fission channel), $n_\gamma(E_n)$ is the rate of counting gamma photons in the energy range from E_1 to E_2 (gamma channel), ν is the number of prompt neutrons emitted per fission, $P(\nu)$ is the probability of the emission of ν neutrons per fission, ε_{nf} is the efficiency of recording a prompt neutron of the fission spectrum in the fission channel, $\nu_\gamma^c(E)dE$ and $\nu_\gamma^f(E)dE$ are the numbers of radiative capture and fission gammas with energies between E and E + dE, $\varepsilon_\gamma^c(E)$ and $\varepsilon_\gamma^f(E)$ are the counting efficiencies for the respective gamma photons in the gamma channel, $\varepsilon_\gamma^{cf}(e)$ is the efficiency of recording captures in the fission channel, and E_a and E_b are the energy ranges of recording gamma rays by the neutron detector.

Translated from Atomnaya Énergiya, Vol. 40, No. 4, pp. 339-342, April, 1976. Original article submitted May 26, 1975; revision submitted August 13, 1975.

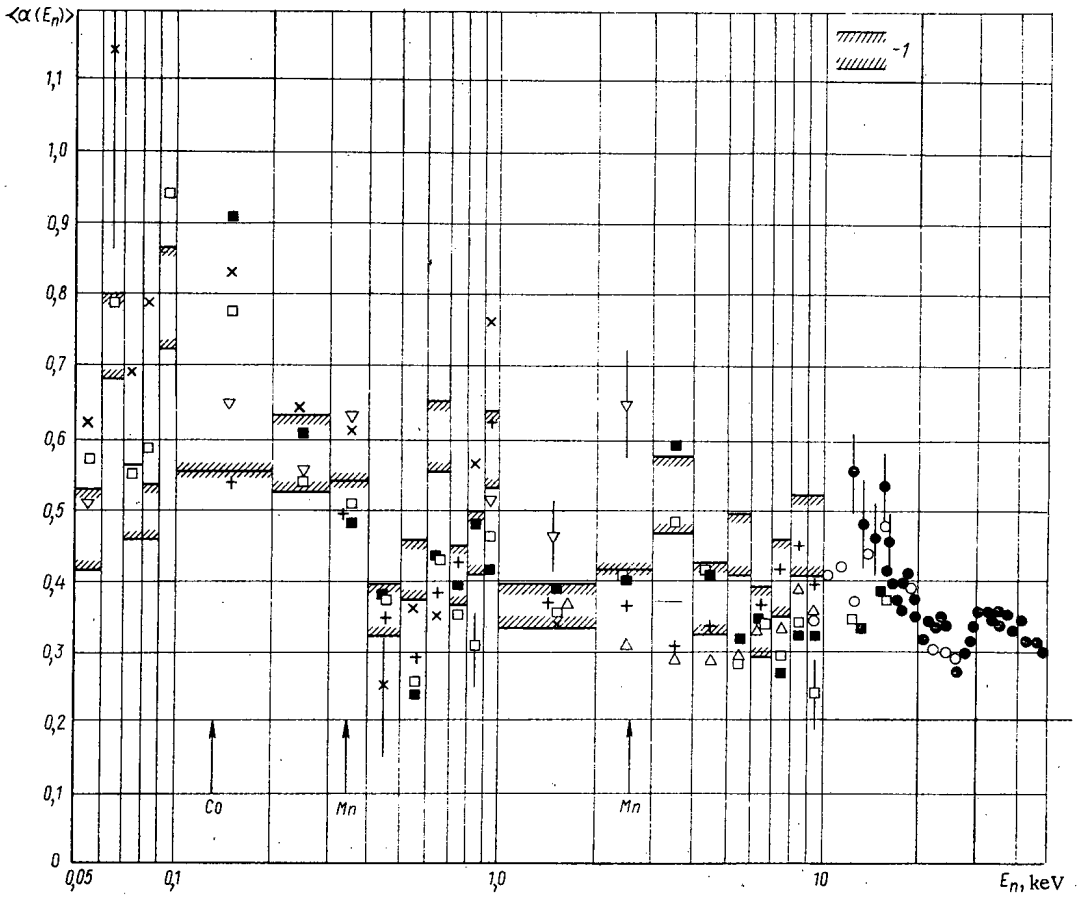

Fig. 1. Comparison of experimental data on $\langle \alpha(E_n) \rangle$ for ^{235}U with results reported in the following papers: 1) our data; ■, □) JINR (1965, 1970) [2, 3]; x, +) ORNL (1965, 1973) [4, 5]; Δ) LRL (1970) [6]; ▽) IAÉ (1970) [7]; ●) FÉI (1973) [18]; ○) KFK (1971) [19].

The quantities A, B, and C are assumed constant and are determined by normalization to known values of α_0 for well-isolated resonances or a certain range of energies [1, 3]. In this case it is always assumed that the spectrum and the multiplicity of the capture and fission gamma radiation are uncorrelated and do not depend on the quantum characteristics of the neutron resonances and consequently on the neutron energy. Similar assumptions are made concerning the characteristics of the neutron radiation accompanying fission. In addition it was previously assumed that the number of counts of gamma photons and prompt fission neutrons is strictly proportional to the number of fission fragment counts, i.e., to the fission cross section. Thus in taking account of the contribution of fission gammas to the total gamma spectrum, and experiment shows they contribute up to 80% [9], we can replace the dependence of the number of counts of fission gammas by the number of counts of prompt neutrons or fission products as follows from Eq. (1). In thorough investigations of recent years performed to increase the accuracy of $\alpha(E_n)$ [3, 5-7] particular attention has been paid to improving the experimental technique but the general approach to the measurements has remained unchanged and is determined by Eq. (1). However, it was noted in [2, 10, 11] that the values of the resonance integrals and the average fission cross sections calculated with high accuracy from differential data depend on whether they were obtained by recording fission fragments or the radiations accompanying fission. Even in this case measurements performed by both methods on the same time-of-flight spectrometer gave results in certain energy ranges which differed by several times the experimental errors [11]. It turned out also that in measuring fission cross sections using secondary neutrons or gamma rays by methods sensitive to the multiplicity of the secondary radiation significantly different results are obtained [12]. Fluctuations of up to 14% were found in the values of $\bar{\nu}$, $E_{\gamma\,tot}$, and $\bar{\nu}_\gamma^f$ for individual fission resonances of ^{239}Pu [13]. It is natural to account for these factors affecting the accuracy of the measurements of $\sigma_f(E_n)$ and $\alpha(E_m)$ by the individual properties of the neutron resonances and primarily by the total momentum, its projection on the axis of symmetry of the nucleus, and the pertinent characteristics of the fission barriers and the subbarrier fluctuations in the fission cross

sections. In this case even for the level of accuracy of the measurements of $\alpha(E_n)$ which has been achieved there is no adequate basis for considering the quantities A, B, and C in Eq. (1) to be strictly constant, and consequently to increase the accuracy further it is necessary either to develop methods which are insensitive to changes in these quantities or to develop new methods taking account of these changes experimentally.

One possible path in the second direction consists in improving the most widely used method of measuring $\alpha(E_n)$ by using low-efficiency detectors. Thus to terms of second order in C ($C \leqslant 10^{-2}$) Eq. (1) can be put in the form

$$\alpha(E_n)=\left[\int_{E_1}^{E_2}\varepsilon_\gamma^c(E)\,\nu_\gamma^c(E)\,dE\right]^{-1}\left\{\frac{n_\gamma(E_n)}{n_f(E_n)}\times\left[\sum_\nu[1-(1-\varepsilon_{nf})^\nu]\,P(\nu)-k\int_{E_a}^{E_b}\varepsilon_\gamma^{cf}(E)\,\nu_\gamma^c(E)\,dE\right]-\frac{n_\gamma^f(E_n)}{n_f(E_n)}\right\}, \tag{2}$$

where $n_\gamma^f(E_n)=\int_{E_1}^{E_2}\varepsilon_\gamma^f(E)\,\nu_\gamma^f(E)\,dE\{\sum_\nu[1-(1-\varepsilon_{nf})^\nu]\times P(\nu)\}N_f$ is the rate of counting gamma photons in coincidence with fissions in those same energy ranges of recording as in the total gamma spectrum; $k \approx 1$. It is clear from (2) that the main source of uncertainty is the quantity $\int_{E_1}^{E_2}\varepsilon_\gamma^c(E)\,\nu_\gamma^c(E)\times dE = f(E_n)$, on which $\alpha(E_n)$ depends linearly. Then in the notation of "generalized efficiencies" when $\varepsilon_{nf} \ll 1$ Eq. (2) can be written in a form convenient for the processing of experimental data:

$$\langle\alpha(E_n)\rangle=\frac{1}{\bar\varepsilon_c}\left\{\frac{\langle n_\gamma(E_n)\rangle}{\langle n_f(E_n)\rangle}[\overline{\varepsilon_{nf}\nu_0}\,\langle R(E_n)\rangle-\bar\varepsilon_{cf}k]-\frac{\langle n_\gamma^f(E_n)\rangle}{\langle n_f(E_n)\rangle}\right\}, \tag{3}$$

where $\langle R(E_n)\rangle = \langle\overline{\nu}(E_n)/\overline{\nu}_0\rangle$ and can be measured in the same experiment by the method of [14]. Here $\langle\,\rangle$ denotes averaging over the selected energy interval and $\overline{\nu}_0$ is the normalized value for an individual resonance or chosen energy range.

Thus all the quantities in (3) except $\bar\varepsilon_c$ and $\bar\varepsilon_{cf}$ can be measured simultaneously in the same experimental arrangement. Since $\overline{\varepsilon_{nf}\nu_0}\langle R(E_n)\rangle \approx 100\,\bar\varepsilon_{cf}k$ the lack of information on the energy dependence of $\bar\varepsilon_{cf}$ cannot affect $\langle\alpha(E_n)\rangle$ in any way comparable with the uncertainty introduced by $\bar\varepsilon_c$. In spite of the fact that so far there is no experimental possibility of determining the dependence of $\bar\varepsilon_c$ on E_n, the proposed method of measurement nevertheless enables one to obtain the energy dependence of $\overline{\varepsilon_c(E_n)}\langle\alpha(E_n)\rangle$ in contrast with the ordinarily obtainable $a(E_n)[\langle\alpha(E_n)\rangle + b(E_n)]$. It is quite clear that under equivalent conditions of measurement the accuracy of the proposed method must be higher than that of previous methods.

Results of Measurements. The proposed method was tested experimentally [13]. The experimental data were obtained by a time-of-flight method with the linear electron accelerator (E_e = 65 MeV) at the Saclay Nuclear Research Center as a pulsed neutron source. The flight path of 12.5 m ensured a nominal resolution of 5.6 nsec/m for a 50-nsec width of the neutron pulse and the analyzer channels. A lead shadow shield was used to decrease the effect of the gamma ray pulse from the neutron source. The neutron beam was shut off by ^{10}B, Mn, and Co filters to eliminate recycled neutrons and to control the background.

Fissions were recorded by two NE-213 liquid scintillation detectors with gamma discrimination by pulse shape ($\bar\varepsilon_{cf} = 10^{-3}$) [14]. Fission and capture gamma rays were recorded by two NaI crystal detectors connected in a coincidence circuit having a lower bias of 0.55 MeV and an upper bias of 2.0 MeV. Gamma radiation in coincidence with fissions was recorded simultaneously.

A sample of ^{235}U metal (93.36%; $2.5\cdot10^{21}$ nuclei/cm^2) and four detectors were located in a plane perpendicular to the direction of the neutron beam. The detectors were covered with 5 mm of lead to shield against the natural radioactivity of the sample, and with filters of amorphous ^{10}B to shield against scattered neutrons. The parameters of the background curve were determined by using background points of the resonance filters for E_n = 132 eV(Co), 0.337 and 2.38 keV (Mn). The background was taken into account as in [2, 3]. Since $R(E_n)$ was not measured in the present work, in the normalization of the resonances to $\alpha_0(E_0$ = 3.14, 4.84, 6.4, 7.09, 11.66, 15.4, 16.66, 26.5, and 33.58 eV) [11, 15, 16] to obtain $\bar\varepsilon_c$ a correction to $\overline{\varepsilon_n\nu_0}$ was introduced in accord with the results of [17] and in the energy range investigated this quantity was assumed constant.

Figure 1 compares our results with those of [2-7, 18, 19]. An experimental account of the contribution of fission gammas to the total spectrum shows that since the ratio $n_\gamma^f(E_n)/(n_f E_n)$ fluctuates by 15-20%, there is an appreciable change in $\langle\alpha(E_n)\rangle$ in the following energy ranges: 0.1-0.2, 0.6-0.7, 3-4, and 5-6 keV. In addition, it should be noted that there is a small systematic decrease in the ratio $N_\gamma^f(E_n)/n_f(E_n)$ with an increase in the neutron interaction energy and consequently also an increase in $\alpha(E_n)$. Over the whole energy range the values of $\alpha(E_n)$ obtained by the proposed method are on the average somewhat higher than the known data, and the values averaged over broader energy ranges (0.1-1, 1-9.74, and 0.1-9.74 keV) are equal to 0.54 ± 0.05, 0.43 ± 0.05, and 0.48 ± 0.05 respectively. Our values of $\langle\alpha(E_n)\rangle$ in the range around 10 keV are in good agreement with the results obtained with electrostatic generators [18, 19].

The proposed method of measurement evidently yields the most reliable information on the energy dependence of α with minimum errors and uncertainties.

The author thanks professors R. Zhol' and A. Mishodon for the opportunity to perform the experiments, Zh. Troshon and B. Lyuka for help with the measurements, and V. N. Kononov and E. A. Poletaev for discussions and critical comments.

LITERATURE CITED

1. M. Sowerby et al., in: Proc. IAEA Symp. on Fast-Reactor Phys., Vol. 1, Karlsruhe, Oct. 30-Nov. 3 (1967), p. 289.
2. Yu. Ryabov, Van-Schi-Di, et al., in: Proc. IAEA Symp. on Phys. and Chem. of Fission, Vol. 1, Vienna (1965), p. 287.
3. M. A. Kurov et al., At. Énerg., 30, No. 3, 258 (1971).
4. G. Saussure et al., ORNL-TM-1804 (1967).
5. R. Perez et al., Nucl. Sci. and Engng., 52, 46 (1973).
6. J. Czirr and J. Lindsey, Nucl. Sci. and Engng., 41, 56 (1970).
7. G. V. Muradyan et al., in: Proc. IAEA Symp. on Nuclear Data for Reactors, Vol. 1, June 15-19, Heksinki (1970), p. 341.
8. P. Gribler et al., Nucl. Appl., 5, 297 (1968).
9. Yu. Ryabov, Preprint IAEA 71-2101 (1971); Preprint DUBNA P3-2101 (1969).
10. Panel Discussion Proc. IAEA Symp. on Nuclear Data for Reactors, Vol. 2, Paris, Oct. 17-21 (1966), p. 397.
11. M. Cao et al., J. Nucl. Energy, 22, 211 (1968).
12. J. Theobald et al., Inter. LINAC Seminar, GEEL (1971). Preprint CEN-239 (1971), p. 18.
13. Yu. Ryabov et al., Nucl. Phys., A 216, 395 (1973).
14. J. Trochon et al., J. Phys., 31, 131 (1973).
15. Yu. V. Ryabov et al., Preprint OIYaI P3-4992 (1970).
16. A. Michaudon et al., Nucl. Phys., 69, 545 (1965).
17. Yu. V. Ryabov et al., Yad. Fiz., 14, No. 5, 927 (1971).
18. V. N. Kononov et al., in: Proc. of Conf. on Neutron Physics [in Russian], Vol. 1, Naukova Dumka, Kiev (1972), p. 256.
19. R. Bandl et al., in: Proc. Third Conf. on Neutron Cross Sections and Technology, Vol. 1, Knoxville, March (1971), p. 273.

IONIZATION ENERGY LOSSES AND RANGES OF ALPHA PARTICLES IN IONIC CRYSTALS

G. N. Potetyunko and E. T. Shipatov

UDC 539.12.04:518.3

In the last few years the most varied problems in solid-state physics have been solved by nuclear physics methods employing beams of accelerated ions. These methods developed particularly rapidly after orientation effects were discovered and understood. Various techniques based on the combination of orientation phenomena and the back-scattering of ions, nuclear reactions, and the production of characteristic x-ray radiation are being more and more widely used to investigate crystal structure, to study the formation and annealing of radiation defects, to analyze defects in surface layers of crystals, to determine the location and depth of impurity atoms in crystal lattices, etc. Most of the work up to the present time has been performed for ion-implanted silicon crystals [1].

The laws of orientation effects in ionic and ion-covalent single crystals, more complex in composition and crystal structure, are being studied in the department of Nuclear Physics of the Scientific-Research Institute of Physics of the Rostov-on-Don State University. Beams of H^+ and He^+ ions with energies from 0.5 to 2.0 MeV are used as analyzing beams.

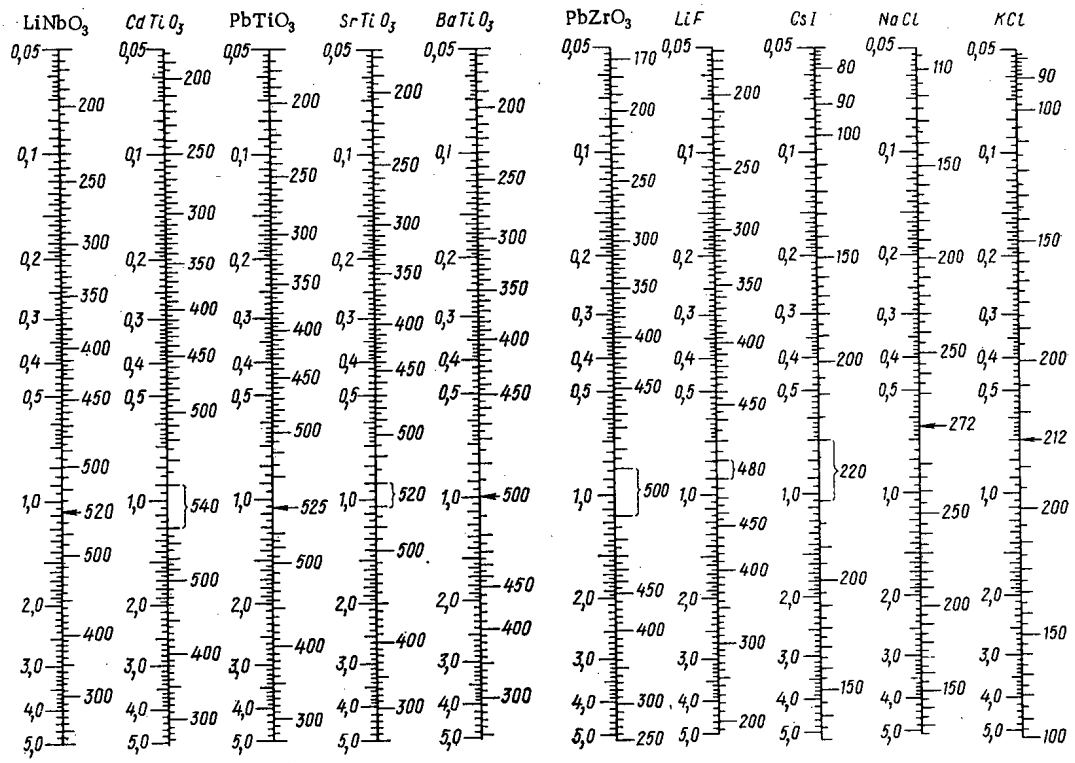

Fig. 1. Ionization energy losses. The left-hand scale is for E in MeV and the right-hand scale for dE/dx in keV/μ.

Translated from Atomnaya Énergiya, Vol. 40, No. 4, pp. 343-345, April, 1976. Original article submitted September 10, 1975.

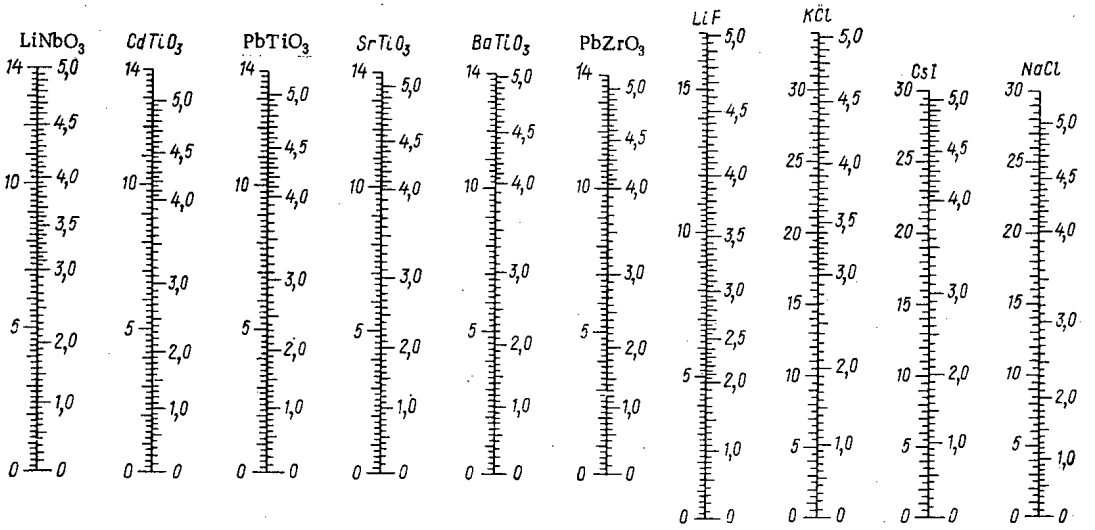

Fig. 2. Alpha particle ranges. The left-hand scale is for R in μ and the right-hand scale for E in MeV.

For a proper choice of the initial ion energy and an analysis of the results it is necessary to know the ionization energy losses and the ranges of the particles of the analyzing beam in the crystals under study. The main difficulty in finding these values is that the energy range indicated either occurs at the maximum of the dE/dx curve (for He^+ ions) or in the immediate vicinity of this maximum (for H^+ ions). For the energies indicated there are no sufficiently reliable theories for calculating dE/dx; the experimental data on ranges and ionization energy losses are poor, and there are few good approximations for the energy dependence of ranges and ionization energy losses. The only source of more or less reliable and relatively complete information is the tables of Northcliffe and Schilling [2]. Having these tables, the problem is to determine the values of the ionization energy losses and ranges of H^+ and He^+ ions in a number of crystals.

The general scheme of the method we used to solve the problem posed is the following:

a) The values of the ionization energy losses in the components of the crystals under study were found by interpolating graphically in the data of the tables in [2];

b) using the Bragg rule, the values of the ionization energy losses in the crystals being studied were found, neglecting channeling effects;

c) having the energy dependence of the ionization energy losses, the values of the ranges were calculated from the expression

$$R(E) = \int_{E_{\min}}^{E} \frac{dE}{dE/dx}. \qquad (1)$$

For the graphical interpolation of the data of [2] points corresponding to the values of the ionization energy losses of a hydrogen or helium ion in various media were plotted on semilog paper for a fixed value of the ion energy. Values of the atomic number of the medium were plotted along the uniform scale and the ionization energy losses along the logarithmic scale. For media with atomic numbers Z > 10 the points fall on a smooth curve except for the rare gases and zirconium and silver (Z = 40 and 47). A smooth curve was passed through the plotted points and used to find the ionization energy losses in the necessary media.

Then the ionization energy losses were found in all the necessary components and the Bragg rule was used to find the ionization energy losses in the crystals. The appropriate equation for finding the ionization energy losses in a $BaTiO_3$ crystal, for example, is

$$\left(\frac{dE}{dx}\right)_{BaTiO_3} = \frac{0.1D}{233}\left[137\left(\frac{dE}{dx}\right)_{Ba} + 48\left(\frac{dE}{dx}\right)_{Ti} + 48\left(\frac{dE}{dx}\right)_{O}\right]. \qquad (2)$$

The values of dE/dx for titanium and oxygen were taken from the tables in [2] and the value for barium was found by the method described above. The factor 0.10, where D is the density of $BaTiO_3$ in g/cm^3, is introduced to transform from $keV/mg/cm^2$ to keV/μ, which are more convenient units in practice.

Taking account of the energy dependence of the ionization energy losses, Eq. (1) was used to find the ranges. The integration was performed by the trapezoidal rule. The value of $R(E_{min})$ was set equal to zero. All the calculations were performed on an ODRA-1204 computer.

In this way the ionization energy losses and ranges of H^+ ions were found in $PbZrO_3$, $SrTiO_3$, $BaTiO_3$, $PbTiO_3$, $CdTiO_3$, CsI, NaCl, KCl and LiF crystals, and for He^+ ions in a $LiNbO_3$ crystal, in addition. The energy ranges used were 12.5 keV to 2.5 MeV for H^+ ions and 50 keV to 5 MeV for He^+ ions. All the results are presented in the form of nomograms. The corresponding nomograms for hydrogen ions are given in [3] and those for helium ions in Figs. 1 and 2 of the present article. The error of the data obtained is about 15-20%. It is clear from the nomograms that the ionization energy losses are higher for both hydrogen and helium ions in three-component crystals with a high packing density and accordingly the ion ranges are shorter than in two-component crystals.

LITERATURE CITED

1. J. W. Mayer, L. Eriksson, and J. A. Davies, Ion Implantation in Semiconductors, Academic Press, New York (1970).
2. L. Northcliffe and R. Schilling, Nuclear Data, A7, Nos. 3-4 (1970).
3. G. N. Potetyunko and É. T. Shipatov, At. Énerg., 39, No. 2, 120 (1975).

A MONOCHROMATIC ANNIHILATION GAMMA-RAY BEAM FROM A 2-GeV LINEAR ELECTRON ACCELERATOR

B. I. Shramenko, G. L. Bochek,
V. I. Vit'ko, I. A. Grishaev,
V. I. Kulibaba, G. D. Kovalenko,
and V. L. Morokhovskii

UDC 539.122:539.124.6:621.384.6

The present study was intended to devise a method of producing and assessing γ-ray beams with linear electron accelerators; the energy K of such a γ ray is related to the angle of observation Θ and positron energy E as follows:

$$K=\frac{m}{1-\sqrt{(E-m)/(E+m)}\cos\Theta};\quad (\hbar=c=1) \tag{1}$$

where m is the rest mass of a positron. The energy spread in the γ rays is dependent on the angular spread S_Θ of the primary positron beam and the energy spread S_E, as well as on the linear angle $\Delta\Theta$ at the detector:

$$\Delta K=[a^2S_E^2+b^2S_\Theta^2+(\Delta\Theta)^2(b^2/12)]^{1/2}, \tag{2}$$

where

$$a=K^2\cos\Theta/(E+m)^2\beta,\quad b=-\sin\Theta K^2(\beta/m).$$

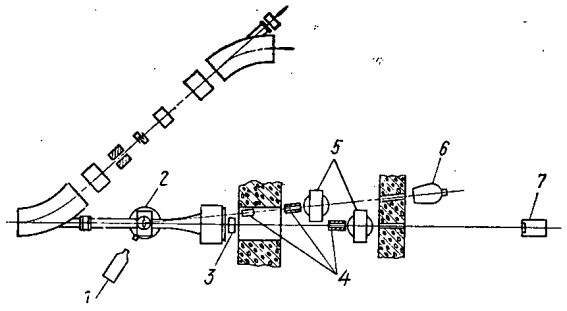

Fig. 1

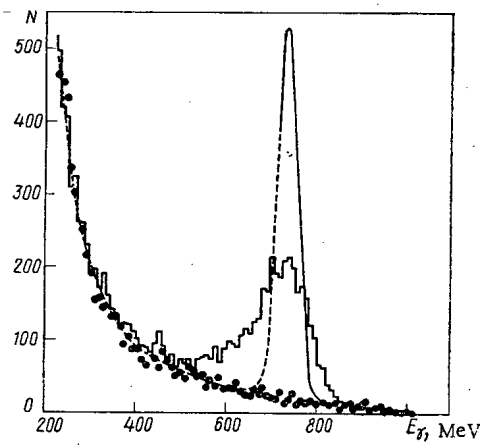

Fig. 2

Fig. 1. The apparatus: 1) TV camera; 2) goniometer; 3) ionization chamber; 4) collimator; 5) separator magnets; 6) total-absorption spectrometer; 7) quantometer.

Fig. 2. Annihilation γ-ray spectra: —— and •) measured spectra of γ rays from positrons and electrons respectively; — — — —) annihilation γ-ray spectrum corrected for spectrometer resolution.

Translated from Atomnaya Énergiya, Vol. 40, No. 4, pp. 345-346, April, 1976. Original article submitted September 4, 1975.

Preliminary results have been given [1] on the spectra of such γ rays; the measurements were made at $\Theta = 1.6 \cdot 10^{-2}$ rad, the positron beam being deflected by a magnetic field.

Here we present new results on the spectrum of quasimonochromatic γ rays produced by the same accelerator; the measurements were made under new conditions in a special photon channel, whose access lay at $\Theta = 2 \cdot 10^{-2}$ rad to the accelerator axis.

Figure 1 shows the system; the 1-GeV positron beam had an energy spread $\Delta E/E = 2\%$ and was directed onto an amorphous beryllium target of thickness 230 μ, which lay at the exit from the accelerator (goniometer), and the resulting beam was deflected by an SP-83 magnet.

The γ rays emitted at $\Theta = 2 \cdot 10^{-2}$ rad (which corresponds to 720 MeV) were collimated by two lead collimators, which isolated a solid angle $d\Omega = 2 \cdot 10^{-6}$ steradian. The value of $\Delta\Theta$ was $7 \cdot 10^{-4}$ rad, which corresponded to $\Delta E/E = 6\%$.

The proper correction for the x rays due to the positron scattering was applied by measuring the spectrum of those x rays under the same conditions with an electron beam having parameters the same as those of the positron beam. The x-ray background at 700 MeV was less than 0.5% in both cases in the absence of the target.

The γ-ray spectrum at 200-1000 MeV was measured with a total-absorption spectrometer based on a KRS-6 crystal [2]. The methods of measuring the γ-ray spectra and calibrating the spectrometer with monoenergetic electrons have previously been described [2, 3]. An improved style of this spectrometer allowed us to provide an energy resolution of 13% at 1 GeV.

The true γ-ray spectrum was derived from the measured one by the method of [4], which enables one to eliminate distortion due to the energy resolution of the spectrometer (Fig. 2); the energy (720 MeV) and the spread in the peak (7%) were in good agreement with the values calculated from (1) and (2); the available positron current ($I_{e+} = 8 \cdot 10^{-10}$ A) resulted in a flux of monochromatic radiation of a few γ rays per second. If the positron flux could be increased by a factor 10-30, physics experiments could be begun with monochromatic high-energy γ rays, e.g., with bubble and spark chambers.

LITERATURE CITED

1. E. V. Bulyak et al., in: Atomic Science and Technology, Nuclear and High-Energy Physics Series [in Russian], Issue 5 (7), Izd. Kharkov, Fiz. Tekh. Inst., Kharkov (1973), p. 66.
2. I. A. Grishaev et al., ibid., Issue 1 (1), Izd. Kharkov, Fiz. Tekh. Inst., Kharkov (1972), p. 87.
3. I. A. Grishaev et al., Ukr. Fiz. Zh., 16, 866 (1971).
4. G. G. Doroshenko, A. M. Zaitov, and M. Z. Tarasko, Applied Nuclear Spectroscopy [in Russian], Issue 3, Atomizdat, Moscow (1972), p. 233.

PARAMETERS OF SEMI-INSULATING GaAs NUCLEAR-RADIATION DETECTORS

S. A. Azimov, S. M. Bukki,
R. A. Miminov, and U. V. Shchebiot

UDC 539.1.074(55):621.382

Semiconductor nuclear detectors are widely used, which requires not only improvements in classical semiconductor materials such as germanium and silicon but also the design of detectors based on other semiconductors such as gallium arsenide, cadmium telluride, and so on. Gallium arsenide as a γ-ray detector should provide improved efficiency by comparison with silicon on account of the higher atomic number (Z = 32), while the temperature range should be wider than that for germanium detectors on account of the greater forbidden-band width (E = 1.4 eV). Such a detector would combine the advantages of silicon (wide forbidden band) and those of germanium (high atomic number) [1].

Here we discuss detectors based on semi-insulating single-crystal gallium arsenide of resistance 10^7-10^8 Ω-cm; the single crystals were cut into wafers of thickness from 200 to 400 μ, which after cutting were ground and mechanically polished with diamond paste of particle size 0.1 μ and then etched in a polishing agent consisting of a mixture of nitric acid, hydrogen peroxide, and water. Then gold was evaporated under vacuum onto both sides and the wafers were mounted in a coaxial device; in this way we made specimens of working area 1.25 cm^2 and thicknesses 100, 200, and 300 μ.

The voltage — current characteristics deviated only slightly from linear and were unaffected by the polarity; this means that these semi-insulating GaAs devices can be used as homogeneous counters, with the electric field uniformly distributed through the crystal. Further evidence for this is that the capacitance is independent of the bias over a wide frequency range (60 Hz-1 MHz), the value being equal to the geometrical capacity, i.e., as calculated for a planar capacitor.

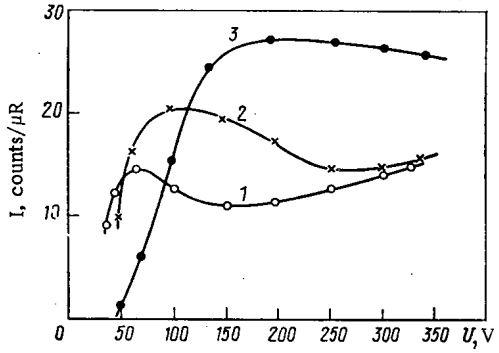

Fig. 1

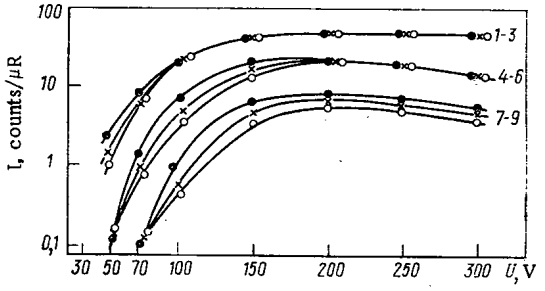

Fig. 2

Fig. 1. Response of GaAs detectors in relation to voltage for E_{thr} = 50 keV, τ = 0.2 μsec.

Fig. 2. Response as a function of voltage for various discrimination thresholds and signal-shaping times: 1-3, 4-6, and 7-9) for E_{thr} of 50, 70, and 100 keV, respectively: ×, ●, and ○) for 0.1, 0.2, and 0.5 μsec.

Translated from Atomnaya Énergiya, Vol. 40, No. 4, pp. 346-347, April, 1976. Original article submitted November 4, 1974; revision submitted September 19, 1975.

The performance was determined from the γ-ray sensitivity; the detector noise level was cut off by an integral discriminator. Figure 1 shows the sensitivity of the GaAs detectors of thicknesses W = 100, 200, and 300 μ, respectively (curves 1-3), in each case as a function of voltage. Figure 2 shows the sensitivity as a function of voltage for a 300-μ detector as measured with various discrimination thresholds and various signal-shaping times. It is clear that the sensitivity of GaAs increases with the thickness, but that the voltage dependence is not monotonic; above a certain field strength (5.5-7 keV/cm), the sensitivity falls, reaching a minimum at 15-18 kV/cm, and then rising slowly. This trend agrees qualitatively with the electron speed as a function of field for high-resistance gallium arsenide [2] and is due to features of the band structure in GaAs.

Theoretical calculations showed that the γ-ray efficiency as actually measured is substantially less than the theoretical value; the discrepancy is due to structural imperfection in the GaAs, which results in a short carrier lifetime in the initial material.

Therefore, the presently available gallium arsenide cannot provide counters having γ-ray efficiencies close to the theoretical value; but structure improvements in the GaAs crystals might improve the γ-ray efficiency and provide detectors having advantages over Si(Li) ones [3].

LITERATURE CITED

1. F. Cappelani and G. Restelli, Semiconductor Detectors, Amsterdam (1968), p. 365.
2. M. E. Levinshtein and I. S. Shur, Fiz. Tekh. Poluprov., 5, No. 9, 1791 (1971).
3. Yu. K. Akimov et al., Applications of Semiconductor Nuclear-Particle Detectors [in Russian], Atomizdat, Moscow (1967).

SIXTH INTERNATIONAL CONFERENCE ON MÖSSBAUER SPECTROSCOPY

A. G. Beda

This conference of COMECON member nations was held August 25-30, 1975 in Krakow; it was attended by 229 researchers, including 115 from eight socialist countries and 114 from 18 capitalist countries. There were 243 papers, for which the abstracts were made available in advance. It is proposed that the complete texts of the review papers will be made available subsequently.

The eight plenary sessions were concerned with 23 requested surveys; the 243 original papers were dealt with by a reporter system. All the papers were distributed over 13 sections. The reporter in each section spoke at the plenary session on the papers presented at the relevant section, which was then followed by a discussion. The topics in the sections were extremely varied and included aspects such as progress in the theory of the Mössbauer effect, charge and spin distributions in solids, relaxation effects, chemical reactions, catalysis and surface phenomena, and the structure dynamics of biological molecules.

The survey by Yu. Kagan (USSR) dealt with coherent effects in the interaction of Mössbauer radiation with crystals; particular attention was given to γ lasers. This was also dealt with in a joint paper by Baldwin and Trammel from the USA and Gol'danskii from the USSR, as well as in a communication from Voitovetskii (USSR), all of which aroused considerable interest and prolonged discussion.

The section concerned with methodology in the Mössbauer effect had notable papers from the USA, Poland, and the USSR, which dealt with the modulation of Mössbauer radiation by radiofrequency magnetic fields. Research has continued on the mechanism of this process, and studies have been made on the parameters of the spectra in relation to field intensity and frequency.

Many papers were also presented on the charge and spin distributions in solids; a very interesting survey dealt with the theoretical determination of these distributions for solids (A. Freeman, USA). He spoke of his modification of the Hartree — Fock method, which provides for reliable interpretation of numerous results; he discussed a series of studies on the precise effects of crystalline environments. Numerous measurements have been made on the hyperfine fields in Heusler alloys. Another group of studies was concerned with ferrites, oxides, and chalcogenides, which are of magnetic semiconductor type.

A survey by Zemcik (Czechoslovakia) dealt with the application of Mössbauer spectroscopy in research on metallic systems; it was observed that the number of applications has increased considerably, especially in aspects of metal physics such as the mechanism of dispersion hardening, order—disorder phenomena in alloys, and migration of alloying elements.

Numerous papers at this section were based on the Mössbauer effect in ^{57}Fe; some papers dealt with the parameters of Mössbauer spectra for various alloys relevant to fundamental metal-physics research. An example is a study by Solomon et al. from the Federal German Republic, in which measurements were made on the isomeric shift and line shape for ^{181}Ta in relation to oxygen and nitrogen concentrations in tantalum. An interesting point here was that the Mössbauer effect in tantalum was there recorded at exceptionally high temperatures, viz., from 300 to 2300°K. A notable paper on the metal physics of practical alloys was that by Belozerskii et al. (USSR) on constructional steel based on iron ($Ni_5Mo_{1.2}$-$Co_{0.9}$); it was shown that the molybdenum concentration can be measured with an error less than 0.15%, and recommendations were made on the optimal means of strengthening the alloy. Many other papers dealt with the magnetic structures and hyperfine interactions, especially for ferrites, intermetallides, and alloys showing phase transitions. Spin-density transfer to diamagnetic atoms was also discussed.

Translated from Atomnaya Énergiya, Vol. 40, No. 4, pp. 349-351, April, 1976.

Dilute impurities, defects, and radiation damage were dealt with in 20 original papers; a series of papers was concerned with minor components showing the Mössbauer effect, especially ones introduced by ion implantation in matrices; isotope separators have been used for this purpose for some time. Measurements have been made of the hyperfine fields, quadrupole splittings, and line widths on implanting ^{57}Fe in transition metals (Sawicka et al., Poland) and group IV elements (Veyer et al., Denmark) and on implantation of rare-earth elements into ferromagnetic metals (Nilson et al., the Netherlands). Much interest and a lively discussion were aroused by two papers by Mansel and Vogl (West Germany) on the kinetics of defects in 99.999% aluminum and silver after exposure to 3-MeV electrons at 4.2°K. The Mössbauer probe ^{57}Co was employed, which was introduced by diffusion. Several other papers dealt with defects and radiation damage produced by electrons, protons, and lasers.

Another section dealt with relaxation phenomena, and there were here two survey papers (Wegener, Federal German Republic), and Shenyoy (USA). In particular, the latter presented his method of calculating relaxation spectra, which gives very good results in the description of Mössbauer spectra in the presence of complex hyperfine interactions. Of the original papers at this section we may note that by Regneaux (France) on the Mössbauer spectra of traces of iron in cubic CaO and KMgO crystals in strong magnetic fields. In these cases the strong field produces not only a magnetic hyperfine structure but also an induced quadrupole splitting. The quadrupole splitting as a function of field strength and direction gives information on the spin-phonon coupling, electronic-state excitation, and characteristics of the ground state. The section also heard many papers on spin—spin relaxation effects in Mössbauer spectra. A new trend was dealt with in a paper by Afanas'ev et al. (USSR). This dealt with the Zeeman electronic splitting in the absorption spectra of Mössbauer γ rays in $Al(NO_3)_3 \cdot 9H_2O : Fe^{3+}$ single crystals, and it was shown that paramagnetic Mössbauer spectra are unusually sensitive to weak external fields. This effect could be of value in the analysis of complex chemical compounds.

Two surveys and about 50 original papers dealt with the chemical applications of the Mössbauer effect; Dayon (Brazil) dealt with the structures, bonds, and general chemistry of polymers. Gol'danskii (USSR) considered the application of Mössbauer spectroscopy in catalysis, his paper being the first in the section on chemical reactions, catalysis, and surface phenomena.

A special section was also devoted to phase transitions and critical phenomena. The papers presented at this section dealt with transitions from the magnetically ordered state to the paramagnetic one, orientation-type magnetic transitions, crystallographic transitions, metal—insulator transitions, and ferroelectric phase transformations.

Another section dealt with the structure and dynamics of biological molecules, at which three surveys were presented: Parak from Western Germany, Frauenfelder from the USA, and Frolov from the USSR. In addition there were eight original papers.

The conference demonstrated the continuing qualitative and quantitative growth of Mössbauer spectroscopy, especially the extension of applications. The next conference of the socialist countries on Mössbauer spectroscopy will be held in 1977 in Romania.

COLLABORATION NOTES

The sixth meeting of the technical committee on research reactors, COMECON Standing Commission on the Peaceful Uses of Atomic Energy, was held in Predeal (Romania) from Sept. 30-Oct. 3, 1975.

The committee discussed and agreed on a plan for the operations of the commission in this area, in particular, research reactors for 1976-1967.

The delegations of specialists discussed and ratified a report on recommendations on collaboration between member countries on research reactors for 1976-1980, which was presented for consideration by the standing commission.

Other discussions and agreements concerned working plans on five topics, which formed parts of the plans for scientific collaboration between COMECON members in the area of atomic-energy use for 1976-1980. There was discussion on a paper by the Czechoslovak delegation on comparison of various plans for VVR-S reactors. Information was presented on investigations completed in 1973-1984 on the design and commissioning of research reactors and on researches with such reactors on reactor physics and technology.

The delegations also welcomed a new participant in the work of the council, viz., a delegation from Cuba.

The sixth meeting of the commission on hydrological problems was held in Eisenach (German Democratic Republic) on Oct. 28-31, 1975; information was presented on the utilization of research results on hydrological conditions, water treatment, and sealing problems for fuel rods at nuclear power stations conducted during 1971-1974. Reports were also heard on studies made in the Republic and in the USSR on nuclear power stations operating with VVÉR reactors during 1971-1974. Discussions led to agreement on a plan for the operations of the commission for 1976-1977, in particular, the working water conditions in nuclear power stations. Other subjects discussed included preparations for the third symposium of COMECON members on the above topic, which is to be held in the German Democratic Republic in Nov. 1976. Specialists on sealing monitoring for fuel rods discussed results from recent studies and ratified recommendations and future research lines.

The 11th meeting of the Council of the International Economic Organization for Nuclear Instrumentation, "Interatominstrument," was held Dec. 9-12, 1975 in Warsaw, Poland. The President of the Council is V. F. Krasov, also President of the All-Union Isotope Organization.

As regards the realization of major decisions of the 10th meeting of the Council, it was reported that from Sept. 15, 1975 in Poland (Zelena Gora) and from Nov. 1, 1975 in the USSR (Dubna) there would be branches of "Interatominstrument" for service support to instrumentation and for preparing the necessary documentation for these branches for service in Bulgaria and the German Democratic Republic; also, measures have been taken to set up a plant to produce nuclear-physics instruments for nuclear power stations.

It was recognized that specialization within the field of production is very important, and the Council confirmed a plan for such specialization for 1976 and made detailed decisions on further lines to be examined.

As regards foreign trade, the performance of their obligations by members of the organization was reported in conformity with the agreed volumes of supplies for 1976-1980, with the conclusion of detailed agreements for 1976.

The Council also ratified the working plan of the organization for 1976, and considered suggestions on the distribution of responsibilities for equipment up to 1980; in addition, agreement was reached on the 12th meeting, which was held May 11-15, 1976.

The President for 1976 was K. Vancl, general director of the Tesla Electronics and Light-Current Engineering Concern.

The meeting of the Council was characterized by a friendly atmosphere and a spirit of complete agreement.

BIBLIOGRAPHY

A. A. Moiseev and P. G. Ramzaev

CESIUM-137 IN THE BIOSPHERE*

Reviewed by R. M. Aleksakhin

Cesium-137 is radiologically one of the most important fission products, since its high mobility in the environment gives it considerable importance in the biosphere. Research shows that ^{137}Cs transport along biological and food chains can result in accumulation in man, and this has become important in the last ten years, particularly, since the observation of elevated mobility of ^{137}Cs in some parts of the world. These areas have unusual biogeochemical conditions (soils of light mechanical composition containing relatively little mineral material, and with elevated water contents, such as forests in European Russia, the Ukraine, and Belorussia, as well as specific food chains with very rapid ^{137}Cs migration, such as from mosses to Arctic animals and man in the extreme north of the USSR, in Scandinavia, and North America). In these areas, the migration rate of ^{137}Cs is above that of ^{90}Sr, whereas the converse applies under normal conditions. Also, ^{137}Cs is a major contributor to the dose resulting from fallout.

This volume deals fully with the migration of ^{137}Cs in the environment.

The first chapter deals with sources of ^{137}Cs in the biosphere (nuclear weapons tests, peaceful uses of nuclear energy, radioactive wastes, and so on).

The second chapter deals with the migration of ^{137}Cs in soils, areas of fresh water, oceans, and plant — soil systems.

The third and fourth chapters deal with the metabolism of ^{137}Cs in animals and man (modes of intake, distribution, excretion, accumulation, and dose — effect relationships).

The fifth chapter deals with the migration of ^{137}Cs in the far north of the USSR and in forested regions in middle latitudes; it thus gives a complete scheme of the circulation of ^{137}Cs in the environment starting from fallout and ending with entry into man via food products, with evaluation of the possible radiation effects.

Unfortunately, the book contains no discussion of research on biogeocenoses as regards the circulation of ^{137}Cs in individual landscapes, such as woodlands. Also, inadequate attention is given to the ^{137}Cs contents of particular objects in the environment and in human foods. The division between the second and third chapters is not entirely satisfactory, since the metabolism of ^{137}Cs in animals is discussed in considerable detail, whereas that in plants is less so. More detailed descriptions should be given of means of reducing the ^{137}Cs migration rates in various biological and food chains (for instance, soil — plant and food — man steps).

The book as a whole is the result of very detailed researches on radiation safety and radioecology in respect of ^{137}Cs in the biosphere, which has produced long-lasting environmental contamination. It is correctly emphasized in the conclusion that the problem of radioactive cesium in the environment cannot be considered as fully resolved in that prolonged researches under natural conditions into the biogeochemistry of ^{137}Cs will be required on a variety of natural landscapes in order to establish the detailed transport along food and biological chains, while laboratory studies must accompany these to establish the metabolism and biological effects of ^{137}Cs, which should provide a means of providing better radiation safety against this nuclide in the environment. The book should prove of interest to radiobiologists, radioecologists, physicists concerned with dosimetry, and environmentalists.

*Atomizdat, Moscow (1975), 11.5 printers sheets, 1 ruble 30 kopecks.

Translated from Atomnaya Énergiya, Vol. 40, No. 4, p. 351, April, 1976.

THE SECOND INTERNATIONAL CONFERENCE ON SOURCES OF HIGHLY CHARGED IONS

B. N. Markov

The second International Conference on sources of heavy, highly charged ions and systems of acceleration was held during Oct. 26-30, 1975 in Gatlinburg (USA). This conference was organized by the Oak Ridge National Laboratory with the support of American national societies. About 140 scientists from 12 countries took part in the work of the conference. The largest delegations were those from the USA, the GFR, and France. The Soviet delegation consisted of five members. More than 50 papers were introduced, two of which came from the USSR. The papers were discussed at seven consecutive sections.

Survey papers and communications were given on the following subjects: fundamental processes in sources, sources of highly charged ions, heavy negative ions, polarized heavy ions, and stripping on foils. The largest number of papers were concerned with the study of sources of highly charged ions and heavy negative ions. Accelerators of highly charged ions obtained directly from ion sources or formed as the result of stripping preaccelerated negative ions were used for studying many problems. In addition to questions relating to the nuclear physics of heavy ions, one of the most important of which concerns the synthesis of transuranic elements, these accelerators have been employed in seeking solutions to a whole series of problems of solid-state physics, such as the implantation of ions during studies in the semiconductor field (the manufacture of integrated circuits for computers), studies of superconducting materials, simulating radiation damage to the structure of metals when selecting or synthesizing materials that are stable in intense neutron fields (thermonuclear reactors, breeder reactors), etc. We should also note that there is an increase in the use of fast ions in biological studies and therapy. It would appear, in this connection, that a significant proportion of the participants at the conference comprised representatives of universities and industrial organizations interested in new information on sources of heavy ions.

The conference considered four sources of highly charged ions: arcs with heated and cold cathodes, which employ the oscillation of electrons in a longitudinal magnetic field; duaplasmatrons; electron beams; and sources with electron-cyclotron heating.

Over the last 20 years only arc sources of highly charged ions have been used for accelerators. Sources with hot cathodes and a heated cathode have been developed by the I. V. Kurchatov Atomic Energy Institute, and cold cathodes by Oak Ridge (USA). The first of these, due to specific features of its discharge characteristics, offers the possibility of producing high-intensity currents of highly charged ions of all elements of the periodic table. This was the reason that the beams of accelerated heavy ions from the cyclotrons of the JINR (Dubna) were for so long the most intensive, which contributed largely to the achievements of heavy ions in nuclear physics in the G. N. Flerov Laboratory. The attractive features of this source have not passed without notice and they have been copied in laboratories of various countries (Belgium, the GFR, France, Sweden, and Japan).

The investigation of physical processes in the discharge columns of arc sources formed the subject of two papers. The question of the existence of nonlinear collective processes was approached by H. Schult and collaborators (Darmstadt, GFR) on the basis of calorimetric and probe measurements. New proposals regarding the distributions of the electric field in the discharge column and their effect on the formation of highly charged ions and the relationships of the energy content of the plasma to various parameters of the source were the subjects of part of the paper presented by B. Makova (USSR Atomic Energy Institute).

Translated from Atomnaya Énergiya, Vol. 40, No. 4, pp. 352-353, April, 1976.

The most convenient and a reasonably effective method of feeding solid matter into the discharge is the method involving cathode atomization by means of ions from the discharge. Such a source using a heated cathode has been developed by the JINR (Dubna) and has operated successfully in a cyclotron. Like the source developed by H. Schult and collaborators (GFR) it incorporates an additional heating cylinder to evaporate the material deposited on the walls of the anode so that it can be reintroduced into the discharge. B. Gavin (Berkeley, USA), in the Super HILAC source, used two annular heating chambers instead of one. These were arranged in relation to the anode core so as to obtain a threefold increased output of Au^{9+}. It was observed that using neon as a carrier gas lead to savings in the expensive isotope ^{48}Ca. The original method of atomizing the sample material by "recovered" ions in a cyclotron source has been used by M. Mellori (Oak Ridge, USA).

The duaplasmatron employed at present as a source of highly charged ions may be used on the UNILAC accelerator (Darmstadt, GRF), insofar as the required ratio of charge to mass of ion is ≥ 0.046 overall; i.e., it can accelerate, e.g., ions of Xe^{7+} and U^{11+}. Considerable successes have been achieved by scientists at Darmstadt and Orsay (France).

The electron-beam sources which are now increasing in popularity enable us to obtain ions with a high degree of ionization, but with relatively weak currents which are insufficient for use in accelerators. The cryogenic pulse source developed by E. Donts (JINR, USSR), having electron energies of 500 eV, has produced beams of Ar^{15+} and Xe^{29+} ions. A great deal of interest was also shown in a paper dealing with the ionization cross section of highly charged ions produced by electron bombardment for C, N, and Ar. R. Bekker (Frankfurt, GFR) has proposed that continuous currents of U^{11+} with intensities up to 100 μA could be achieved, which satisfy the requirements of UNILAC.

An important step has recently been taken in the development of highly charged ion sources using heated plasma by electron—cyclotron resonance. This formed the subject of four papers (Grenoble and Orsay, France; Marburg, GFR; Oak Ridge, USA). Of these, the modular source of R. Zhel and collaborators comprised a three-stage combination of magnetic "bottles" in which the plasma flows from one section to another with a higher charge state. Currents of 10^{14} particles/sec of C^{5+} and O^{6+} have been achieved together with a maximum charge of Kr^{15+} ions. The value of nT is $6 \cdot 10^{15}$ eV/cm^3, which is four times greater than the value of nT in arc sources (IAÉ). It is clear that future lines of development of highly-charged-ion sources are anticipated in the direction of obtaining U^{60+} ions in sufficient quantities to drive accelerators, and the possibility of employing such a source in the GANIL project (France) was discussed.

The formation of negative ions of the heavy elements in sources being actively developed at the present time is effected by cathode atomization of the sample material by Cs^+ ions (E ~ 20 keV). The "linear" design of the ion source has taken on a "reflex" form, in which conical (K. Chapman, USA) or plane (G. Elton, USA) targets are also bombarded by Cs^+ ions accelerated from the surface of a thermoionizer, while negative ions are accelerated in the opposite direction by the same electron-ion optics which accelerate the Cs^+ ions. N. Smith (USA) noted the existence of a correlation between the electron properties and the output of negative ions in various types of ion source (i.e., the lower the electron properties, the lower the output). The intensities of beams of ions of various elements are compared; for example: Li^- ~ 5, C^- ~ 70, O^- ~ 130, Si^- ~ 45, S^- ~ 55 μA. Besides the sources already noted, improvements are still being made to plasma sources of negative ions: triplasmotrons (Lejeun, France) and other sources with oscillating electrons (N. Smith, USA). The paper by E. Steffens (GFR) and similar ones were discussed on the development of sources of polarized negative heavy ions for a Heidelberg tandem. Currents of 200 nA of Li^{3+} on a target are shown to be a possible way of obtaining polarized ions of Na, Cl, I, and Br. Amongst the theoretical works, the papers of P. Olson (USA) on the processes of development of negative hydrogen ions and D. Kaufman (USA) on electron affinity are worthy of note.

G. Frick and others (France) reported interesting results of stripping Ni, I, and Au ions with energies of 0.5-0.85 MeV/A on carbon foils with thicknesses of 2-200 μg/cm^2, work which was carried out in connection with the GANIL project. K. Bete and collaborators (GFR) used a supersonic jet of approximately the same range of thickness, the expenditure of argon on a target thickness of 100 μg/cm^2 being 0.4 g/sec with a 2-mm-diameter jet.

More attention is now being devoted to surveying the parameters of ion beams and measuring the emittance for beams with high phase densities. The emittance of beams obtained from arc ion sources with radial (D. Clark and collaborators, USA) and axial (K. Bete and collaborators, GFR) extraction of

ions has been measured. The emittance of beams of negative ions was measured by N. Anderson (Denmark), N. Smith (USA), and G. Dukas (UK). The last paper reported on the development of a system for measuring emittance with the aid of a computer and employing an ion-energy analyzer with a high resolution.

New experimental equipment built for investigating and developing sources of highly charged ions over the last three years in the leading foreign centers Berkeley, Oak Ridge (USA), and Darmstadt (GFR) shows the directions of future development of sources, insofar as the expenditure on this work cannot conceivably be warranted by any simplification of the design of accelerators and any increase in the efficiency of the way they are used.

The conference marks an important milestone in the development of sources of highly charged ions; it recorded the results of the basic achievements in this field, demonstrated an ever-growing interest in the study and development of sources of heavy ions in many countries of the world, and enabled specialists to assess the results of the work of research laboratories of other countries over recent years. The work of Soviet specialists on arc-type sources of highly charged ions with hot cathodes and electron-beam sources occupies a leading place on the world scene. The Soviet contributions drew considerable interest from the participants at the conference. Sources with heated cathodes are the most efficient at the present time for use with accelerators.

The proceedings of the conference will be published in the IEEE journal NS-23, No. 2, April 1976.

THE THIRD INTERNATIONAL CONFERENCE ON IMPULSE PLASMA WITH HIGH β

S. S. Tserevitinov

Despite the widely publicized successes achieved by the established classical tokamak programs, the search is still continuing for other and more effective systems of obtaining and maintaining high-temperature plasma.

The results of studies carried out on systems in which the β-ratio of the hydrokinetic pressure of the plasma to the pressure of the external containing magnetic field is of the order of unity or greater were discussed at the third International Conference on impulse plasma with high β. The conference took place at the Culham laboratories (UK) from Sept. 9-12, 1975. More than 120 delegates from 14 countries participated. The conference was organized by the UK Atomic Energy Commission, the Institute of Physics, London, the American Physical Society, and MAGATE. Similar conferences were held in 1969 and 1972.

The organizing committee (which operated both during the preparatory stage and during the conference itself) selected about 100 papers on the subjects: stellarators and tokamaks with high β, reversed-field, pinches, screw-pinches, plasma focus, and the theory of plasma with high β. Seven survey papers were presented at the conference: M. Kaufman (GRF) "Stellarators with high β," H. Bodine (UK) "Reversed-field pinches," D. Tailor (UK) "The relaxation of toroidal discharges," A. Bernar (France) "Plasma focus," K. Hirano (Japan) "Screw-pinches and the tokamak of circular section," D. Schluter (GFR) "Screw-pinches and the tokamak with high β and a noncircular section," D. Freiberg (USA) "The theory of plasma stability with high β."

A new period in the development of investigations in the pinch program (straight and closed) and particularly of stabilized reversed-field pinches (RFP) has begun over the last five years. Reversed-field systems are attractive for the following reasons:

1) In these systems, the containment field which is strong at the surface of the plasma tends to fall away towards the walls of the chamber, which improves the utilization factor of the field and the effectiveness of reactors based on RFP;

2) as the azimuthal current (I_z) through the plasma increases, the temperature, the value of β, and the magnetic width also increase.

The role of the reversed field in stabilizing the pinch was shown experimentally a long time ago. However, the fact that the physics of the phenomenon was not understood for a long time held back development in this direction. Now, as the result of theoretical and experimental work, important progress has been made in understanding the dynamics of such systems and the laws governing them.

In a similar manner, the conference discussed the problem of MHD stability, particle and field diffusion, particle loss, microinstabilities, the effects of plasma heating, energy balance, etc. in reversed-field θ pinches.

There has been considerable success in obtaining an understanding of the process of achieving stable configurations under conditions in which the reversed field is spontaneously created by the current flowing through the plasma. This occurs when the longitudinal plasma current lies within the framework of some calculated boundary values. Such an RFP regime is highly attractive from the point of view of the engineering problems of future thermonuclear reactors, as it greatly simplifies their design.

Translated from Atomnaya Énergiya, Vol. 40, No. 4, pp. 353-356, April, 1976.

In much the same way, the present state of theory and experiment relating to reversed field pinches was examined in the survey papers of H. Bonin and D. Taylor, and, particularly, that of D. Freidberg. These showed that for low-temperature collision plasma, equipment NVTKh-1 (employing a programmed field) attained the classical configuration and energy lifetimes (τ_K and τ_E) at $\beta \approx 30\%$. The possibilities of the experiment were limited by too low a value of $\omega\tau$, and also by too rapid an increase in β and pressure gradient up to a value exceeding that permissible from the point of view of MHD stability.

In Zeta equipment in which the stable configuration with a reverse field is self-generated, the values of τ_E and $n\tau$ are observed with relatively high $\omega\tau$, compared with those obtained today on tokamaks, and at $T_e \approx 150$-200 eV and $\beta \approx 10\%$. However, the configuration lifetime is limited by the low-electron temperature. At present, there is a good basis for the construction of large equipment in which a self-reversal of the field will be accompanied also by its programming at the formation stage and the containment of the plasma at $I_z \approx 1$ MA. Detailed engineering design of the future NVTKh-2 equipment is already in train. It is proposed that the property of the plasma in this will be close to that required for the creation of a reactor, while the lifetime of the plasma will be measured in tens of milliseconds at $\beta = 20$-40%.

The papers presented by collaborators from Los Alamos give the results of experiments and calculations on stabilizing MHD instabilities by feedback on a Scillac installation. In 1975, tests were conducted on a 120° sector system. To reduce the speed of development of unstabilities at m = 1 up to a value at which an existing system of feedback can operate, the magnetic field was reduced to 17 kG. Under these conditions, the plasma configuration with sufficiently high parameters [$n = (2 \text{ to } 4) \cdot 10^{16}$ cm^{-3}; plasma radius ~1 cm; $\beta = 0.6$ to 0.7; $T_e = T_i \approx 120$ eV] was contained for more than 25 μsec. In these same tests, the applicability of the stabilization theory of D. Freidberg for suppressing feedback instabilities of mode m = 2 was tested and confirmed.

Papers on the θ pinch confirmed that there has been notable progress over the last five years in understanding plasma physics at high β. Theoretical work is in agreement with experimental results. Unfortunately, this does not apply to any great extent in the case of belt pinches, screw pinches and tokamaks at high β. Attempts to find the conditions for stable operation with densities of the order $(10^{15}$-$10^{16})$ cm^{-3} in these systems are attractive from the point of view of achieving the Lawson criteria at high densities. Marked progress in understanding the processes taking place in such systems has been assured by the interesting theoretical work of D. Freidberg and V. Grossman, H. Liu, K. Ch'u, D. Beiker, D. Schluter, and K. Hirano, in which relationships have been found between the basic parameters of the plasma and the configurations of the magnetic fields.

The numerical methods of H. Liu and K. Ch'u for a single-liquid model produce dose agreement with the experiments carried out in Holland on the SPICA equipment with relatively low-temperature plasma.

Up to the present, studies of plasma with T_i and T_e of the order of 40 eV have been carried out on equipment of the belt-pinch type. Plasma with $n_e \approx 5 \cdot 10^{13}$ cm^{-3} and $T_i \approx 180$ eV has only been achieved and studied on a TENQ installation in Ulich. However, even here, attempts to achieve a sufficiently stable plasma failed. The dynamics of this system were shown to be fairly complex. Regardless of the attempts, which involved varying the values of q, β, and b/a over wide ranges, the plasma remained unstable.

The unanimous opinion was expressed that a higher temperature in the toroidal pinch would significantly increase the life of a stable configuration. The basic problem at the present time for belt pinches remains that of checking stability and the energy lifetime of the plasma at higher temperatures.

R. Krakovskii has shown that heating plasma with $n_e \approx 10^{15}$ cm^{-3} to a temperature of $T_i \approx 1$ keV by surge waves is difficult by means of present-day high-voltage techniques. In direct θ pinches, adiabatic compression is used to provide an additional rise in temperature. Powerful compression is not employed with belt pinches, as it leads to loss of stability, as was demonstrated in the paper presented by D. Schluter. The effectiveness of surge heating by the use of low-inductive capacitor banks has been studied in Garking and Los Alamos on installations with direct θ pinches at voltages of 250-500 kV. Belt pinches have been operated at these voltages in Garking (VP-II-a at 160 and VR at 250 kV) in Yulikh (TENQ at 160 and HVBP at 250 kV). Variants with even higher voltages (500 kV and 1 MV) were discussed. An original method of obtaining a rapidly increasing magnetic field (with a time of increase of the order of 1 μsec) was proposed by R. Wilhelm. He considered that our solution to the energy problem lay with the belt pinch, although from the point of view of the engineering problems of a thermonuclear reactor, this project, with its complex steel cores and switched windings, was no less complex than the megavolt systems.

Interesting results were obtained on the BICASP and TORMAC equipments. These created a toroidal configuration of plasma with a high β, while possessing the properties of a system with "minimum B." Maintenance of plasma density ($n \approx 10^{15}$ cm^{-3}) and temperature ($T_e \approx 30$ eV) over the lifetime of the field (60 μsec) showed the equilibrium and MHD stability of the plasma in these systems. The plasma was heated by magnetic sonic waves propagated perpendicularly to the external toroidal magnetic field. TORMAC is one of the most convenient systems for the creation of a reactor. Work on the system has been under the direction of M. Levin in the University of California, Berkeley, in collaboration with scientists from Princeton University. For configurations of this sort, an important problem is the mechanism of ejection of particles through the magnetic slot, therefore, in recent years, Berkeley and Princeton have proposed a more serious study of this problem.

Among the various programs of toroidal equipment with high plasma, the reverse-field toroidal pinch is now the most advanced in theoretical experimental, and engineering relationships.

The conference discussed several projects for thermonuclear reactors.

Scientists at Los Alamos have proposed a project consisting of two reactors: straight (based on a linear θ pinch) and toroidal (SFTR). The straight reactor is 500 m long, while the large diameter of the SFTR is 80 m. Experience accumulated during the operation of the Scillac equipment (with a chamber length of the order of 25 m) permits a bolder approach to the search for ways of solving the problems of controlled thermonuclear synthesis on such grandiose systems. The complexity of creating a stable closed configuration and the closeness of the linear dimensions of the toroidal (~250 m) and straight (~500 m) versions compel us to think seriously about the type of reactor based on the θ pinch. All representations at the conference reaffirmed that interest in the straight θ pinch is still maintained. A study in this program has begun at Los Alamos on two large installations with specially developed high-voltage techniques (using voltages of 250-500 kV).

Interest has also been maintained in systems with compression of flux and plasma by metallic liners. It is generally accepted that these studies are most purposefully carried out at the I. V. Kurchatov IAÉ and in the US Navy Research Laboratories (Washington). The latter presented two papers: by program director A. Robson and by P. Terch. The first examined the possibilities of creating a very compact reactor with liner, in which multifold utilization of rotating liners of liquid metal is proposed. The second describes tests on a new experimental installation specially designed and constructed for conducting liner investigations. In this installation, stable compression of metallic liners is being developed (with degrees of compression up to 28 and with a terminal field of 1.3 MG, while experiments have begun with liquid liners made of a mixture of sodium (22%) and potassium (78%). Numerical experiments on a computer are widely used by this laboratory as a way of analyzing the dynamics of liners. The papers show that calculation and experiment are in close agreement.

The Soviet Union presented two papers on liners which evoked a great deal of interest. One of these reported on the successful compression of neutral argon (up to a pressure of 10^5 atm) by a threefold collapsing metallic liner (attaining a degree of compression of ~10^3), while ideas on the nonmagnetic compression and containment ($\beta \gg 1$) of plasma with cold gas was discussed. The second paper indicated the possibility of using fluxes of plasma, generated by equipment type MK-200, for injection into systems with collapsing liners. Plasma having parameters near to those needed for the creation of a demonstration reactor was used in tests.

As before, plasma focus retained its interest from the reactor point of view as a means of obtaining a dense high-temperature plasma, and also as sources of thermonuclear irradiation for materials technology. The conference papers did not include any sensational reports. All the "focus buffs" are waiting impatiently for the results from Frascatti (Italy). However, the equipment of K. Mezone was not yet adjusted and did not produce a large flux of neutrons. The impression was created that without the K. Mezone results, nobody would have the nerve to charge the capacitor banks of a focus system, as the paper of H. Sachlin of Livermore showed that quantitative variations in the "neutron output — bank energy" curve can be expected with further increase in power. H. Sachlin gives a similar analysis of equipment of the "plasma focus" type with the aim of creating a high-power source of radiation with the possibility of obtaining powerful relativistic electron and ion beams in such installations. In a verbal statement, H. Sachlin discussed some interesting tests on the use of an electron-beam plasma focus for ablation of deuterium in the capillary space of a glass bottle established in the axis of symmetry of the anode. This work is related to other work at the Livermore laboratory by D. Shearer and a collaborator at the University of Santa Clara (California), D. Chen, involving an experiment with a Z pinch with ambient gas: This work

studied the numerical and experimental problems of the rapid excitation of energy in a Z pinch in a time which is less than the development time of MHD instability, and producing suitable conditions for the capture and utilization for heating of the plasma of energy liberated during the reactions of synthesizing α particles. The results of these tests can be considered encouraging: They also show experimentally the possibility of rapid heating and maintenance of an energy balance due to the energy of the α particles.

The original plasma focus, the "hypocyloidal pinch," is being studied at Vanderbilt University (Tennessee) in cooperation with NASA. The experiment is similarly described in the paper by G. Lee and D. Macfarland. With "three-dimensional" compression of plasma in a system which can be referred to as a "double plasma focus," a density of $n_p > 10^{18}$ cm^{-3} and a temperature of ~1 keV was achieved.* Containment was accompanied by radiations of neutrons and soft x rays. It is interesting that the plasma configuration is extremely long-lived. In this connection, there is self-maintained interest in the results of a study of the interaction of the radiation from a CO_2 laser (50 J in light, pulse duration τ = 150 nsec, beam diameter 5 mm) with plasma; the laser radiation was practically fully absorbed during the 70 μsec of the hypocycloidal pinch.

The conference considered projects for reactors on the basis of Scillac, the reverse-field pinch, the screw-pinch, the straight θ pinch and also projects for equipment for use in materials investigations. This was discussion, without any form of revolutionary novelty, very useful for plotting the most promising lines of future development.

Despite the fullness of the conference program, the participants and guests found time for useful conversation and discussion. The confidence of the majority of the conference participants in the need for further development and investigation of systems with $\beta \geqslant 1$, both from the viewpoint of the thermonuclear reactor and from the viewpoint of their use in applied problems, should be noted.

*Plasma with such parameters has a life of more than 5 μsec.

A SOVIET–AMERICAN PROJECT FOR A DIVERTER FOR A TOKAMAK REACTOR

A. M. Stefanovskii

In Oct., 1975, a group of Soviet and American physicists and engineers completed the initial stages of a joint project for a divertor for a tokamak reactor. The need for this type of development was sharply felt in connection with the planned construction of a large tokamak. In recent times, diverters have come to be considered as a possible means of dealing with contaminants in tokamaks. However, in the case of the two-component tokamaks operating at low values of $n\tau$, diverters are the one and only method of pumping out hydrogen injected into the discharge chamber.

The designed diverter is based on parameters ($R = 6.25$ m, $a = 2$ m, $B_T = 50$ kOe, $I_{op} = 7$ MA) which would allow it to be used in a T-20, ORNL EPR, or ANL EPR reactor.

The basic physical and engineering requirements for a diverter system can be formulated in the following way. First, to ensure reliable insulation of the plasma from the walls of the discharge chamber and form a screening diversion layer. Second, to create conditions under which it would be possible to ensure a high rate of pumping-out and a low return flow of neutral atoms of hydrogen into the discharge chamber. Third, to ensure a maximum reduction in the specific thermal load on the contact plates and facilitate heat extraction. Fourth, to select the optimum arrangement and design of the coils in the diverter which would provide reliable protection from neutron fluxes, break them down, and create the necessary magnetic configuration by the simplest and most economical method, while at the same time making the best possible use of the volume of the toroidal coils.

In the project under consideration (see Fig. 1) all these problems have been solved in a satisfactory manner. Thanks to the length of the diverter channel, it was possible to use the so-called "plasma trap," producing significant ionization of the neutral particles within the channel and increasing the pressure in

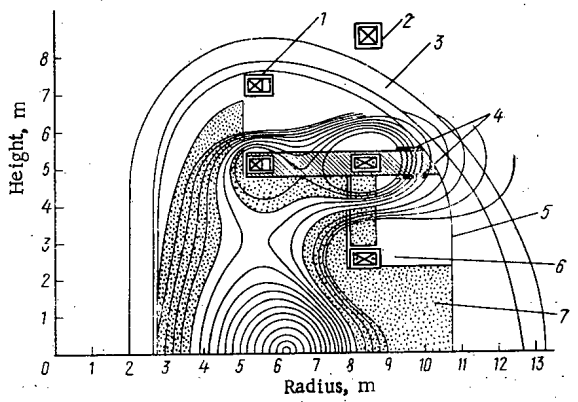

Fig. 1. Scheme of diverter project for a tokamak reactor. 1) DF-1 winding; 2) EF-1; 3) TF coil; 4) contact (neutralizing) plate; 5) dischare chamber; 6) DF-2 winding; 7) blanket and neutron protection.

Translated from Atomnaya Énergiya, Vol. 40, No. 4, pp. 356-357, April, 1976.

the diverter channels to (2 to 3)·10^{-5} mm Hg, at which it becomes possible to ensure the necessary speed of pumping-out, with positive diffusion of plasma from the current-carrying flexible conductor. The output of the plasma fluxes to the outer periphery of the toroidal system reduces the specific thermal load on the contact (neutralizing) plates and reduces the problem of heat extraction, while at the same time enabling us to use a diverter chamber of large volume, which in its turn offers the possibility of using a highly efficient built-in pumping system. The characteristic feature of the diverter windings is that their summated current within the toroidal coil is zero (currents in the DF-1 and DF-2 windings are equal and opposite in direction), and consequently, they can be fabricated in the form of two half rings; this allows the whole system to be dismantled into two half-toruses. The effectiveness with which the volume is utilized and the arrangement of the neutron shield are clearly shown in Fig. 1.

The problems of insulating the plasma from the walls and screening the diverter layer in the proposed project, as in other projects, demand further investigation, chiefly by means of special experiments. The completed part of the work on the project has defined, naturally, only the basic features of the diverter system to be developed. And while many of the details will need to be further developed and optimized, and some of them will require experimental proving, the basic idea of the project shows considerable promise.

S. Gralnik, D. Dzessbi, D. Mid, F. Tenni, A. Georgievskii, G. Saksaganskii, and the present author have participated in work on the project.

A CONFERENCE ON NUCLEAR DATA FOR TRANSACTINOIDAL ELEMENTS

S. M. Kalebin

A conference on nuclear data for transactinoidal elements organized by MAGATE was held in the GFR on Nov. 3-7. Specialists in various fields of applied science employing the nuclear-physical constants of transactinoidal isotopes participated in the conference, together with specialists concerned with the measurements of these constants. One of the aims of the conference consisted in establishing a close contact between the activities of these two groups of specialists. There were 47 participants in all from various countries: Belgium, Great Britain, Holland, Spain, Italy, Poland, the USSR, the USA, the Phillipines, France, the GFR, Switzerland, and Japan, while representatives were present from Euratom and MAGATE. The conference was held in the Nuclear Physics Center, located near Karlsruhe.

This was the first international conference at which all the transactinoidal isotopes were considered both from the point of view of the consumer, as regards their nuclear physical data for applications, and also from the point of view of measuring the data and coordinating the work of the national centers on their collection and assessment. In this connection, survey papers were presented at the conference dealing with problems of employing and utilizing the transactinoidal isotopes. These papers dealt with: the role of the transactinoidal isotopes in the design of reactors, the effect of these isotopes on the operation of the reactors, the problems of accumulating transactinoidal isotopes in reactor fuels, etc. Various papers were concerned with the use of transactinoidal isotopes in medicine, agriculture, and industry.

Problems connected with the accumulation of transactinoidal isotopes in nuclear-fuel wastes formed the subject of serious discussion. As the US delegates indicated, by the year 2000, the US reactors will have produced up to 1300 tons of transactinoidal isotopes. What can one do with wastes which contain such vast quantities of highly toxic transactinoidal isotopes, representing a considerable danger to the world biosphere? One of the solutions to this problem, which US specialists have in mind, is for the transactinoidal isotopes, after chemical separation from the wastes, to be returned to the reactors for "burning-up." It is possible that special "incinerator" reactors will be built for this purpose. In this regard, a large program has been instituted in the United States for measuring the nuclear-physical constants of the transactinoidal isotopes. Representative of the European states noted that the problem of reusing transactinoidal isotopes in reactors is too complex, and is hardly likely to be solved in this century. At the present time, in particular, there is not even the chemical technology developed for the separation of large quantities of transactinoidal isotopes from reactor wastes. To implement a program of reuse would demand very extensive means. During the discussion, it was noted that of all the various ways of burying wastes containing transactinoidal isotopes (in outer space, at the bottom of the oceans, in rocks) the most reasonable would appear to be burial in rocks. In this case, a large quantity must not be buried in a single locality, as unintentional criticality might then arise. The burial should be carried out in such a way that it remains possible to remove small amounts of the waste for investigation.

Successive sessions were concerned with a survey of contemporary methods of measuring and estimating nuclear data. An account was given of the composition of data relating to neutron cross sections in thermal, resonance, and fast-energy regions, the composition of data on α, β, and γ decays. A notable discussion arose in connection with the proposition of the American delegation regarding the further use of underground nuclear explosions for measuring neutron constants for the transactinoidal isotopes. During this discussion, it was noted that the method of measurement involving nuclear explosions has a number of serious drawbacks, including the fact that it is extremely expensive, so that this proposal requires

Translated from Atomnaya Énergiya, Vol. 40, No. 4, p. 357, April, 1976.

detailed examination. The need for closer cooperation between interested countries in the collection and assessment of nuclear physical constants for transactinoidal isotopes was stated. In particular, the US delegation proposed that a special journal on transactinoidal isotopes be published in the USA, in order to facilitate the exchange of experimental information.

The end of the conference was taken up with meetings of the three working groups, in which the achievements in accuracy of nuclear data are compared with the accuracy requirements existing at the present time for the various fields of use of transactinoidal isotopes.

At the final plenary session, the recommendations of the working groups were considered, together with the proposals made by the various participants. This material formed the basis on which the final recommendations of the conference were formulated.

AN INTERNATIONAL SCHOOL-SEMINAR ON THE INTERACTIONS OF HEAVY IONS WITH NUCLEI AND THE SYNTHESIS OF NEW ELEMENTS

K. G. Kaun and B. I. Pustyl'nik

An international school-seminar on the interaction of heavy ions with nuclei, and the synthesis of new elements, organized by the USSR Joint Institute for Nuclear Research was held in Dubna during Sept. 23-Oct. 4, 1975. A total of 200 delegates from 15 countries participated in the work of the seminar.

An exceedingly high level of lectures and discussions was maintained. In essence, the school-seminar was turned into a large international conference, at which current problems of further research were considered at length and in depth.

The 16 sessions comprising the seminar were taken up with 40 survey papers, in addition to which there was a discussion seminar on the mechanism of the interactions of complex nuclei and a general discussion of the whole problem. After an introductory speech by the president of the Organizing Committee, Academician G. N. Flerov (JINR), there was an introductory lecture devoted to a survey of theoretical models and experimental material related to nuclear aspects of the astrophysical problems of "black holes" given by Academician Ya. B. Zel'dovich (USSR Institute of Cosmic Research).

The remaining papers covered all the most urgent problems of the physics of heavy ions.

The Synthesis of New Transuranic and Superheavy Nuclei. This division included six experimental and five theoretical papers. A great deal of interest was aroused by the papers presented by A. Giorso (USA) and Yu. Ts. Oranesyan (JINR), in which the latest results were given from the programs for synthesizing new transuranic elements being carried out at Berkeley (USA) and Dubna. The chairman of the session on transuranic nuclei was G. Siborg (USA).

A. Giorso presented his paper on work related to the synthesis of isotope $^{263}106$ in a fusion reaction of californium with oxygen. The isotope was identified from the α decay, which resulted in a considerable methodological difficulty connected with the extremely low formation cross section of element 106 and the large level of background α radioactivity. A. Giroso's paper showed that the problem of synthesizing new transuranic elements with $Z > 105$ using the traditional Berkeley method of changing to a target with a higher atomic number, i.e., to nuclei of Bk, Cf, and Es, and accelerated ions of carbon and nitrogen, has encountered very serious difficulties.

As the paper by Yu. Ts. Oganesyan indicated, this situation can be altered radically if the traditional direction of synthesis is dropped and a new method employed instead. This has been proposed and realized at Dubna during the synthesis of a series of new isotopes of elements with $102 \leq Z \leq 106$ and $142 \leq N \leq 154$, including isotopes of element 104: ^{253}Ku, ^{254}Ku, ^{255}Ku, ^{256}Ku, and isotopes of element 1.05: ^{255}Ns, ^{257}Ns, $^{257}106$, $^{259}106$.

The essence of the method lies in the fact that when targets of lead and bismuth are irradiated with ions of mass greater than 40, i.e., argon, titanium, chromium, iron, etc., nuclei are observed in a weakly excited state, and they revert to the ground state by emitting 1 to 3 neutrons, which results in a significant increase in the formation cross section of the nucleus in the ground state. The paper presents preliminary results of work on the synthesis of element 107.

Translated from Atomnaya Énergiya, Vol. 40, No. 4, pp. 358-260, April, 1976.

The paper presented by Yu. Ts. Oganesyan proposed a new system, testifying to the possibility of increasing the stability of relatively spontaneous fission of nuclei during transmutation from nuclei with Z = 104 to a superheavy element.

The paper presented by E. Hewlet (USA) was concerned with the synthesis of the heaviest isotope of the 100th element ^{259}Fm by bombarding ^{257}Fm with tritium ions having a 16-MeV energy accelerated in a tandem generator at the Los Alamos laboratory. The life of ^{259}Fm (1.5 sec) is 10^7 times greater than the life of ^{258}Fm (~1 msec). The distributions of the fission fragments of ^{259}Fm by mass and kinetic energy were also studied. The results of this work have considerable value for the further analyses of the stability of transuranic and superheavy elements.

The papers presented by I. Zvara (JINR) and G. Herrman (GFR) gave surveys of the principles and methods of rapid radiochemistry. The thermochromatograph method for studying volatile nonwater compounds has a record speed of action with relative technical simplicity, and enables the more important chemical characteristics of atoms to be studied.

The paper presented by G. Herrman indicated that the use of automatic equipment for separating short-lived isotopes from the products of nuclear fission enables preparations to be prepared for γ spectroscopy in a few seconds. This method was aimed at studying radiators of delayed neutrons, obtaining the spectra of the delayed neutrons with an energy resolution of ~20 keV, which enables the fine structure of the spectra to be analyzed.

The search for superheavy elements in nature formed the subject of the paper presented by T. M. Ter-Akop'yan (JINR). These investigations have a history of more than five years, and a large number of investigators from various countries have taken part. The paper gave a brief outline of the results of work carried out by the JINR in this direction. Exceedingly sensitive methods have been developed, which enable the search for superheavy elements in natural samples to be conducted at sensitivities of 10^{-15}-10^{-16} g/g. A large number of different samples were surveyed. Attention was drawn to data on observations of rare occurrences of spontaneous fission in some meteorites of the carbonaceous chondrite type, obtained by the JINR with the aid of multiple neutron-emission spectrometers of record sensitivity.

The theoretical papers presented by A. Sendulesku (JINR), S. Nielson (Switzerland), and T. Ledergerber (GFR) dealt with analyses of the properties of elements with Z = 104-108, giving a prediction of the half-lives of these nuclei relative to the energy of α decay. A. Sobichevski (Poland), on the basis of existing models for calculating the properties of superheavy nuclei, showed that a marked level of stability could also exist for nuclei with Z $\approx$ 160 to 200. G. Nix (USA) considered possible ways of synthesizing superheavy nuclei.

Studies of the Mechanism of the Interaction of Complex Nuclei. The problem of the interaction of complex nuclei was examined in nine experimental and theoretical papers. In addition, a special discussion seminar was arranged in response to requests from the delegates. This was held under the direction of Academician S. G. Belyaev and covered the more urgent problems of the interaction of complex nuclei.

New experimental data obtained at the JINR, the USA, and France from studies of deep inelastic reactions of the transmission of nucleons, quasifission, and fission of excited nuclei, by the use of a wide assortment of accelerated ions from carbon to xenon, were dealt with in papers presented by V. V. Volkov (JINR), V. Svyatetski (USA), J. Jaqmar (France), J. Peter (France), etc., and lead to significant progress in the qualitative understanding of the interactions between complex nuclei, the role of the large number of angular momentums, viscosities, and deformations of the nuclei in the collision process; it also assisted in the development of a number of theoretical models.

A great deal of interest was expressed in the paper presented by R. Klapish (France) on the results of joint experiments conducted by physicists of Orsay (France) and Dubna (USSR) to study the mechanism of interaction of complex nuclei and the fission of excited nuclei, obtained on a U-300 accelerator at the JINR, using a French slot-element mass separator. A fortunate combination of the unique possibilities of ion beams in the JINR accelerator and precision methods previously prepared in France enabled a large amount of experimental material to be obtained in a short period of time (3 months).

Obtaining Nuclei Remote from Lines of β Stability and Studying Their Properties. The proton decay of nuclei formed the subject of a paper presented by V. A. Karnaukhov (JINR) which presented results obtained at Dubna during studies of new proton sources in the region of alkali and rare-earth isotopes, while G. Hardy (Canada) presented data on sources of delayed protons obtained at Chalk River (Canada).

The paper presented by A. Khrinkevich (Poland) presented experimental data on the measurement of g factors and magnitudes of internal magnetic fields for a number of nuclear states.

New Problems of the Physics of Heavy Ions. Three groups of studies along these lines were reported at the school-seminar.

The papers presented by V. Grainer (USA), A. Poscantser (USA), and G. Nix (USA) discussed the problem of the shock waves which arise during the interaction of relativistic ions with nuclei. This new and extremely topical field of study can apparently only be approached with the aid of heavy ions. By studying experimentally the mechanism of formation of these shock waves, it is possible to gain some insight into the fundamental properties of nuclear material, its compressibility, and to check the hypothesis regarding the existance of superdense states of the nucleus: the stable density isomers.

The session studied quantum electrodynamics under the conditions of superpowerful fields, which formed the subject of papers presented by V. S. Popov (ITÉF, Moscow), V. Grainer (GFR), and K. G. Kaun (JINR). V. S. Popov and V. Grainer examined in their papers the contemporary state of the theory of formation of electron shells in supercritical magnetic fields of nuclear systems with $Z \geqslant 172$. They showed that for nuclei with $Z \geqslant 172$ the lower level of electrons $1S_{1/2}$ collapses into the negative continuum of dirac electron states with the possibility of the creation of an electron—positron pair. It is proposed that the effect of a spontaneous generation of positrons can be studied with the aid of collisions of very heavy nuclei such as uranium and uranium, californium and californium, etc. With collision energies below the coulomb barrier, these nuclei must be momentarily formed into quasiatoms with $Z \geqslant 172$, which enables the emission of positrons to be observed, i.e., the decay of a neutral vacuum, if the nuclei are close enough to each other.

K. G. Kaun in his paper reported experimental data obtained at Dubna during the investigation of KX radiation, which gave rise to transmutations between quasiatoms of systems with Z = 100-114. In these works, the quasiatomic origin of this radiation is shown, and the structure of the spectra analyzed. The investigation showed the existance of a real possibility of experimentally studying superheavy quasiatoms with $Z \geqslant 172$, which would answer a number of questions of principle relating to quantum electrodynamics and superpowerful fields, and also relating to field theory and elementary particles.

Finally, the third group of investigations, concerned with obtaining and studying weakly excited nuclei with large angular momentums by means of heavy ions, was represented by the papers of S. Ogazy (Poland) and V. V. Pashkevich (JINR). This was also a new field of study, in which new qualitative effects connected with isomers of high-spin states could be expected to be brought to light. This would lead to a delay in the cascade of γ quanta or an increase in the fissionability of some nuclei.

Future Developments in Heavy-Ion Accelerators. At the present time, a number of the world's leading centers are designing and building accelerators for producing intensive beans of heavy ions. Five papers were concerned with the future development of heavy-ion accelerators: G. N. Flerov (JINR), P. Armbruster (GFR), J. Jaqmar (France), M. Sakai (Japan), and S. Khoinatkii (Poland).

The construction of a powerful linear accelerator — the UNILAC — has been completed at Darmstadt (GFR), capable of generating beams of ions from neon to uranium inclusive, with intensities of $5 \cdot (10^{13}\text{-}10^{11})$ particles per second at an energy of 8.5 MeV/nucleon. The physical start-up was marked at the end of 1975. The total cost of the accelerator was ~ $65 million.

Construction has begun at the Oak Ridge laboratory (USA) of an accelerator complex for heavy ions. A tandem generator with a potential on the collector of 25 MV serves as injector, while an existing ORIC isochronous cyclotron with a pole diameter of 190 cm acts as the main accelerator. This accelerator complex is capable of producing heavy ions up to mass 150 with intensities of 10^{12} to 10^{10} particles per second. It is proposed that the accelerator starts operating in 1979, and its construction will cost $17.5 million.

It is proposed to start up a heavy-ion accelerator in England in 1979 at the Deresbern research center. A tandem generator with a collector potential of 30 MV is being built at a cost of ~ $30 million.

In France, the decisive has been taken to build a national heavy-ion accelerator GANIL, being a combination of two isochronous cyclotrons with divided sectors, having pole diameters of 3.3 m each. It is proposed that the accelerator starts operating in 1980-1981. The construction costs are expected to run to ~ $55 million.

An extensive program for the design and creation of heavy-ion accelerators has been carried out in

Japan. Developments have been taking place in two directions: the creation of low-energy accelerators (~10 MeV/nucleon) and an annular synchrotron for producing beams of heavy ions with energies of ~500 MeV/nucleon (Project NUMATRON).

A 4-m cyclotron — the U-400 — is being constructed at Dubna, capable of generating beams of heavy ions all the way up to xenon, with intensities from $5 \cdot 10^{14}$ particles per second for neon to $2 \cdot 10^{11}$ particles per second for xenon. It is proposed that the U-400 will produce beams of carbon, nitrogen, and oxygen ions with energies of 50 to 60 MeV per nucleon.

Work on the creation of a multipurpose 2-m isochronous cyclotron for heavy ions is proceeding successfully in Poland, in cooperation with scientists from JINR.

The Various Uses for Heavy Ions. The field of application of heavy ions is rapidly expanding into new directions of research. The paper presented by V. S. Barashenkov (JINR) showed that the use of the unique methodical possibilities of the JINR heavy-ion accelerator, producing intensive beams of heavy ions right up to xenon, would enable a number of problems of considerable importance to the national economy to be solved in the shortest possible time. In particular, a method was developed at Dubna, together with the necessary industrial technology, for manufacturing nuclear filters, which has found application in various fields of science and technology; work has been carried out on the modeling of radiation damage and the development of new superconducting materials by using beams of heavy ions.

At the close of the session a general discussion was convened. The results of the work bore witness to the rate with which the physics of heavy ions is developing, the great scientific importance of the results that have been achieved and the extensive possibilities of practical application. Work with heavy ions is being carried out in a number of the leading scientific centers of the USA, the GFR, France, and other countries in addition to that taking place at the JINR and member countries. New high-powered accelerators for heavy ions are being built in many countries.

The school-seminar has shown that scientists of the JINR occupy leading positions in all the basic lines of study with heavy ions, they have carried out a number of fundamental initiatory investigations on the synthesis of new transuranic elements, the detection of new forms of radioactivity, and the observation of new types of nuclear reaction involving the transmission of large numbers of nucleons.

engineering science

continued from back cover

Title	# of Issues	Subscription Price
Metallurgist *Metallurg*	12	$225.00
Metal Science and Heat Treatment *Metallovedenie i termicheskaya obrabotka metallov*	12	$215.00
Polymer Mechanics *Mekhanika polimerov*	6	$195.00
Problems of Information Transmission *Problemy peredachi informatsii*	4	$175.00
Programming and Computer Softwave *Programmirovanie*	6	$95.00
Protection of Metals *Zashchita metallov*	6	$195.00
Radiophysics and Quantum Electronics (Formerly Soviet Radiophysics) *Izvestiya VUZ. radiofizika*	12	$225.00
Refractories *Ogneupory*	12	$195.00
Soil Mechanics and Foundation Engineering *Osnovaniya, fundamenty i mekhanika gruntov*	6	$195.00
Soviet Applied Mechanics *Prikladnaya mekhanika*	12	$225.00
Soviet Atomic Energy *Atomnaya energiya*	12 (2 vols./yr. 6 issues ea.)	$235.00
Soviet Journal of Glass Physics and Chemistry *Fizika i khimiya stekla*	6	$ 95.00
Soviet Journal of Nondestructive Testing (Formerly Defectoscopy) *Defektoskopiya*	6	$225.00
Soviet Materials Science *Fiziko-khimicheskaya mekhanika materialov*	6	$195.00
Soviet Microelectronics *Mikroelektronika*	6	$135.00
Soviet Mining Science *Fiziko-tekhnicheskie problemy razrabotki poleznykh iskopaemykh*	6	$225.00
Soviet Powder Metallurgy and Metal Ceramics *Poroshkovaya metallurgiya*	12	$245.00
Strength of Materials *Problemy prochnosti*	12	$295.00
Theoretical Foundations of Chemical Engineering *Teoreticheskie osnovy khimicheskoi tekhnologii*	6	$195.00
Water Resources *Vodnye Resursy*	6	$190.00

SEND FOR YOUR FREE EXAMINATION COPIES

Plenum Publishing Corporation

Plenum Press • Consultants Bureau
• IFI/Plenum Data Corporation
227 WEST 17th STREET
NEW YORK, N. Y. 10011

United Kingdom: Black Arrow House
2 Chandos Road, London NW10 6NR England

Back volumes are available. For further information, please contact the Publishers.

Declassified and Approved For Release 2013/04/10 : CIA-RDP10-02196R000700070004-7

breaking the language barrier

WITH COVER-TO-COVER
ENGLISH TRANSLATIONS
OF SOVIET JOURNALS

in engineering science

Title	# of Issues	Subscription Price
Automation and Remote Control *Avtomatika i telemekhanika*	24	$260.00
Biomedical Engineering *Meditsinskaya tekhnika*	6	$195.00
Chemical and Petroleum Engineering *Khimicheskoe i neftyanoe mashinostroenie*	12	$275.00
Chemistry and Technology of Fuels and Oils *Khimiya i tekhnologiya topliv i masel*	12	$275.00
Combustion, Explosion, and Shock Waves *Fizika goreniya i vzryva*	6	$195.00
Cosmic Research (Formerly Artificial Earth Satellites) *Kosmicheskie issledovaniya*	6	$215.00
Cybernetics *Kibernetika*	6	$195.00
Doklady Chemical Technology *Doklady Akademii Nauk SSSR*	2	$65.00
Fibre Chemistry *Khimicheskie volokna*	6	$175.00
Fluid Dynamics *Izvestiya Akademii Nauk SSSR mekhanika zhidkosti i gaza*	6	$225.00
Functional Analysis and Its Applications *Funktsional'nyi analiz i ego prilozheniya*	4	$150.00
Glass and Ceramics *Steklo i keramika*	12	$245.00
High Temperature *Teplofizika vysokikh temperatur*	6	$195.00
Industrial Laboratory *Zavodskaya laboratoriya*	12	$215.00
Inorganic Materials *Izvestiya Akademii Nauk SSSR, Seriya neorganicheskie materialy*	12	$275.00
Instruments and Experimental Techniques *Pribory i tekhnika éksperimenta*	12	$265.00
Journal of Applied Mechanics and Technical Physics *Zhurnal prikladnoi mekhaniki i tekhnicheskoi fiziki*	6	$225.00
Journal of Engineering Physics *Inzhenerno-fizicheskii zhurnal*	12 (2 vols./yr. 6 issues ea.)	$225.00
Magnetohydrodynamics *Magnitnaya gidrodinamika*	4	$175.00
Measurement Techniques *Izmeritel'naya tekhnika*	12	$195.00

SEND FOR YOUR FREE EXAMINATION COPIES

Back volumes are available.
For further information,
please contact the Publishers.

continued on inside back cover